TU WIEN
TECHNISCHE
UNIVERSITÄT
WIEN
Vienna University of Technology

Diplomarbeit

Combustion of Dimethylether and Dimethylether/Iso-Octane Fuel Mixtures in Non-Premixed and Partial Premixed Flows

ausgeführt unter der Leitung von

Ao. Univ. Prof. Dipl.-Ing. Dr.techn. Ernst Pucher
Institut für Fahrzeugantriebe und Automobiltechnik
Technische Universität Wien

und

Prof. Dr. Kalyanasundaram Seshadri
Department of Mechanical and Aerospace Engineering
University of California, San Diego.

Eingereicht an der Technischen Universität Wien
Fakultät für Maschinenwesen und Betriebswirtschaftenvon

von

Thomas Knoblinger

Matrikel Nr.: 0925292
Josefstädterstraße 14/69
A - 1080 Wien

Wien und San Diego, April 2015

Master Thesis

Combustion of Dimethylether and Dimethylether/Iso-Octane Fuel Mixtures in Non-Premixed and Partial Premixed Flows

Vienna University of Technology
Faculty of Mechanical and Industrial Engineering

Advisors:

Ao. Univ. Prof. Dipl.-Ing. Dr.techn. Ernst Pucher
Institute for Powertrains and Automotive Technology
Vienna University of Technology

and

Prof. Dr. Kalyanasundaram Seshadri
Department of Mechanical and Aerospace Engineering
University of California, San Diego.

Thomas Knoblinger

Matrikel Nr.: 0925292
Josefstädterstraße 14/69
A - 1080 Wien

Vienna and San Diego, April 2015

Abstract

Different experimental and computational studies on combustion of dimethyl ether (DME), a very promising non petroleum fuel alternative, are carried out in this thesis. DME can be manufactured out of various types of biomass and BioDME belongs to the group of second-generation biofuels. Experimental studies are carried out emplyoing the counterflow configuration. The burner used in the experiments is made up of two ducts. In the counterflow configuration, two axys-symemtric reactant streams flow from opposite directions towards a stagnation plane.

In the first investigation critical conditions of autoignition and extinction of DME/iso-octane fuel mixtures are measured. The fuels are dimethyl ether (DME) and 2,2,4-Trimethylpentane (iso-octane) and their mixtures. In this investigation the counterflow configuration consists of an oxidizer stream of oxygen (O_2) and nitrogen (N_2) coming from one side and a fuel stream of fuel and nitrogen (N_2) coming from the other side. The Reynolds numbers of the flow are considered to be large.

Critical conditions of autoignition are measured under ambient pressure and a fixed fuel mass fraction of $Y_F = 0{,}4$ in the fuel stream. At fixed values of the oxidizer strain rate a_2 autoignition temperatures are higher for fuel mixtures of DME and iso-octane then for pure DME. By rising the amount of iso-octane in the fuel composition the level of increase in temperature by adding iso-octane is becoming smaller.

Previous studies have established that the scalar dissipation rate at extinction depends on the stochiometric mixture fraction Z_{ST} and the adiabatic flame temperature T_{AD}. To clarify the influence of mixing iso-octane and DME on extinction, studies are carried out at fixed values of Z_{ST} and T_{AD}. A previous developed Burke-Schumann (flame-sheet) formulation is employed to estiamte the boundary values of the mass fractions of the reactants. Critical conditions of extinction are measured under ambient pressure. The strain rate at extinction is found to be positively correleated to an increase of DME in the combustile mixture.

In the second investigation critical conditions of extinction of laminar partially premixed DME flames are measured. The fuel is dimethyl ether (DME). A premixed fuel-rich mixture of DME (C_2H_6O), oxygen (O_2) and nitrogen (N_2) is injected from one duct while a fuel-lean mixture of C_2H_6O, O_2 and N_2 is injected from the other duct.

The level of partial premixing is given by the equivalence ratio $\Phi = Y_F/(v Y_{O2})$ where Y_F and Y_{O2} are respectively the mass fractions of fuel and oxygen at the injection planes (exit of the ducts) and $v = W_F/(3\ W_{O2})$. Here W_F and W_{O2} are the molecular weights of fuel and oxygen respectively. The equivalence ratio of the premixed fuel-rich mixture is Φ_1 and the equivalence ratio of the premixed fuel-lean mixture is Φ_2. Previous studies have established that the scalar dissipation rate at extinction depends on the stochiometric mixture fraction Z_{ST} and the adiabatic flame temperature T_{AD}. To clarify the influence of partial premixing on extinction, studies are carried out at fixed values of Z_{ST} and T_{AD}. A previous developed Burke-Schumann (flame-sheet) formulation is employed to estiamte the boundary values of the mass fractions of the reactants. Critical conditions of extinction are measured under ambient pressure. Two sets of expriments are conducted, in one set $\Phi_1^{-1} = 0$ and in the other set $\Phi_2 = 0$. The computations are carried out using two different detailed chemical kinteic mechanism for DME oxidation. For $\Phi_1^{-1} = 0$ experiments show that the value of the strain rate at extinction increases with increasing Φ_2. For $\Phi_2 = 0$, experiments show very little change in the values of the oxidizer strain rate a_2 at extinction with increasing Φ_1^{-1}. The values of the strain rate at extinction calculated using detailed chemistry are found to agree quite well with the experiments. The key observation is that addition of DME to the fuel lean mixture enhance the overall recativity while addition of oxygen to the fuel-rich mixture has little influence on the overall reactivity.

As one of the two used chemical kinetic mechanism, a new at UC San Diego developed short reaction mechanism for the combustion of dimethyl ether, was found to agree very well for the non premixed case ($\Phi_1^{-1} = 0$; $\Phi_2 = 0$) and little levels of partial premixing it was decided to start another set of expriments only considering non premixed diffusion flames. Critical conditions of extinction are measured for a fixed value of the stochiometric mixture fraction Z_{ST}. The values of the strain rate at extinction calculated with the detailed chemistry of the new developed short DME mechanism show a very well agreement with the experimental results.

Kurzfassung

Verschiedene experimentelle Versuche und numerische Simulationen zur Verbrennung von Dimethylether (DME), einer vielversprechenden Alternative zu fossilen Kraftstoffen, werden in dieser Diplomarbeit durchgeführt. Dimethylether kann aus unterschiedlichsten Arten von Biomasse hergestellt werden und BioDME gilt as Biokraftstoff der zweiten Generation. Für die experimentellen Untersuchungen wird die Gegenstromdiffusionsanlage verwendet, in der zwei achsensymetrische Ströme frontal aufeinander strömen, sodass eine Stauebene entsteht.

In der ersten Untersuchung werden kritische Bedingungen der Selbstenzündung und Verlöschung von DME/Iso-Octan – Flammen gemessen. Die verwendeten Kraftstoffe sind Dimethylether(DME), 2,2,4-Trimethylpenthan (Iso-Octan) und ihre Mischungen. In dieser Untersuchung besteht die Gegenstromdiffusionsanlage aus einem Oxidationsstrom aus Sauerstoff (O_2) und Stickstoff (N_2) von einer Seite kommend und aus einem Kraftstoffstrom aus Kraftstoff und Stickstoff (N_2) von der anderen Seite kommend. Die Reynoldszahlen des Stromes werden als groß angenommen.

Die kritischen Bedingungen der Selbstentzündung werden unter Umgebungsdruck und mit einem konstanten Krafstoffmassenanteil $Y_F = 0,4$ im Kraftstoffstrom gemessen. Für stationäre Werte der „Streckungs-Rate" (Strain Rate) a_2 werden höhere Selbstenzündungstemperaturen für Mischungen aus DME und Iso-Octan gemessen als für reines DME. Mit höheren Anteilen von Iso-Octan in der Krafstoffmischung wird dieser Effekt jedoch geringer.

In vorangegangenen Untersuchungen wurde festgestellt, dass der skalare Verlustfaktor bei der Verlöschung von der stöchiomterischen Mischungsrate Z_{ST} und der adiabaten Flammentemperatur T_{AD} abhängt. Um die Verlöschung von DME/Iso-Octan – Flammen zu bestimmen werden die Versuche deshalb mit konstanten Werten für die stöchiometrische Mischungsrate Z_{ST} und die adiabate Flammentemperatur T_{AD} durchgeführt. Eine zuvor durchgeführte Burke-Schumann Berechnung wird verwendet um die Randbedingugen für die Massenanteile der Ausgangsstoffe zu bestimmen. Die kritischen Bedingungen der Auslöschung werden unter Umgebunsdruck gemessen. Die Ergebnisse der Versuche zeigen, dass die „Strain-Rate" bei der Verlöschung positiv mit einem höheren Anteil von DME in der Kraftstoffmischung korreliert.

In der zweiten Untersuchung werden kritische Bedingungen von laminaren, teilweise vorgemischten DME Flammen gemessen. Der verwendete Kraftsoff ist Dimethylether. Eine kraftstoffreiche Mischung aus DME (C_2H_6O), Sauerstoff (O_2) und Stickstoff (N_2) strömt von einer Seite ein, eine kraftstoffarme Mischung aus C_2H_6O, O_2 and N_2 strömt von der anderen Seite ein. Der Grad der teilweisen Vormischung wird mit Hilfe der Äquivalenzrate $\Phi = Y_F/(vYO_2)$ bestimmt in der Y_F and Y_{O2} die Massenanteile von Kraftstoff und Sauerstoff sind und $v = W_F/(3\ W_{O2})$. Hier sind W_F und W_{O2} die Molmassen von Kraftstoff und Sauerstoff. Die Äquivalenzrate der kraftstoffreichen Mischung ist Φ_1 und die Äquivalenzrate der kraftstoffarmen Mischung ist Φ_2. In vorangegangenen Untersuchungen wurde festgestellt, dass der skalare Verlustfaktor bei der Auslöschung von der stöchiometrischen Mischungsrate Z_{ST} und der adiabaten Flammentemperatur T_{AD} abhängt. Um den Einfluss der laminaren, teilweisen Vormischung auf die Verlöschung von DME-Flammen festzustellen werden deshalb die Versuche mit einer konstanten stöchiometrischen Mischungrate Z_{ST} und einer konstanten adiabaten Flammentemperatur T_{AD} durchgeführt. Eine zuvor durchgeführte Burke-Schumann Berechnung wird verwendet um die Randbedingugen für die Massenanteile der Ausgangsstoffe zu bestimmen. Die kritischen Bedingungen der Verlöschung werden unter Umgebungsdruck gemessen. Zwei Versuchsreihen werden durchgeführt, in der ersten Versuchsreihe wird $\Phi_1^{-1} = 0$ gesetzt und in der zweiten Versuchsreihe wird $\Phi_2 = 0$ gesetzt. Numerische Simulationen werden mit der Hilfe von zwei verschiedenen detaillierten chemischen Reaktionsmechanismen für DME-Oxidation durchgeführt. Für $\Phi_1^{-1} = 0$ zeigen die Experimente einen Anstieg der "Strain Rate" bei der Verlöschung für einen höheren Vormischungsgrad. Für $\Phi_2 = 0$ zeigen die Experimente nur sehr kleine Änderungen der "Strain Rate" für höhere Vormischungsgrade. Die Ergebnisse der numerischen Unersuchungen zeigen eine gute Übereinstimmung mit den experimentellen Untersuchungen. Die zentrale Schlussfolgerung ist, dass eine Erhöhung des DME-Anteils in der kraftstoffarmen Mischung die generelle Reaktionsfähigkeit erhöht, während eine Erhöhung des Sauerstoffanteils in der kraftstoffreichen Mischung nur einen geringen Einfluss auf die generelle Reaktionsfähigkeit hat.

Da einer der beiden verwendeten chemischen Reaktionsmechanismen, ein neuer an der UC San Diego entwickelter verkürzter Reaktionsmechanismus für DME Verbrennung eine sehr gute Übereinstimmung für nichtvorgemischte Mischungen ergab wurde eine weitere Versuchsreihe für nicht vorgemischte Diffusionsflammen durchgeführt. Die kritischen Bedingungen der Verlöschung werden für konstante Werte der stöchiometrischen Mischungsrate Z_{ST} gemessen. Die berechneten Werte der „Strain Rate" bei der Verlöschung des neu entwickelten DME Mechanismus zeigen eine außerordentlch gute Übereinstimmung mit den experimentellen Untersuchungen.

Acknowledgements

Table of Content

List of Symbols

A	frequency factor for Arrhenius Equation [1/s]
A_1	area of fuel duct [m^2]
A_2	area of oxidizer duct [m^2]
$A_{CURT,1}$	area of fuel curtain [m^2]
$A_{CURT,2}$	area of oxidizer curtain [m^2]
A_{RAD}	surface of the thermocouple wire and bead [m^2]
A_W	surface of the thermocouple wire
a_1	fuel strain rate [1/s]
a_2	oxidizer strain rate [1/s]
B	pre-exponential constant for Frequency Factor of Arrh. equation [1/K]
c_P	specific heat capacity (isobaric) [J/kgK]
d_{SC}	diameter of the oxidizer screen [m]
d_W	diameter of the thermocouple wire [m]
Da	Damköhler number [ ]
E_A	activation energy [cal/mol]
F_{SC}	view factor of the oxidizer stream [ ]
$F_{UpperSUR}$	view factor of the upper surroundings [ ]
$F_{LowerSUR}$	view factor of the lower surroundings [ ]
ΔH	heat of reaction [cal/mol]
k	reaction rate constant [ ]
k_F	thermal conductivity of air [W/mK]
L	distance between the screens of oxidizer and fuel duct [mm]
L_2	distance between the thermocouple bead and the lowest screen [mm]
Le_{DME}	Lewis number dimethyl ether [ ]
Le_{ISO}	Lewis number iso-octane [ ]
M_{AIR}	molecular weight air [g/mol]
M_{DME}	molecular weight dimethyl ether [g/mol]
M_{ISO}	molecular weight iso-octane [g/mol]
M_{N_2}	molecular weight nitrogen [g/mol]
M_{O_2}	molecular weight oxygen [g/mol]

$\dot{m}_1$	mass flux of the fuel stream [kg/s]
$\dot{m}_2$	mass flux of the oxidizer stream [kg/s]
Nu_{CYL}	nusselt number [ ]
p	ambient pressure [Pa]
Q_{DME}	heat release of dimethyl ether [J/mol]
Q_{ISO}	heat release of iso-octane [J/mol]
$\dot{Q}_{CAT}$	heat losses due to surface-induced catalytic reactions [W]
$\dot{Q}_{COND}$	heat losses due to conduction [W]
$\dot{Q}_{CONV}$	heat losses due to convection [W]
$\dot{Q}_{RAD}$	heat losses due to radiation [W]
R	gas constant [J/molK]
Re	Reynolds number of air [ ]
T	absolute temperature (Arrhenius Equation) [K]
T_1	fuel duct temperature [K]
T_2	oxidizer duct temperature [K]
T_{AD}	adiabatic flame temperature [K]
T_F	film temperature [K]
T_{SC}	screen temperature [K]
T_{SUR}	surrounding temperature [K]
T_{TC}	thermocuouple temperature [K]
T_U	temperature of the environment [K]
t_c	chemical time of combustion [s]
t_m	residence time [s]
V	Volume (Energy balance thermocouple) [m^3]
V_1	normalcomponent of fuel stream velocity at duct exit [1/s]
V_2	normalcomponent of oxidizer stream velocity at duct exit [1/s]
$\dot{V}_{AIR,1}$	volume stream of air in the fuel stream [m^3/s]
$\dot{V}_{AIR,2}$	volume stream of air in the oxidizer stream [m^3/s]
$\dot{V}_{CURT,1}$	volume stream of the fuel curtain [m^3/s]
$\dot{V}_{CURT,2}$	volume stream of the oxidizer curtain [m^3/s]
$\dot{V}_{DME,1}$	volume stream of dimethyl ether in the fuel stream [m^3/s]

$\dot{V}_{DME,2}$	volume stream of dimethyl ether in the oxidizer stream [m^3/s]
$\dot{V}_{ISO,1}$	volume stream of iso-octane in the fuel stream [m^3/s]
$\dot{V}_{N_2,1}$	volume stream of nitrogen in the fuel stream [m^3/s]
$\dot{V}_{N_2,2}$	volume stream of nitrogen in the oxidizer stream [m^3/s]
$\dot{V}_{SLM,i,j}$	volume stream scaled to the normal temperature [m^3/s]
$\upsilon_{REL,1}$	relative velocity of fuel curtain to the inner ducht [ ]
$\upsilon_{REL,2}$	relative velocity of oxidizer curtain to the inner ducht [ ]
$X_{AIR,1}$	mole fraction of air in the fuel stream [ ]
$X_{AIR,2}$	mole fraction of air in the oxidizer stream [ ]
$X_{DME,1}$	mole fraction of dimethyl ether in the fuel stream [ ]
$X_{DME,2}$	mole fraction of dimethyl ether in the oxidizer stream [ ]
$X_{ISO,1}$	mole fraction of iso-octane in the fuel stream [ ]
$X_{N_2,1}$	mole fraction of nitrogen in the fuel stream [ ]
$X_{N_2,2}$	mole fraction of nitrogen in the oxidizer stream [ ]
$X_{O_2,1}$	mole fraction of oxygen in the fuel stream [ ]
$X_{O_2,2}$	mole fraction of oxygen in the oxidizer stream [ ]
$Y_{AIR,1}$	mass fraction of air in the fuel stream [ ]
$Y_{AIR,2}$	mass fraction of air in the oxidizer stream [ ]
$Y_{DME,1}$	mass fraction of dimethyl ether in the fuel stream [ ]
$Y_{DME,2}$	mass fraction of dimethyl ether in the oxidizer stream [ ]
$Y_{ISO,1}$	mass fraction of iso-octane in the fuel stream [ ]
$Y_{N_2,1}$	mass fraction of nitrogen in the fuel stream [ ]
$Y_{N_2,2}$	mass fraction of nitrogen in the oxidizer stream [ ]
$Y_{O_2,1}$	mass fraction of oxygen in the fuel stream [ ]
$Y_{O_2,2}$	mass fraction of oxygen in the oxidizer stream [ ]
Z	mixture fraction [ ]
Z_{ST}	stochiometric mixture fraction [ ]
$Z_{ST,DME}$	stochiometric mixture fraction dimethylether [ ]
$Z_{ST,ISO}$	stochiometric mixture fraction iso-octane [ ]

α	temperature exponent for frequency factor of Arrh. equation [ ]
ε_{TH}	emissivity of the thermocouple [ ]
ρ	density [kg/m^3]
ρ_1	density at fuel duct exit [kg/m^3]
ρ_2	density at the oxidizer duct exit [kg/m^3]
σ	Stefan-Boltzmann constant 5,67e-8 [W/m^{2}K^4]
Φ	equivalence ratio [ ]
Φ_1	equivalence ratio fuel stream [ ]
Φ_2	equivalence ratio oxidizer stream[ ]

Subscripts

$_1$ fuel duct side

$_2$ oxidizer duct side

$_b$ burnt

$_u$ unburnt

Nomenclature

AKI	Anti Knock Index
C_2H_6O	Dimethyl Ether
CO	Carbon Monoxide
CO_2	Carbon Dioxide
DME	Dimethyl Ether
H_2	Hydrogen
H_2O	Water
HCCI	Homogeneous Charge Compression Ignition
LLNL	Lawrence Livermore National Laboratory
LPG	Liquified Petroleum Gas
MFC	Mass Flow Controller
MON	Motor Octane Number
NO_x	Nitrogen Oxides
O_2	Oxygen
PID	Proportional Integral Derivative
RON	Research Octane Number
UC	University of California
UCSD	Universtiy of California, San Diego

1. Introduction

The combustion process is central to for many applications and is required for developing prosperity in the modern world. On a hisorical basis the first discovery of combustion dates back over 500000 years as source of heat and light, but it took until the 18th century combustion was used as method to produce energy on an industrial scale. Combustion of fossil fuels became the basis for transportation, manufacturing and producing elecricity in power plants and had a huge impact on economic progress. Even nowadays human life without combustion is not conceivable although many new technologies were developed. Especially transportation still requires the combustion of fossil fuels as other possible energy storages like batteries cannot provide the required high energy densities.

From a chemical perspective, combustion can be simplified as the transformation of chemical bond energy into thermal energy by conversion of reactants into products. This simplification represents also the two main challenges for combustion of fossil fuels in the future. First to supply the demand of crude oil for the ever growing world energy consumption and second to deal with the products and their impact on the world climate. The first challenge will probably rather be a long term concern as technology for exploration and production of oil has improved enormous and an expected increasing of the oil price in long term makes this technologies affordable. Regardless there are a lot of countries without or rather difficult to acces reserves of fossil fuels who want to decrease their energy dependence. The second challenge is already affecting us for a long time thinking for example of smog, high fine dust and NO_x concentrations in big cites and global warming triggered by increasing CO_2 concentrations in the world atmosphere. Hence, it´s important to search for alternatives and develop infrastructure that can gradually replace fossil fuels. Governments of various regions and countries, especially in high developed areas, try to accelerate this progress in the last decades by introducing restrictions and regulations for emissions for both factories and vehicles.

Although the combustion process is well known for decades now, there still exists very limited knowledge in this field. In a flame for example thousand of reactions take place, in a small lengths scale and very short amount of time. Most fuels show high
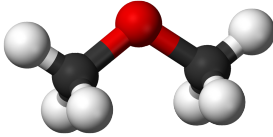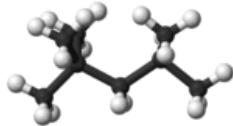
temperature chemistry and autoignition occurs in a one stage process. However, there are also fuels that show low temperature chemistry and autoignite in a two-step process in which a transient cool flame (650 - 950 K) appears before a hot flame (>2000K) is established. One such fuel is dimethyl ether (DME). The existence of cool flames is highly dependent on the structure of the fuel molecule and a better knowledge of the cool flame behaviour is helpful to improve the efficiency of spark ignition internal combustion engines as well as diesel engines and HCCI research.

The focus of this thesis is the combustion behaviour of dimethyl ether which is seen as potential alternative fuel and additive fuel for diesel engines and can be produced ouf of various types of biomass. For this approach several investigations on DME are carried out in this thesis. Critical conditions of autoignition and extinction of dimethyl ether, iso-octane and their mixtures and critical conditions of extinction of partially premixed DME flames are studied under ambient pressures. For an improved understanding of the combustion behaviour of a fuel it´s also important to know how the fuel interacts with other fuels. Improved knowledge of partially premixed flames is very helpful modelling turbulent combustion. [20, 22, 30]

1.1. Tested Fuels

In this thesis investigations on the combustion behaviour of dimethyl ether and dimethyl ether/iso-octane fuel mixtures are conducted. Iso-octane can be used as surrogate fuel for gasoline together with heptane. There have been several studies about DME since it is considered as an alternative for Diesel and bio-production is applicable. For a better understanding of the combustion behaviour of a chosen fuel it´s also important to know how a fuel interacts with others. Recently there have been studies carried out at UCSD about critical conditions of autoigntion and extinction of Ethanol/DME fuel mixtures as these molecules are isomers. However there are limited number of published investigations on DME/gasoline blends. As iso-octane can be used as Gasoline surrogate this investigation will give us basic knowledge about the combustion behaviour of DME/gasoline fuel blends. The following table compares the most important properties of DME and iso-octane.

Table 1.1: Comparison of the tested fuels dimetyhl ether and iso-octane

	Dimethyl Ether (DME) [12, 23]	2,2,4-Trimethylpentane (iso-octane) [12]
Chemical structure		
Chemical Formula	CH_3OCH_3	$CH_3(CH_2)_6CH_3$
Molecular Weight [kg/mol]	0,04607	0,1142285
Density [kg/m^3]	661	690
Normal boiling point [K]	248,25	372,4

1.1.1. Dimethyl Ether (DME)

Dimethyl Ether (DME) is a very promising non petroleum fuel alternative with the chemical formula CH_3OCH_3. It´s been investigated as an oxygen-rich fuel additive or replacement of diesel in compression ignition engines to decrease emissions. Major global concerns like the greenhouse effect and decreasing accessible petroleum reserves have put more attention on dimethyl ether in recent years as it´s global warming potential can be neglected and it´s production is not limited to one feedstock. DME can be manufactured out of various types of biomass and BioDME belongs to the group of second generation biofuels. Its similar properties to LPG are an additional benefit as they allow DME to be handled in LPG infrastructure with only small modifications. Currently DME is primary used in developing countries where it is blended to LPG and used for heating and cooking. [23]

Dimethyl ether is the simplest of all ethers and with its low normal boiling point at 248,25 K it is gaseous at standard atmosphere pressure and liquid above 6,1 atm at 293,15 K. During the combustion process it shows a visible blue flame and it doesn´t require an odorant as it has an ether-like scent. [6]

Dimethyl ether is non-toxic, non-mutagenic, non-teratogenic, non-carcinogenic and doesn´t corrode any metals. It´s high cetane number (55 – 60) makes it a remarkable alternative for diesel (55) and leads to short ignition delay times and low engine

noise. In engines, the simplicity of the carbon chain also leads to low NO_x and CO emissions and only moderate modifications are required to burn dimethyl ether. DME does not deplete the ozone layer and enables soot free operation. Another benefit is the fact that it doesn´t contain sulfur and nitrogen. Due the high oxygen content DME has a lower energy content compared to petroleum based fuels which leads to higher fuel consumption. For commercial use a larger fuel storage tank is required and a larger volume has to be injected to provide the same performance as Diesel fuels. [6, 23]

1.1.1.1.   BioDME – Production Methods

As mentioned before DME production is not limited to a single feedstock. DME produced out of bio sources or biogas is called BioDME and belongs to the group of second generation biofuels. There are two different production methods, the conventional indirect synthesis and the recently new developed direct synthesis which both require Syngas (synthetic gas) as feedstock. Syngas can be produced by multiple sources including biogas by steam reforming and by bio sources or waste materials such as straw or black liquor by gasification.

In a conventional two-step process (indirect synthesis) the Syngas is first converted to methanol followed by the dehydration of methanol to form DME. In the newly developed direct synthesis process, both methanol synthesis and the dehydration process take place in the same reactor. The efficieny rate of this method can be increased by methanol preparation since the thermodynamic limitations for methanol synthesis can be obviated. [6, 13, 23]
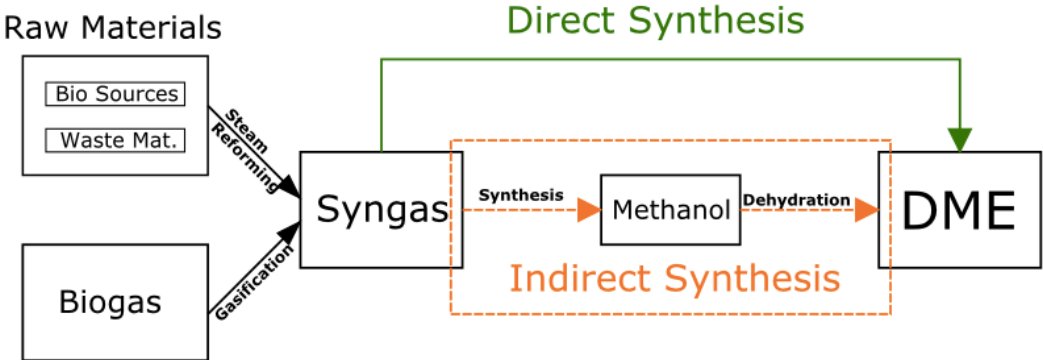

Figure 1.1: BioDME production methods – direct and indirect Synthesis

1.1.2.   2,2,4-Trimethylpentane (Iso-Octane)

2,2,4-Trimethylpentane, also well-known as iso-octane is used as a reference fuel for the octane–rating which describes the knock resistance of different fuels in internal combustion engines.

In the 1920s Graham Edgar found out that engine knocking stopped when 2,2,4-Trimethylpentane was added to gasoline. After this discovery he developed the octane-rating scale in 1927. The RON testing method was first published in 1932. 2,2,4-Trimethylpentane which has a very high level of knock resistance and n-heptane which has a very low level of knock resistance where chosen as reference fuels and assigned octane numbers of 100 and 0, respectively.

Both fuels have a certain performance in a test engine and the octane rating of every other fuel is defined by a comparison with a mixture of 2,2,4-Trimethylpentane and n-heptane with the same knocking resistance as the tested fuel. The octane rating of the tested fuel equates the percentage by volume of 2,2,4-trimethylpentane in that mixture. [26]

High octane numbers are crucial for high compression rates in internal combustion engines to provide optimum energy efficiency. The two main measurement methods used are called RON and MON.

Research octane number (RON):
- Definition of knocking performance at low and medium speeds ("acceleration knocking")
- according to EN 25164, ASTM D 2699 (600 rpm, no prewarming of the mixture, constant ignition timing).

Motor octane number (MON):
- Definition of knocking perfomance at high speeds and loads ("High speed knocking")
- according to the EN 25163, ASTM D 2700 (900 rpm, prewarming of the mixture to 150 °C, and variable ignition timing).

Generally the MON is lower than the RON, the difference between the two indexes is called sensitvity. [5]

Gas stations in Europe generally use the RON to describe the knocking behaviour of their fuels. In other countries including the United States and Canada the anti knock Index (AKI) is used which is the average of the RON and MON.
(AKI = (RON + MON) / 2)

1.2. Counterflow Configuration

To carry out the autoignition and extinciton experiments of the tested fuels a counterflow configuration is used. Combustion in a counterflow burner is different than that in conventional internal combustion engines (gasoline and diesel) where the fuel is burnt discontinously in a cylinder under varying pressure levels. In some types of the internal combustion engines (gasoline, HCCI) furthermore the reactants (fuel) and the oxidizer (air) are already premixed.
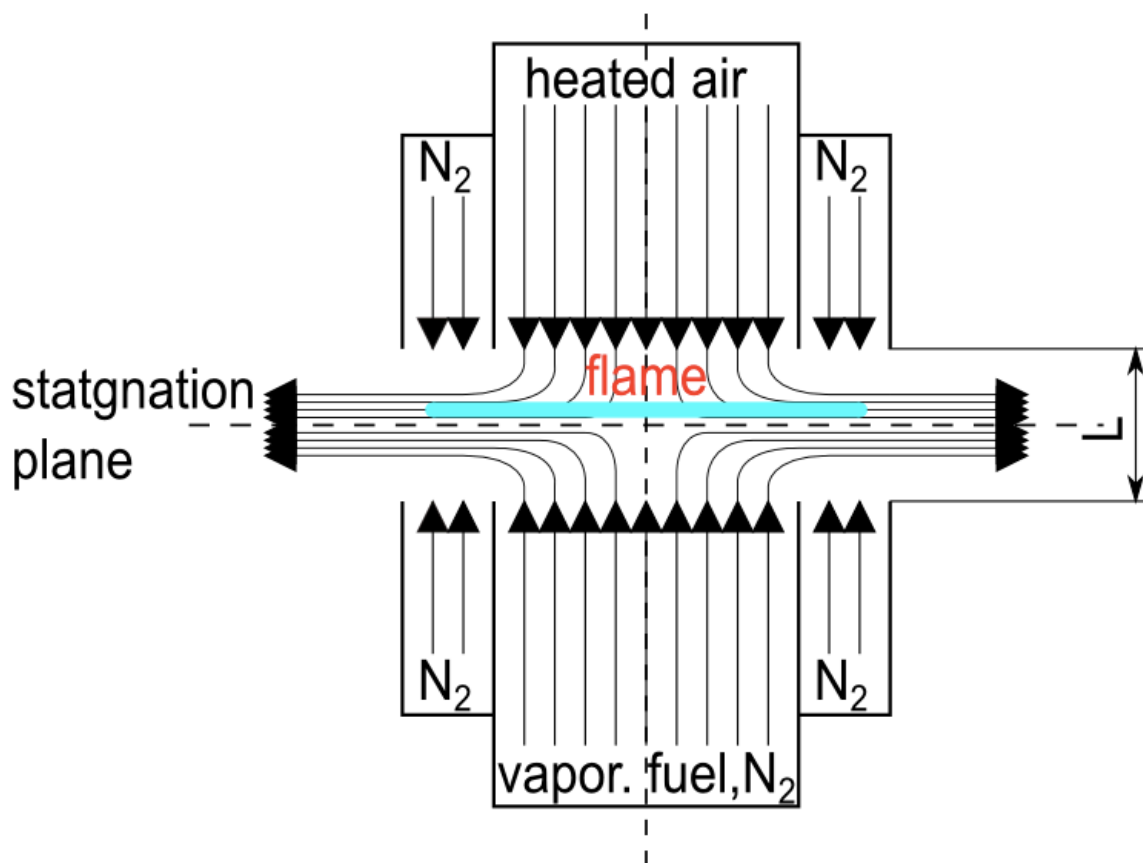

Figure 1.2: schematic illustration of the counterflow configuration in order to create a diffusion flame with non premixed flows

Figure 1.1 shows a schematic illustration of the counterflow configuration that is used to carry out the autoignition and extinction experiments. The experimental apparatus consists of two ducts which are arranged opposite to each other. The distance between the two ducts can be changed. From each duct leaves a laminar flow which stagnates against the flow of the opposed duct and together they create a special flow field and a stagnation plane. The lower duct is called fuel duct and is indicated by index 1, the upper duct is called oxidizer duct and indicated by index 2. The exits of the two ducts are called fuel and oxidizer boundary. Both ducts are encircled by another concentric ring duct which provides a nitrogen curtain in order to shield the reaction zone from the surroundings. A detailed description of the burner is given elsewhere. [7, 21]

Experimental investigations include studies on diffusion flames and partially premixed flames.

1.2.1.   Premixed Flames

In order to create a premixed flame a premixed reactant stream of fuel, oxygen and nitrogen are injected from the fuel duct and an inert nitrogen stream is injected by the oxidizer duct. The reactants are mixed together before they enter the reaction zone. A specific characteristic of the premixed flame is that the flame propagates with an finite velocity. [7, 27]

1.2.2.   Diffusion Flames (Non-Premixed Flames)

Creating a diffusion flame on the contrary assume that the reactant and the oxidizer are separated before the they enter the reaction zone where they are mixed at the same time as the reaction takes place. Fuel together with nitrogen is injected from the fuel duct and air diluted with nitrogen is injected from the oxidizer duct. A flammable mixture is formed in a narrow region of the stagnation plane where the reaction takes place and a diffusion flame is established. The flame is always stabilized at the place of maximum energy output, thus the place of stochiometric conditions and does not propagate in contrast to the premixed flame. According to [27] the reaction zone becomes infinitesimally thin when the reaction rate is infinitely fast and the combustion zone becomes a flame sheet. The characteristics of diffusion

flames is related to the time of the chemcial reaction and the aerodynamics of the particular flow situation. [7, 27]

1.2.3. Partial Premixed Flames

A part of this thesis is concerned with investigation of structure and extinction of partially premixed DME flames. Improved knowledge of laminar partially premixed flames is extremely helpful in modelling turbulent combustion. Employing the counterflow configuration it is assumed that partially premixed combustion takes place, if one or both reactant streams of a non-premixed flame are premixed with the other reactant. Figure 1.3 shows a schematric illustration of partially premixing. A mixture of the fuel and nitrogen (N_2) or a premixed fuel-rich mixture of the fuel, oxygen (O_2) and nitrogen (N_2) is injected from the fuel side, also called fuel-rich boundary, a mixture of O_2 and N_2 or a premixed fuel-lean mixture of fuel, O_2 and N_2 is injected from the oxidizer side, also called fuel-lean boundary. The level of premixing in each stream is determined by the equivalence ratio Φ where Y_F and Y_{O2} are the mass fractions of fuel and oxygen and ν is the stochiometric mass ratio of fuel to oxygen. [22]

$$\Phi = \frac{Y_F}{\nu Y_{O_2}}$$ (1.1)
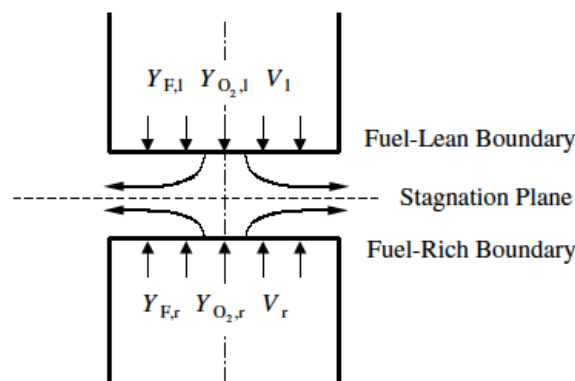
Figure 1.3: schematic illustration of counterflow configuration for partial premixed flames [22]

1.2.4. Strain Rate

To characterize the flow field in the counterflow setup the strain rate, a, is introduced. The value of the strain rate equates the normal gradient of the normal component of the flow velocity and it changes from the fuel boundary to the oxidizer boundary. It is obtained from an asymptotic theory where the Reynolds numbers of laminar flow at

the boundaries are presumed to be large. The strain rate used to characterize the flow field is the characteristic strain rate of the oxidizer stream at the stagnation plane and it is given by. [7, 11, 24]

$$a_2 = \frac{2|V_2|}{L}\left(1 + \frac{|V_1|\sqrt{\rho_1}}{|V_2|\sqrt{\rho_2}}\right)$$
(1.2)

Index 1 indicates the fuel side and index 2 indicates the oxidizer side. L is the distance between the screens of the ducts and V_1, V_2, ρ_1, ρ_2 are the velocities and densities of the fuel and the oxidizer side normal to the stagnation plane. Equation 1.2 is reduced to following simplification using the momentum balance and assuming equal duct diameters.

$$a_2 = \frac{4V_2}{L}$$
(1.3)

Now the velocity of the oxidizer stream can be calculated with an given oxidizer strain rate using equation (1.3).

1.3. Autoignition and Extinction

Autoignition and Extinction are the burning limits which are investigated in this thesis. By calculating the maximum temperature in a reactive flow field the characeristic S-shaped curve, shown in figure 1.4 can be obtained as a solution where the maximum temperature T_{max} is shown as function of the strain rate [29]. The curve consists of a stable upper, an unstable middle and a stable lower branch, describing three different solutions. The upper branch describes the temperature of the burning flame, the lower branch describes the temperature of the reactans before ignition and the middle branch is physically unstable. For better understanding what is happening at each branch the knowledge of the Damköhler number, Da, is helpful. The Damköhler number is the ratio of the characteristic time of convection and diffusion t_m (residence time) to the characteristic chemical reaction time t_c of combustion.

$$Da = \frac{t_m}{t_c}$$
(1.4)

Fast chemical reactions show high Damköhler numbers, slow chemical recations show small Damköhler numbers. Diffusion flames show very high Damköhler numbers as the time for transport and mixing the reactants t_m is large.

At the lower branch the flow is considered as frozen and no important chemical reactions are taking place. Decreasing the strain rate only leads to a slight increase of the maximum temperature but the Damköhler number increases because of a rise in residence time of the reactants and at a certain point the mixture autoignites. The temperature immediately jumps to the upper branch, which describes the temperature of an established flame. Another way to achieve autoignition is to increase the temperature at a constant strain rate.

Considering the upper branch an established flame can be extinguished by increasing the strain rate. At higher strain rates the residential time of the reactants in the mixing layer decreases and the maximum temperatures decreases until a certain point, where extinction occurs and the temperature is jumping down to the lower branch.

The middle branch is physically unstable and therefore no flames can be observed. [7]
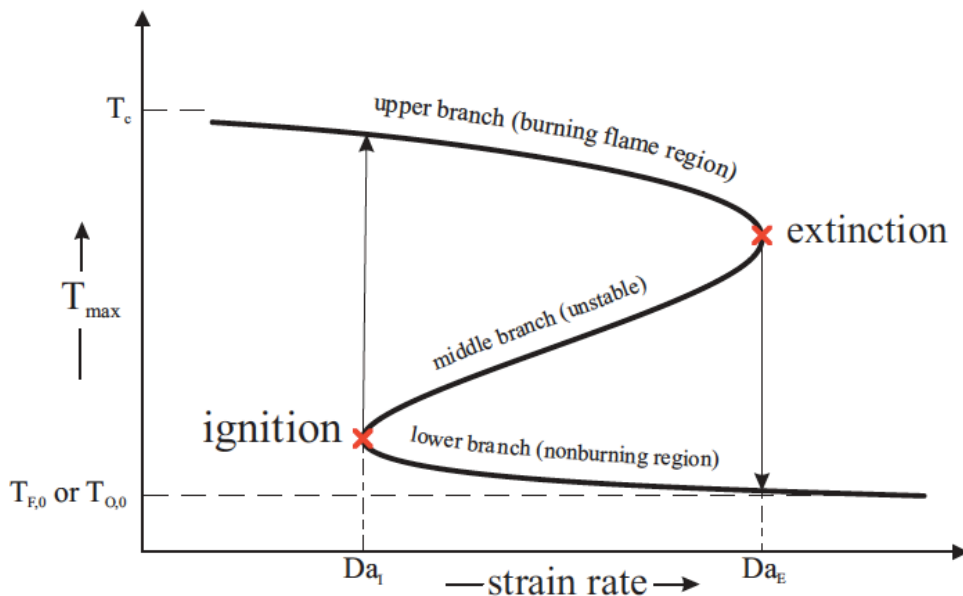

Figure 1.4: S-Shaped Curve for calculating maximum temperature in the reacting flow field [7]

1.4. Arrhenius Equation

To describe the temperature dependency of the reaction rate in diuffusion flames a common form is to use the Arrhenius eqation. The reaction rate constant k is given by

$$k = A * e^{\frac{-E}{R^0 T}} \qquad (1.5)$$

where R^0 [J/molK] is the universal gas constant, E [J/mol] represents the activation energy, A [1/s] represents the frequency factor of the reaction step and T [K] is the local temperature. In Equation 1.5 the activation Energy E is constant but A can be dependent on the temperature as shown in equation 1.6 where the pre-exponential factor B [1/K] and the temperature exponent α [ ] are constant and T [K] represents again the local absolute temperature.

$$A = BT^\alpha \qquad (1.6)$$

The activation energy E can be imagined as an energy barrier that needs to be overbeard to start the raction as shown in figure 1.5 which shows the chemical bond energy for a whole chemical reaction. The activated complex during the reaction has an higher chemical bond energy as the reactants at the beginning. By decomposing the activated complex to the products beside the activation energy also the heat of reaction is released. $E \geq 0$ for exothermic reactions and $E \geq \Delta H$ for endothermic reactions. ($-\Delta H \equiv$ heat of reaction) The heat of reaction ist the maximum theoretical energy that can be generated by an exothermic reaction. [29]
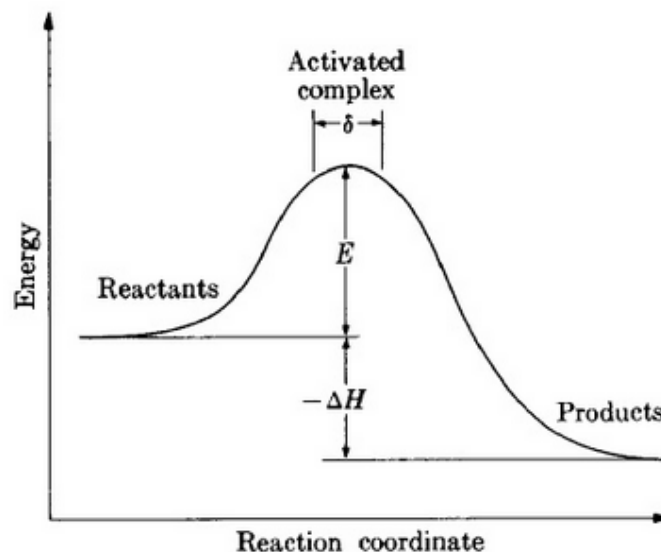

Figure 1.5: Schematic illustration of potential-energy surface [29]

2.   Experimental Setup

The experimental setup shown in figure 2.1 consists of the counterflow burner, the piping, air-, N_2- and fuel supply as well as a vaporizer for vaporizing the liquid fuel. Gaseous and liquid fuel flows are controlled by mass flow controllers and the syringe pump. The burner itself consists of an upper and and lower part that are both exchangeable in order to run different types of experiments including autoignition and extinction.
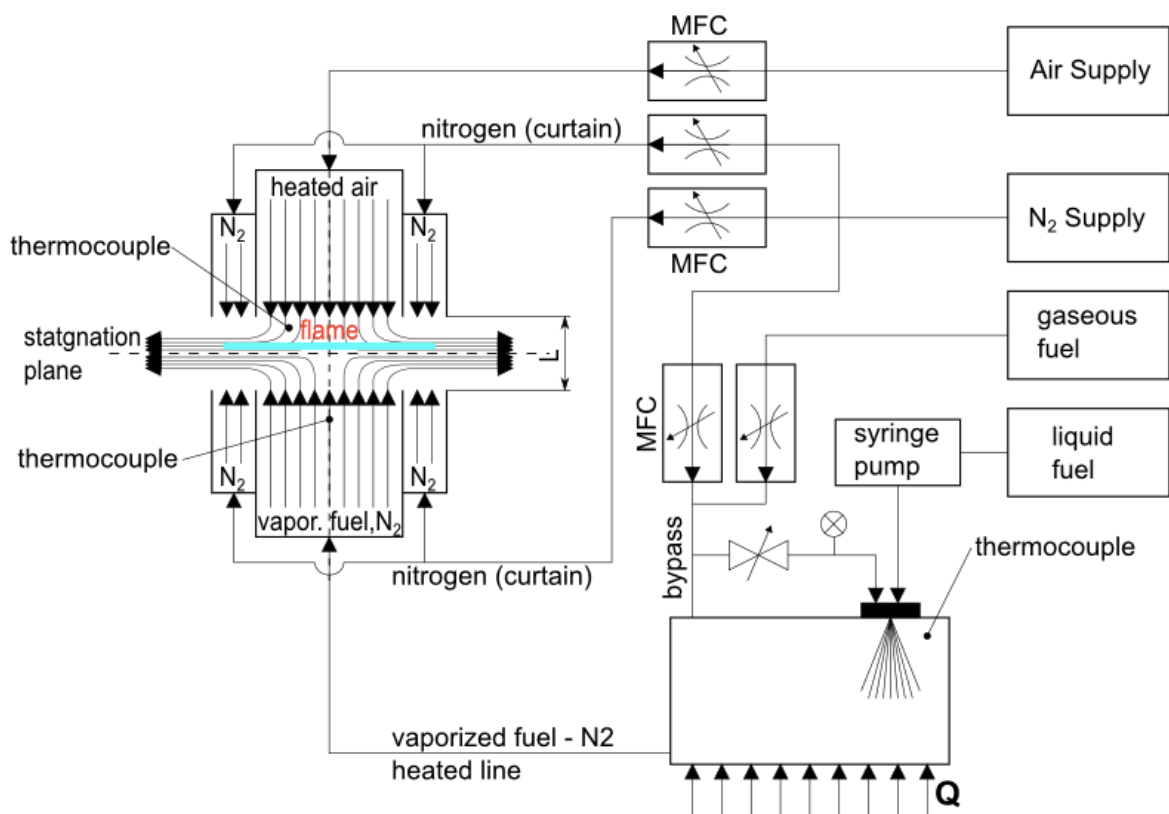

Figure 2.1: Schematic illustration of the experimental setup. The figure shows the counterflow burner as well as the fuel and gas supply including vaporizer and syringe pump.

2.1. Lower Part of the Burner

The main purpose of the lower part of the burner is to direct the fuel stream towards the reactive flow field. It mainly consists of two concentric ducts. The center duct is called fuel duct and responsible for the fuel supply. It´s surrounded by the annular curtain duct that provides a nitrogen curtain to shield the reaction zone from the environment. The exhaust gases are removed into the outlying exhaust with a moderate vacuum of the building exhaust system. The hot exhaust gases are cooled with the help of injecting through six water spray nozzles to ensure that no further reactions are taking place as shown in Figure 2.2.

Three screens out of stainless steel with a mesh of 200 lines per inch are placed at the end of the fuel duct to ensure a uniform velocity profile (plug flow profile) and to prevent flashback. The screens are mounted with the help of four steel clips which reduce the effective diameter of the fuel stream to 23 mm.
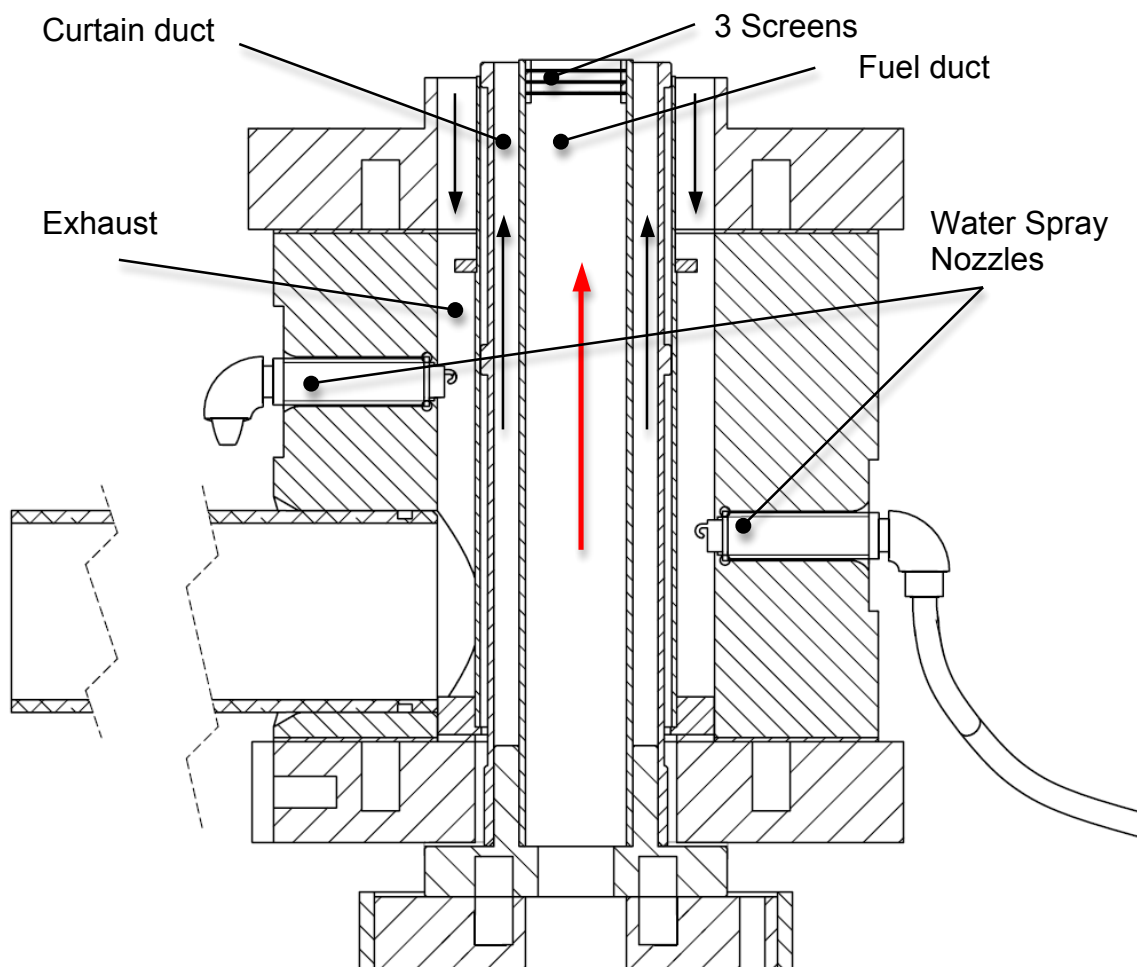
Figure 2.2: Section View of the lower part of the burner

2.2. Upper Part of the Burner

Depending on which experiments are carried out different upper parts, also called oxidizer tops are used in this work. The interchangeable tops are connected to the lower part of the burner with three adjustable pins that also determine the desired distance between the oxidizer and the fuel duct.
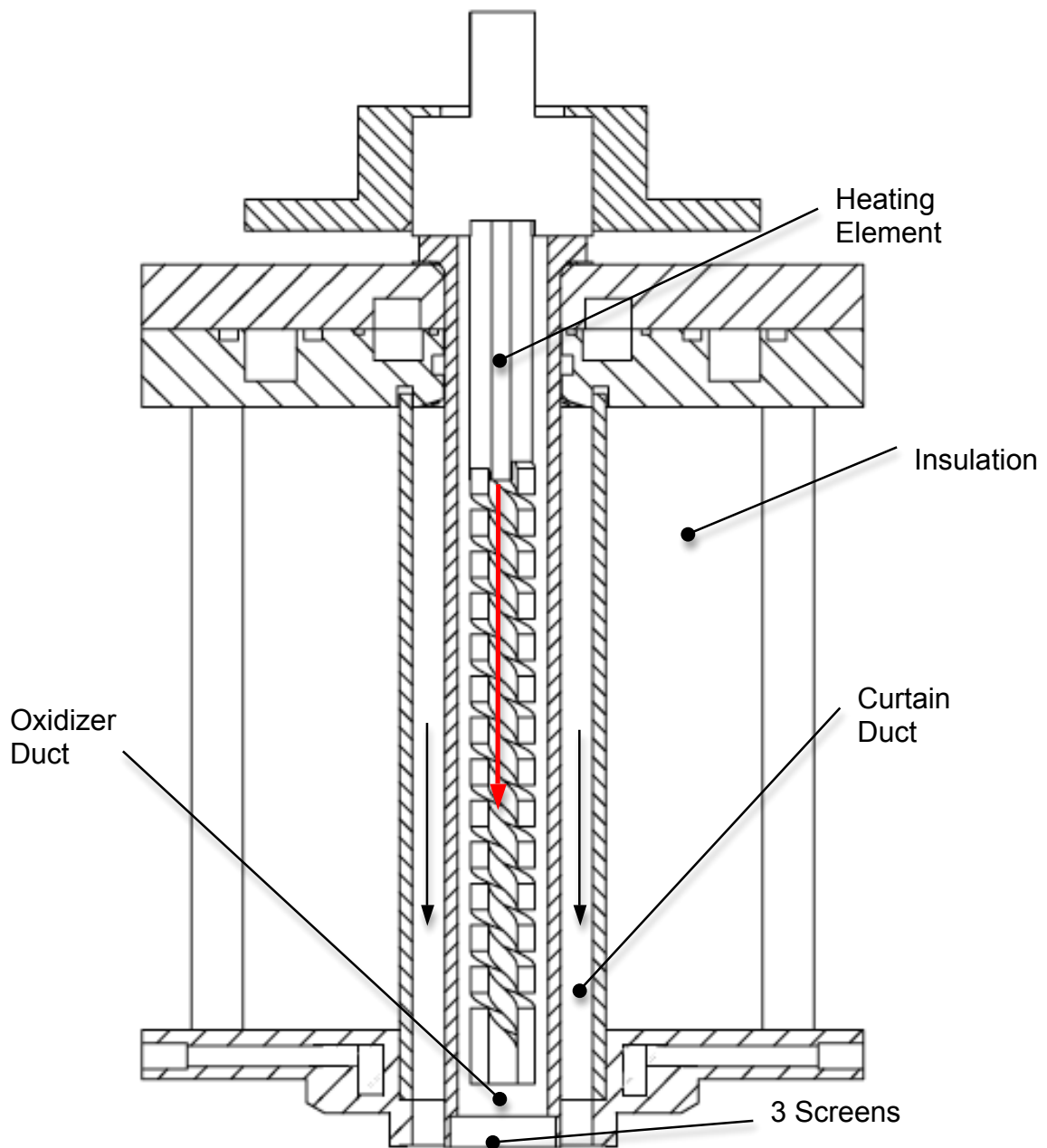
2.2.1. Autoignition Top

Figure 2.3: Section View of the autoignition top

The main task of the autoignition top is to heat up the oxidizer stream to the autoignition temperature of the fuel-air mixture and lead it to the reactive flow field. To reach these high temperatures a powerful heating element is placed in the center of the oxidizer duct which is made out of quartz to withstand the high temperatures. The heating element and the quartz tube have to be aligned very precisely to guarantee circular symmetric heating which is crucial for the appearance of autoignition in the middle of the flame zone. Due to the high temperatures in the autoignition top (> 2000 K) also the surrounding concentric curtain duct is made out of quartz and all surrounding metal parts of the quartz are constantly cooled by water. Various layers of Insulfac ® alkaline earth silicate fiber blanket insulation material around the curtain duct are used to reduce heat losses.

Just as in the lower part of the burner three screens at the end of the oxidizer duct are used to ensure again uniform velocity profile (plug flow profile) and prevent flashback. Due to the high temperatures in the autoignition top the screens are made out of Inconel 600 to withstand the high temperatures. Inconel clips are used for mounting and prevent the screens from falling out of the oxidizer duct. The effective diameter of the oxidzer stream is 23 mm. For autoigntion the distance between the screens of fuel and oxidizer duct is L = 14,5 mm.
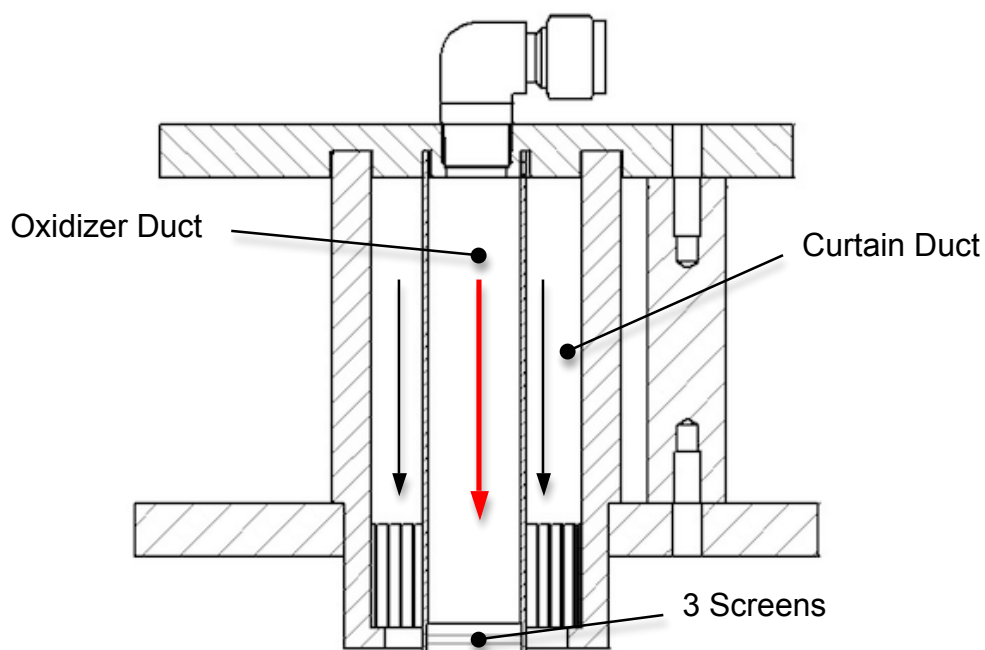
2.2.2. Extinction Top

Figure 2.4: Section View of the extinction top

The main purpose of the extinction top is to direct the oxidizer stream towards the reactive flow field. It mainly consists of two concentring ducts that separate oxidizer gas and curtain gas. The same screens and clips as in the lower part of the burner are used to ensure a uniform velocity profile and prevent flashbacks of the flame. No heating and cooling is necessary. For extinction the distance between the last screens of the fuel and oxidizer duct is L = 12,5 mm. A section view of the Extinction top is shown in Figure 2.4.

2.3. Gas and Fuel Supply

For the carried out experiments in this thesis all reactants have to be gaseous. nitrogen and DME are supplied from high pressure gas bottles, air is injected from an in-house system. Pressure reducing valves provide a stable supply pressure. The liquid fuel iso-octane is supplied with a syringe pump and gets vaporized before entering the fuel duct. (Figure 2.5)
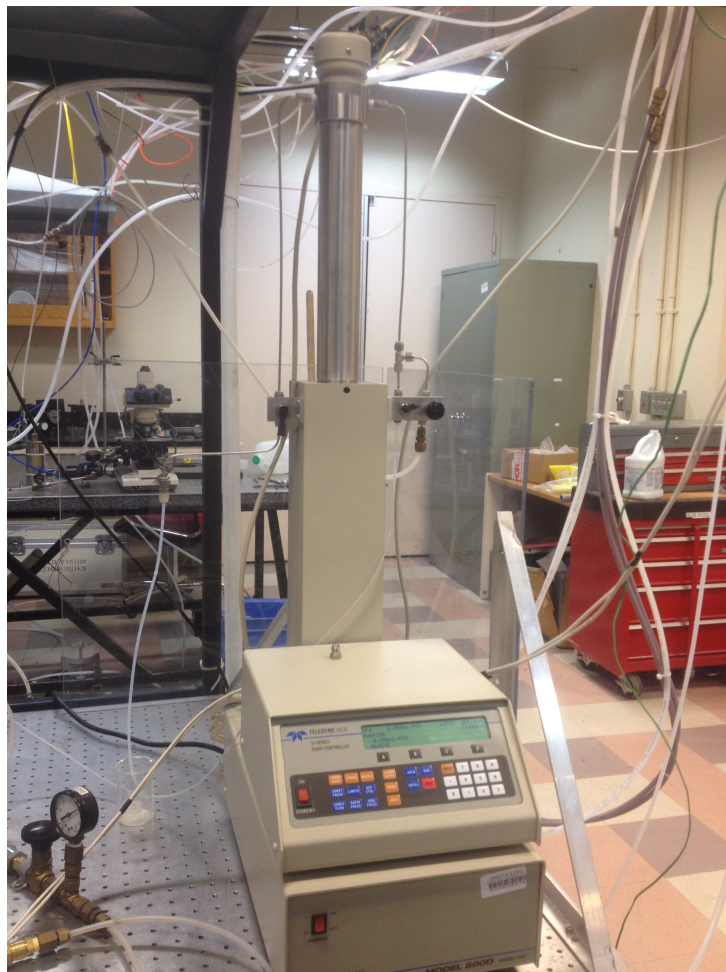

Figure 2.5: A Teledyne Hastings 500D Syringe pump is used to provide flow control of liquid fuels to a vaporizer

2.3.1. Vaporizer

The vaporizer is situated between the fuel duct and the fuel supply and ensures a steady vaporized supply of a fuel/nitrogen mixture to the lower part of the burner. Nitrogen and DME are supplied gaseous anyway but iso-octane and many other fuels are liquid under normal conditions and have to be vaporized before entering the fuel duct.

The main part of the vaporizer is a heated aluminium box where a nozzle injects liquid fuel together with gaseous nitrogen. The nozzle vaporizes the liquid fuel and nitrogen is used as carrier gas. To ensure proper vaporization and a constant, steady flow, the nozzle is installed into a cooling plate to avoid vaporization of the liquid fuel in the nozzle or the tubing which would influence the constant flow. During the experiment an aluminium box is held at a constant temperature above the boiling point of the liquid fuel to make sure that no condensation of the liquid fuel occurs. The bottom is heated by a heating plate, the entire vaporizer as well as the tubings to the burner are insulated and heated with a heating tape, all controlled by an auto-transformer.

2.4. LabVIEW Controlling Software

Controlling the gaseous and liquid flow and the corresponding mass fractions in the experimental site is crucial for combustion experiments. For the carried out experiments in this thesis a LabVIEW software was used which controls all input and output parameters. LabVIEW (Laboratory Virtual Instrument Engineering Workbench) is a graphical programming language from National Instruments. The created LabVIEW software is able to control up to five gaseous reactans and an additional liquid reactant in each stream. It was improved recently and is now also capable to avoid human errors as it displays standard errors like too high strain rates when the maximum of a gasflow of a mass flow controller is reached. The program was also adapted to high pressure experiments and includes now an procedure to calibrate the mass flow controllers. As several parameters change very quickly during the experiments all the data processed is recalculated and refreshed every two seconds.
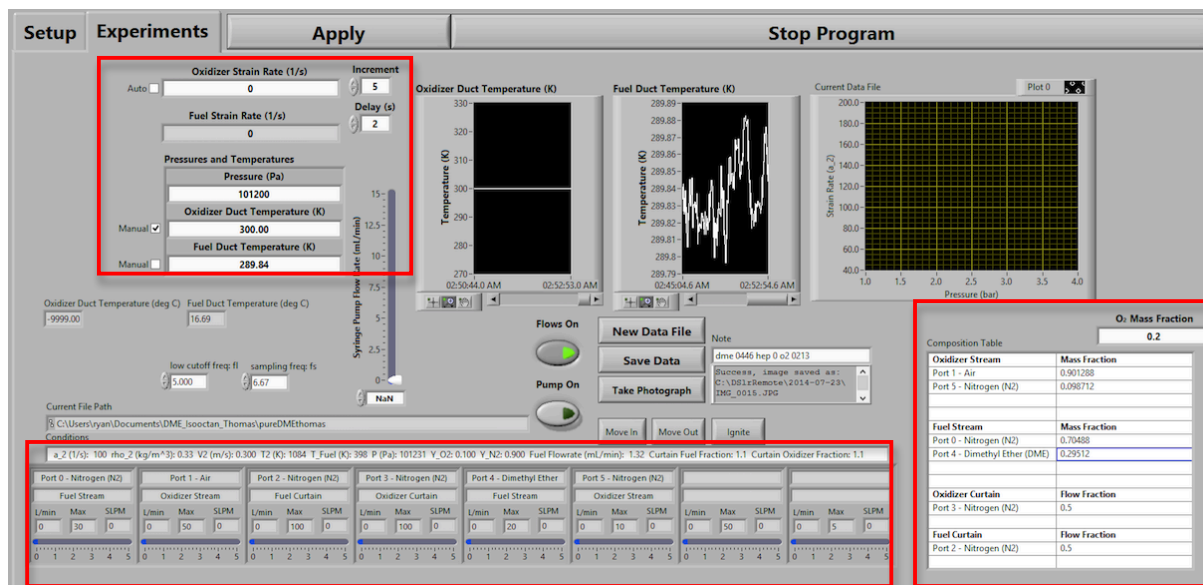
Figure 2.6: Control experiment screen of the counterflow control software. User can control reactant mass fractions, gaseous and liquid flow rates, temperatures and data saving routines.

Figure 2.6 shows the main control screen for the carried out experiments of the LabVIEW software. On the lower right the user can choose the desired reactant mass fractions of the oxidizer and the fuel stream. On the plane on the lower left the user can control the actual gas flow rates of the used mass flow controllers.

The main conrol unit is the plan on the upper left side where the user can change the oxidizer strain rate manually. To change the oxidizer strain rate and the reactant mass fractions the „Apply"- Button has to be pressed.

The screen also shows two temperature charts which show the oxidizer and fuel duct temperature. By pressing the „Save Data" Button the current data is saved in a text file including informations about strain rates, flow rates, velocities, mass fractions, mole fractions, temperatures, densities of the fuel and oxidizer stream.

Figure 2.7 shows the main setup control screen. The user can assign the desired massflow controllers to each port and select the used ports for fuel and oxidizer stream as well as for the curtains.

At the bottom the user can choose the desired compuation in the background by choosing autoignition or extinction depending on the carried out experiment.

Each port can be calibrated separately by pressing the calibration button. All changes of the setup can be applied by pressing the "Apply" button.
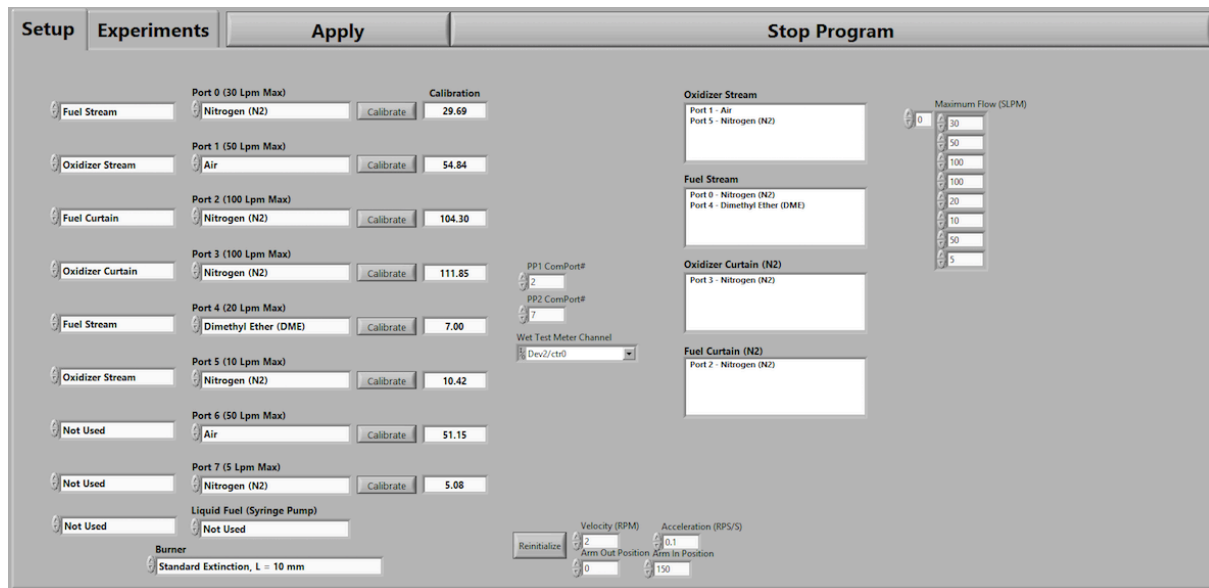
Figure 2.7: Control Setup screen of the counterflow control software. From this screen user can select the computation programme for the desired experiments, set up all ports and start the calibration procedure of the mass flow controllers.

2.4.1. Fixed Parameters

Certain input parameters are supposed to stay constant during the experiments.

- Distance L between Oxidizer and Fuel Duct, by setting the software to „Autoignition" or „Extinction" the distance is automatically set
- Pressure is set to 101200 Pa as experiments are carried out under atmospheric pressure
- Density of the liquid fuel at a temperature of 296 K for calculating the flow rate of the syringe pump
- The areas of the duct exits $A_1 = A_2$ and the areas of the curtain exits $A_{CURT,1} = A_{CURT,2}$

2.4.2. Calculated Parameters

As in this thesis different kind of experiments are carried out we have to distinguish two cases:

- Case 1: Autoigntion and Extinction of DME/Isooctane Fuel mixtures
- Case 2: Extinction of partial premixed DME flames

2.4.3. Autoignition and Extinction of DME/Iso-Octane Fuel Mixtures

According to the carried out experiments the fuel and air mass fractions are set. The range of the fuel fractions are limited by the maximum flow rates of the chosen mass flow controllers and the temperatures in the fuel and oxidizer duct. With the following formulas the N_2 mass fractions of the fuel and oxidizer stream can be calculated.

$$Y_{N_2,1} = 1 - Y_{DME,1} - Y_{ISO,1} \qquad (2.1)$$

$$Y_{N_2,2} = 1 - Y_{AIR,2} \qquad (2.2)$$

The mole fractions of the fuel and oxidizer stream can be calculated then with equations 2.3 and 2.4, where the indexes ISO, DME, N_2 and AIR are used for iso-octane, dimethyl ether, nitrogen and air. M_i is the molecular weight of the relevant element.

$$X_{i,1} = \frac{\dfrac{Y_{i,1}}{M_{i,1}}}{\displaystyle\sum_{ISO,DME,N_2} \dfrac{Y_{i,1}}{M_{i,1}}} \qquad (2.3)$$

$$X_{i,2} = \frac{\dfrac{Y_{i,2}}{M_{i,2}}}{\displaystyle\sum_{AIR,N_2} \dfrac{Y_{i,2}}{M_{i,2}}} \qquad (2.4)$$

The densities of the fuel and oxidizer stream can be calculated with the help of the ideal gas equation where T_1 is the temperature of the fuel duct and T_2 is the temperature of the oxidizer duct. In all carried out experiment T_2 is set at 296 K as the oxidizer stream is not preheated and T_1 is measured with an thermocouple that is located at the end of the fuel duct below the first screen. R = 8,314 [J/molK] is the ideal gas constant and p the ambient pressure.

$$\rho_1 = \frac{p\displaystyle\sum_{i=ISO,DME,N_2} X_{i,1}M_{i,1}}{RT_1} \qquad (2.5)$$

$$\rho_2 = \frac{p\displaystyle\sum_{i=AIR,N_2} X_{i,2}M_{i,2}}{RT_2} \qquad (2.6)$$

2.4.4. Extinction of Partial Premixed DME Flames

For the extinction experiements of partial premixed DME flames the LabVIEW code was adapted to set all fuel, air and N_2 mass fractions manually. The mole fractions and the densities of the fuel and air stream are calculated using following equations.

$$X_{i,1} = \frac{\frac{Y_{i,1}}{M_{i,1}}}{\sum_{DME,AIR,N_2} \frac{Y_{i,1}}{M_{i,1}}} \tag{2.7}$$

$$X_{i,2} = \frac{\frac{Y_{i,2}}{M_{i,2}}}{\sum_{AIR,DME,N_2} \frac{Y_{i,2}}{M_{i,2}}} \tag{2.8}$$

$$\rho_1 = \frac{p \sum_{i=DME,AIR,N_2} X_{i,1} M_{i,1}}{RT_1} \tag{2.9}$$

$$\rho_2 = \frac{p \sum_{i=AIR,DME,N_2} X_{i,2} M_{i,2}}{RT_2} \tag{2.10}$$

As the velocity of the oxidizer stream is known by setting the value of the oxidizer strain rate a_2 the velocity of the fuel stream is calculated by introducing the momentum balance.

$$V_1 = \frac{V_2}{\sqrt{\frac{\rho_1}{\rho_2}}} \tag{2.11}$$

The flow rates of the fuel and the oxidizer stream can now be calculated and an appropriate mass flow controller can be chosen employing the following equations.

$$\dot{V}_{N_2,1} = X_{N_2,1} V_1 A_1 \tag{2.12}$$

$$\dot{V}_{DME,1} = X_{DME,1} V_1 A_1 \tag{2.13}$$

$$\dot{V}_{ISO,1} = X_{ISO,1} V_1 A_1 \qquad \text{(only case 1)} \tag{2.14}$$

$$\dot{V}_{AIR,1} = X_{AIR,1} V_1 A_1 \qquad \text{(only case 2)} \tag{2.15}$$

$$\dot{V}_{N_2,2} = X_{N_2,2}V_2A_2 \tag{2.16}$$

$$\dot{V}_{AIR,2} = X_{AIR,2}V_2A_2 \tag{2.17}$$

$$\dot{V}_{DME,2} = X_{DME,2}V_2A_2 \quad \text{(only case 2)} \tag{2.18}$$

Since the curtain flows should be adjusted to the fuel and oxidizer stream the relative curtain velocities $\upsilon_{REL,1}$ and $\upsilon_{REL,2}$ are introduced with the result that the flow rate of the curtains increase and decrease in direct proportion as the fuel and oxidizer stream. For all experiments $\upsilon_{REL,1}$ and $\upsilon_{REL,2}$ are set at 0,5 [ ].

$$\dot{V}_{CURT,1} = \upsilon_{REL,1}V_1A_1 \tag{2.19}$$

$$\dot{V}_{CURT,2} = \upsilon_{REL,2}V_2A_2 \tag{2.20}$$

The ideal gas equation is used to output the volume fluxes in standard liter per minute using the values of standard conditions.

$$\dot{V}_{SLM,i,j} = \dot{V}_{i,j}\frac{273,15K}{T_{i,j}} \tag{2.21}$$

2.5. Controlling Units

2.5.1. Mass Flow Controller

Mass flow controllers (MFC) use the density of gases to calculate familiar volumetric units out of mass units. The measurements are carried out in mass units, converted into standard liter per minute and are independent from pressure and temperature changes. In the experimental apparatus several Teledyne Hastings mass flow controllers of different ranges (1 to 100 standard liter per minute) and types (HFC-303 and HFC-302) are used to control the massflow. The massflow controllers are connected to the controlling LabVIEW software and are powered and controlled by two Teledyne Power Pod 400 modules. The power pods convert the signal of the controlling software to analog signals for the mass flow controllers and provide voltage for the MFCs that is linear to the mass flow rate.

To ensure accurate mass flow control calibration of the mass flow controllers is crucial. The mass flow controllers are calibrated by determining the maximum flow rate. As mass flow controllers are most accurate when carefully calibrated near the range at which they will be used the expected flows are set in the flow control program and the flow is piped in a calibration unit. As calibration unit a Ritter TG5/5-ER wet test meter with a flow range of 0.167 l/min to 33,3 l/min is used. The measurement principle of the wet test meter is positive displacement. The drum is leveled and packed with a fluid and the gas flow through the meter causes a rotation of the drum. The drum measures the gas flow by periodically filling and emptying the rigid measuring chambers. With the measurements the maximum flow rate is calculated. The process is repeated as often until the derivation of the maximum flow rate is less than 1% of the maxiumum flow rate of the previous calibration. [19]

2.5.2. Temperature Measurement

Temperature is measured at different locations and the condition in each location has different requirements. For the temperature measurements different types of thermocouples are used. A thermocouple consists of two dissimilar metal conductors that are connected at one end by a bead. The bead is postioned at the point of temperature measurement and a change of the voltage can be measured when the temperature of the bead is changing. A function in the background calculates the temperature difference out of the voltage change.

For the measurement of the autoignition temperature (T_2) below the screen of the oxidizer duct a type R thermocouple (platinum-13%rhodium vs. Platinum) is used. It is mounted on a 3-axle rack to be positioned 1 mm below the last screen of the oxidizer duct of the autoignition top.

To ensure proper vaporization in the fuel duct type E thermocouples (nickel-chromium vs. copper-nickel) are used to measure the temperature in the Vaporizer and at the end of the fuel duct (T_1).

To control the fuel duct temprature two type E thermoucouples are positioned at the end of the fuel duct (3 mm below the first screen), one is connected together with the heating tape with a proportional integral derivative (PID) control, the other one to the computer and the LabVIEW system control. Two more type E thermocouples are positioned inside the vaporizer, where the temperature can set manually and another PID is conrolling the heated bottom and the heating tape covering the vaporizer.

2.5.3. Exhaust System

A slight vacuum is used to remove the combustion gases from the combustion zone without influencing the flame. The lower part of the burner is connected to the in-house exhaust system of the building which provides the vaccum through the exhaust duct. To ensure that no further reactions are taking place, the combustion gases are cooled by six water spray nozzles. Water is separated from the lighter fuel components in a vertical tube.

3. Experiments

3.1. Autoignition

3.1.1. Experimental Procedure and Preparation

For the autoignition experiments the autoignition top has to be aligned and mounted concentrically to the lower part of the burner. On the basis of recent investigations on accuracies of laminar counterflow experiments [11] the distance between the last screens of the two ducts is set to L = 14,5 mm for autoignition experiments at working temperature. (ca. 1100 K)

For all experiments the fuel fraction in the fuel stream $Y_{F,1}$ is held constant at 0,4 with varying amounts of iso-octane and DME. The oxidizer stream is pure air with an O_2 mass fraction $Y_{O2,1}$ = 0,233 and ambient pressure. The fuel stream is preheated to approximately T_2 = 385 K to ensure the vaporization of iso-octane.

After the cooling water is turned on and the burner is provided with air and nitrogen to establish a flow field the autoigntion top can be heated up. It´s important to heat up the apparatus very slowly as the high temperatures could cause thermal stresses otherwise. The temperature is steadily increased until autoignition occurs. After autoignition the established flame is blown out and the oxidizer temperature is lowered down a bit. The procedure is repeated a second time to ensure accurate results.

The described procedure is carried out for different fuel compositions of DME and iso-octane at five different strain rates between 80 s^{-1} and 250 s^{-1}.

In addition a highspeed camera is set up to record autoignition visually. Figure 3.1 shows snapshots of autoignition of a 80%DME/20% iso-octane fuel mixture at an oxidizer strain rate a_2 = 166 s^{-1}. The first three pictures show a blue flame right at the beginning of the autoignition process. The time interval between this pictures is just two miliseconds. The fourth picture shows the established blue flame in comparison.
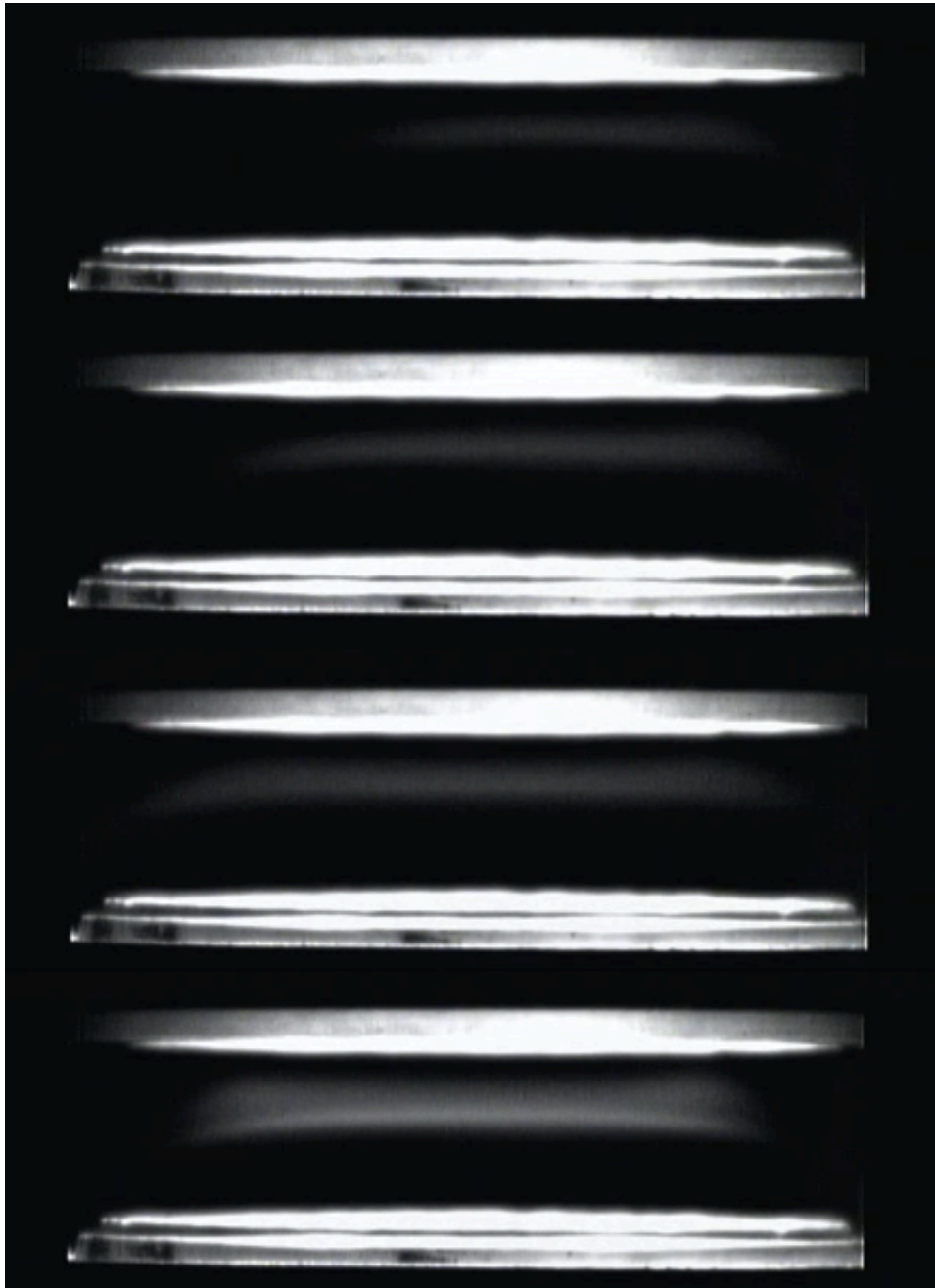
Figure 3.1: Snapshots of autoigntion of a fuel mixture with $Y_{DME,1}$ = 0,32 and $Y_{ISO,1}$ =0.08 at an oxidizer strain rate a_2 = 166 s^{-1}. The first three pictures show a blue flame right at the beginning of the autoignition process. The fourth pictures shows an established blue flame in comparison.

3.1.2. Temperature Correction

As already mentioned in 2.5.2 a unsheated fine gage thermocouple type R of OMEGA engineering is used for temperature measuring. It consists of two different wire materials that are welded together (Pt/13%Rh-Pt). Unsheated fine gage thermocouples ensure fast response and the chosen type R can be used at temperatures up to 1450°C. According to the manufacturer the error limits are 1,5 °C respectively 0,25%. [14] The wires of the thermocouples have a diameter of

0,076 mm and the bead diameter of the connecting welding is 0,3048 mm. The thermocouple wires are welded to two additional lead wires which are seperately routed through a ceramic tube with two holes to avoid shortcircuiting. The thermocouple wires and the lead wires loom about 2 cm out of the ceramic tube to avoid thermal losses.

The thermocouple is integrated on a two-dimensional moveable mounting to guarantee repeatable, proper positioning. The actual measuring point, the bead and respectively the thermocouple wires have to be positioned horizontally in the gas flow to obtain accurate measurements of the gas flow temperature by preventing heat conduction. The bead of the thermocouple is positioned about 1 mm below the last screen of the oxidizer duct at a third of the duct diameter, where the highest temperatures can be measured according to a previous measured temperature profile over the duct diameter. [7]

To determine accurate autoignition temperatures it´s crucial to completely understand all the possible heat transfer modes of the thermocouple and its environment. With the chosen measuring setup surface induced catalytic reactions, conduction along the thermocouple wires, convection between the thermocouple and the gases and radiation losses as shown in figure 3.2 have to be considered and the initially measured temperature has to be corrected. [25]
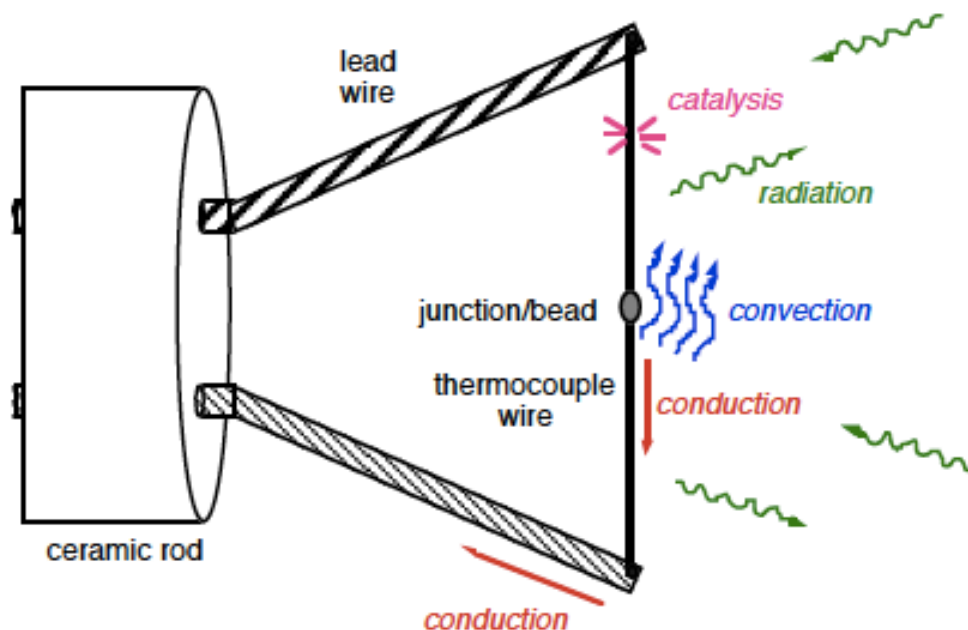

Figure 3.2: Heat transfer modes associated to the thermocouple for combustion system measurements [25]

Equation 3.1 summarizes the thermocouple associated heat transfer modes as result of an energy balance of the thermocouple.

$$\dot{Q}_{CAT} + \dot{Q}_{CONV} + \dot{Q}_{RAD} + \dot{Q}_{COND} = \rho c_p V \frac{dT_{TC}}{dt} \tag{3.1}$$

Equation 3.1 can be simplified in practice as conduction along the thermocouple is avoidable if the thermocouple length/diameter ratio is large enough (>200). Conduction losses are neglected because the wires are placed along an isoterm. Catalytic effects are neglected because no chemical reactions are taking place at the exit of the duct. [25]

To determine the radiation asscociated to the thermocouple all surroundings are treated as hypothetical black surfaces. This assumption can be made as the dimensions of the thermocouple wires are a lot smaller than the dimensions of the surroundings. Even if the surroundings reflect some of the radiation of the thermocouple it´s much more likely that the surroundings absorb before they hit a very small point on the thermocouple surface. [8, 10]

Several assumptions are made to calculate the temperature correction according to [8]:

- Temperature of the screen is the same temperature as the temperature of the oxidizer stream ($T_{SC} = T_2$)
- Temperature of the surroundings is assumed to be T_{SUR} = *296 K*
- Thermocouple is a small plane surface compared to a large disk of the surroundings.

With this assumptions the view factors can be calculated with the help of the view factor intgral and the view factor summation rule.

$$F_{ij} = \frac{1}{A_i} \int_{A_i} \int_{A_j} \frac{\cos \Theta_i \Theta_j}{\pi R^2} dA_i dA_j \tag{3.2}$$

$$\sum_{j=1}^{N} F_{ij} = 1 \tag{3.3}$$

F_{SC} [ ] is the view factor of the screen, $F_{UpperSUR}$ [ ] is the view factor of the upper surroundings and $F_{LowerSUR}$ [ ] is the view factor of the lower surroundings. d_{SC} [m] is

the diameter of the screen and L_2 [m] is the distance between the thermocouple bead and the lowest screen.

$$F_{SC} = \frac{d_{SC}^{\,2}}{d_{SC}^{\,2} + 4L_2^{\,2}}$$

$$F_{UpperSUR} = 1 - F_{SC} \qquad\qquad (3.4)$$

$$F_{LowerSUR} = 1$$

With these approximations and a steady state measurement ($dT_{TC}/dt = 0$) as assumption a new equation for determing the real oxidizer gas temperature can be introduced by applying equation 3.1 and this equation can be solved with MATLAB.

$$\frac{Nu_{CYL}k_f}{d_W} = A_W(T_2 - T_{TC}) = \frac{A_{RAD}}{2}\sigma\varepsilon_{TH}\left[F_{SC}(T_{TC}^{\,4} - T_2^{\,4}) + (2 - F_{SC})(T_{TC}^{\,4} - T_{SUR}^{\,4})\right] \qquad (3.5)$$

A_W [m^2] is the surface of the thermocouple wire, d_W [m] is the diameter of the thermocouple wire, T_2 [K] is the oxidizer gas temperature, T_{TC} [K] is the measured temperature of the thermocouple, A_{RAD} [m^2] is the suface of both bead and thermocouple wire, σ [W/m^{2}K^4] is the Stefan-Boltzmann constant and has the value 5,67e^{-8}, T_{SUR} [K] is the temperature of the surroundings, k_f [W/mK] is the thermal conductivity of air and depending on the temperture, ε_{TH} [ ] is the emissivity of the thermocouple and is set to 0,2 according to [1]

The Nusselt number Nu_{CYL} [ ] can be calculated with

$$Nu_{CYL} = (0,24 + 0,56\,\mathrm{Re}^{0,45})(\frac{T_F}{T_2})^{0,17} \qquad\qquad (3.6)$$

where Re [ ] is the Reynolds number of air, T_F [K] the film temperature [K] which equates to the average of the thermocouple temperature T_{TC} and the gas temperature T_2. Equation 3.6 is valdid for Reynolds numbers from 0,02 up to 40. [25]

3.2. Extinction

3.2.1. Experimental Procedure and Preparation

For the extinction experiments the extinction top has to be aligned and mounted concentrically to the lower part of the burner. On the basis of recent investigations on accuracies of laminar counterflow experiments [11] the distance between the last screens of the two ducts is set to L = 12,5 mm for extinction experiments. Before starting the experiments the cooling water for the lower part of the burner has to be turned on and the both ducts have to be provided with the corresponding gaseous flows.

According to the carried out experiments it can be necessary to heat up the fuel stream to ensure proper vaporization. For the extinction experiments on DME/iso-octane fuel blends the fuel stream is preheated to approximately T_2 = 380 K to avoid condensation of the liquid fuel (iso-octane). During the experiments it was found out that the fuel stream temperature has significant influence on the values of the extinction strain rate and accurate extinction results can only be measured at relative small deviations (+/- 10 K) of the set fuel stream temperatures which requires appropriate time until the PID temperatrue control has settled into the temperature tolerances as after every calibration of the system has to be heated up again. The experiments on partial premixed DME flames don´t require preheating of the fuel stream as DME is already gaseous at atmospheric temperature.

Following experimental procedure is applied for different fuel compositions:

A flame is ignited with a blowtorch at a strain rate close to the extinction strain rate. After the flame is established the oxidizer strain a_2 rate is increased in very small steps, normally by 1 s^{-1} every 2 seconds until the flame extinguishes. This procedure is repeated at least 5 times or until the extinction rate doesn´t change significantly anymore to obtain very accurate results.

All experiments are carried out for a constant stochiometric mixture fraction Z_{st} = 0,318 and a constant adiabatic flame temperature T_{AD} = 1850 K.

3.2.2. Adiabatic Flame Temperature

The adiabatic flame temperature is that temperature that theroetically occurs at a complete combustion process without loosing any energy to the outside ennvironment (performing work, changings in kinetic or potential energy, heat transfer from or to the reaction zone) for either constant volume or pressure. This implicates an ideal combustion process where the resulting products are only water and carbon dioxide and that the enthalpy of the burnt and unburnt mixture have the same value. The adiabatic flame temperature is the maximum temperature for given reactants which can be reached during combustion because an incomplete combustion or any heat transfer of the reactants would lower the flame temperature. The adiabatic flame temperature is dependent from the initial mixture fractions, the initial temperatures of the reactants and the pressure. [7, 28]

For all carried out experiments the adiabatic flame temperature is selected to be T_{AD} = 1850 K.

3.2.3. Mixture Fraction

The mixture fraction, Z, is an extremely useful tool to describe important properties in combustion theory. Z can have a value between zero and one. In the fuel stream the mixture fraction is one and in the oxidizer stream the mixture fraction is zero.

For a stochiometric mixture where $\nu Y_F = Y_{O_2}$

$$Z_{ST} = \left(1 + \frac{\nu Y_{F,1}}{Y_{O_2,2}}\right)^{-1}$$

(3.7)

can be calculated. $Y_{F,1}$ is the mass fraction of fuel in the fuel stream, $Y_{O2,2}$ is the mass fraction of oxygen in the oxidizer stream and ν is the stochiometric oxygen to fuel mass ratio. [15]

The flamelet model of Burke Schumann developed in 1928 requires that combustion in diffusion flames takes place at the stochiometric mixture fraction. In the counterflow configuration fuel and oxygen diffuse from opposite sides into the flame area and immediately vanish. The products of the chemical reaction and the temperature reach a maximum which implicates that the characteristic chemical reaction time is assumed to be significantly smaller than the characteristic residence

times. To solve this problem mathematically it´s also assumed that the reaction takes place under infinite residence time and under complete combustion for a one-step reaction. With this underlying theory the mass fractions of the reactants and products can be showed as a function of the stochiometric mixture fraction for the burning and unburnt mixture. [15, 16]
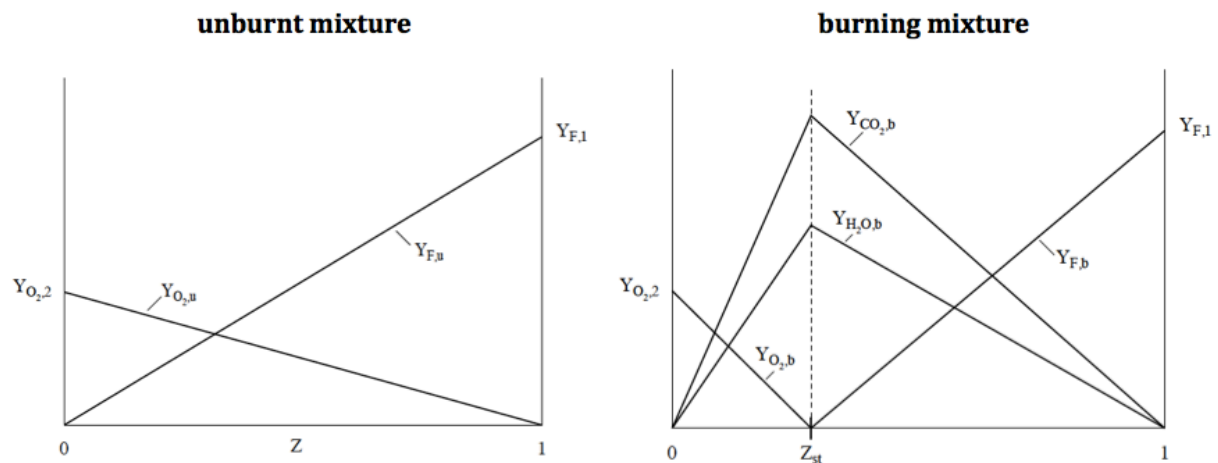

Figure 3.3: The left side shows the mass fractions of oxygen and fuel in the unburnt mixture, the right side shows the mass fractions of the reactants oxygen and fuel and the products CO_2 and H_2O in the burning mixture [15]

The left side of figure 3.3 shows the mass fractions of oxidizer and fuel as a function of the mixture fraction in the unburnt mixture before combustion. The right side of figure 3.3 shows the mass fractions of all reactants and products in the burning mixture. Z_{ST} represents the point where fuel and oxygen are mixed in stochiomtric ratio and react completely during combustion to its products water and carbon dioxide. For all carried out experiments the stochiometric mixture fraction is selected to be Z_{ST} = 0,318.

To calculate the mass fractions for oxygen and fuel in the unburnt condition Professor Seshadri developed an asymptotic formulation with fixed values for stochiometric mixture fraction Z_{ST} and adiabatic flame temperature T_{AD}. Furthermore the formulation assumes that the Damköhler numbers are high due to the assumption that reactions take place simultaneously with the mix of the fuel. In the following chapters 3.2.4 and 3.2.5 the results of this assymptotic analysis are obtained for extinction of DME/iso-octane fuel blends and extinction of partial premixed DME flames. The whole asymptotic models of both cases are attached in Appendix B.

3.2.4. Extinction of DME/Iso-Octane Fuel Mixtures

By determining x_{ST} from

$$Z_{ST} = \frac{1}{2} erfc\left(x_{ST}\sqrt{\frac{1}{2}}\right) \tag{3.8}$$

and with the chosen Lewis numbers for DME and iso-octane Le_{DME} = 1,5 and Le_{ISO} = 2 the stochiometric mixture fractions for DME ($Z_{DME,ST}$) and iso-octane ($Z_{ISO,ST}$) can be calculated.

$$Z_{ISO,ST} = \frac{1}{2} erfc\left(x_{ST}\sqrt{\frac{Le_{ISO}}{2}}\right) \tag{3.9}$$

$$Z_{DME,ST} = \frac{1}{2} erfc\left(x_{ST}\sqrt{\frac{Le_{DME}}{2}}\right) \tag{3.10}$$

The mass fraction of iso-octane $Y_{ISO,1}$ and oxygen $Y_{O2,2}$ are calculated by choosing a value for $Y_{DME,1}$ and solving equation 3.12 with the help of the following equations 3.13 – 3.17 where $X_{ISO,1}$, $X_{DME,1}$ and $X_{O2,2}$ are the mole fractions of iso-octane, DME and oxygen and W_{ISO}, W_{DME}, W_{O2} and W_{N2} are their molecular weights respectively.

$$25g + 6m = 2c \tag{3.11}$$

$$g = \frac{1}{\sqrt{Le_{ISO}}} \frac{X_{ISO,1}}{1 - Z_{ISO,ST}} \left\{ \exp\left[\frac{x_{ST}^2(1 - Le_{ISO})}{2}\right]\right\} \tag{3.12}$$

$$m = \frac{1}{\sqrt{Le_{DME}}} \frac{X_{DME,1}}{1 - Z_{DME,ST}} \left\{ \exp\left[\frac{x_{ST}^2(1 - Le_{DME})}{2}\right]\right\} \tag{3.13}$$

$$c = \frac{X_{O_2,2}}{Z_{ST}} \tag{3.14}$$

$$T_{AD} = T_U + \frac{1}{c_p W_{N_2}} \left(Q_{ISO}g + Q_{DME}\right)Z_{ST}\left(1 - Z_{ST}\right) \tag{3.15}$$

$$X_{ISO,1} = \frac{Y_{ISO,1}W_{N_2}}{W_{ISO}} \qquad X_{DME,1} = \frac{Y_{DME,1}W_{N_2}}{W_{DME}} \qquad X_{O_2,2} = \frac{Y_{O_2,2}W_{N_2}}{W_{O_2}} \tag{3.16}$$

Q_{ISO} = 50,98 10^3 [J/mole] and Q_{DME} = 13,28 10^3 [J/mole] are the heat releases of iso-octane and DME and c_p = 1300 J/kgK is the heat capacity. T_{AD} = 1850 K is the chosen adiabatic temperature and T_U = 296 K is the temperature of the environment. By iterating solving of this formulation for values of $Y_{DME,1}$ from zero to one following figures show the results of $Y_{O2,2}$ and $Y_{ISO,1}$ as function of $Y_{DME,1}$.
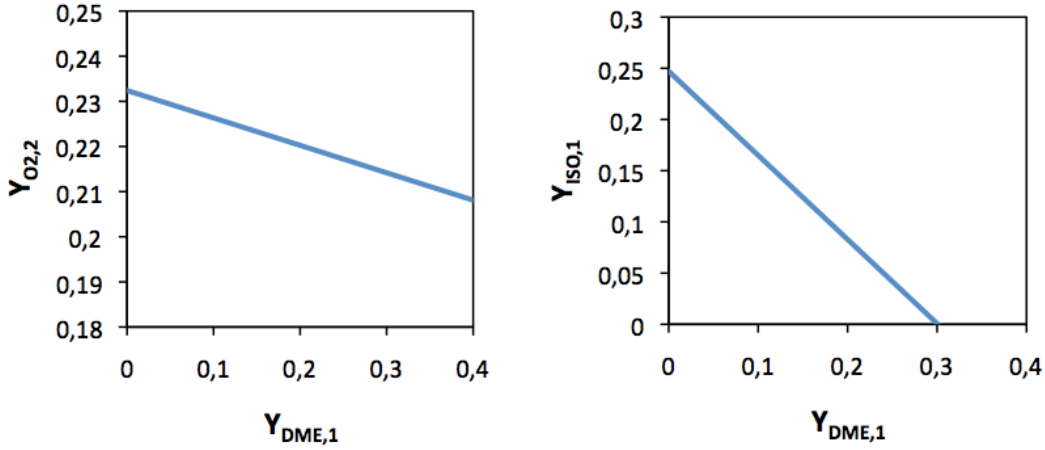
Figure 3.4: Mass fractions of oxygen $Y_{O2,2}$ and iso-octane $Y_{ISO,1}$ as result of asymptotic analysis for a fixed $Z_{ST} = 0,318$ and fixed $T_{AD} = 1850$ K as function of $Y_{DME,1}$

Table 3.1 shows the mass fractions of all reactants of the fuel and oxidizer stream for the 13 measuring points which have been selected from the results of the asymptotic analysis showed in Figure 3.4.

Table 3.1: Mass fractions of the reactants in fuel and oxidizer stream chosen for the experiment

Point	$Y_{O2,2}$ [ ]	$Y_{N2,2}$ [ ]	$Y_{DME,1}$ [ ]	$Y_{ISO,1}$ [ ]	$Y_{N2,1}$ [ ]
1	0,2324	0,7676	0,000	0,2471	0,7529
2	0,2309	0,7691	0,025	0,2266	0,7484
3	0,2294	0,7706	0,050	0,2060	0,7440
4	0,2279	0,7721	0,075	0,1855	0,7395
5	0,2263	0,7737	0,100	0,1650	0,7350
6	0,2248	0,7752	0,125	0,1444	0,7306
7	0,2233	0,7767	0,150	0,1239	0,7261
8	0,2218	0,7782	0,175	0,1034	0,7216
9	0,2203	0,7797	0,200	0,0829	0,7171
10	0,2187	0,7813	0,225	0,0623	0,7127
11	0,2172	0,7828	0,250	0,0418	0,7082
12	0,2157	0,7843	0,275	0,0213	0,7037
13	0,2142	0,7858	0,300	0,0008	0,6992

3.2.5. Extinction of Partial Premixed DME Flames

The asymptotic analysis for partial premixed DME Flames is similar to the formulation before. Calculating fuel and oxidizer mass fractions however is different and therefore the measuring variable for the level of premixing, the equivalence ratio Φ, is introduced for the fuel lean and the fuel rich side as [22] did in similar investigations on methane . The equivalence ratio Φ is defined by

$$\Phi = \frac{Y_F}{\nu Y_{O_2}} \qquad \text{and respectively} \quad \Phi^{-1} = \frac{\nu Y_{O_2}}{Y_F} \qquad (3.17)$$

where Y_F is mass fraction of fuel in one stream, Y_{O2} the mass fraction of oxygen in the same stream and v the stochiometric air-fuel ratio. In this investigation pure DME flames are investigated and there is no iso-octane involved. All DME related values are the same as in the previous experiment and Z_{ST} = 0,318 and T_{AD} = 1850 K are set at the same values as for the previous experiment on DME/iso-octane fuel blends.

The mass fractions of all reactants are calculated by three steps:

1. Calculating the mass fractions of DME and oxygen for the non premixed case
2. Calculating mass fractions for the addition of DME to the oxidizer side
3. Calculating the mass fractions for the addition of air at the fuel side

1) Non Premixed Case (Φ = 0)

x_{ST} and $Z_{ST,DME}$ have the same values as in 3.2.4 and are calculated by 3.9 and 3.11. The mass fractions of DME in the fuel side $Y^0_{DME,1}$ and Oxygen $Y^0_{O2,2}$ in the oxdizer side are calculated by solving following equations.

$$3m^0 = c^0 \tag{3.18}$$

$$m^0 = \frac{1}{\sqrt{Le_{DME}}} \frac{X^0_{DME,1}}{1 - Z_{DME,ST}} \left\{ \exp\left[\frac{x_{ST}^2 (1 - Le_{DME})}{2} \right] \right\} \tag{3.19}$$

$$c^0 = \frac{X^0_{O_2,2}}{Z_{ST}} \tag{3.20}$$

$$T_{AD} = T_U + \frac{1}{c_p W_{N_2}} Q_{DME} m^0 Z_{ST} (1 - Z_{ST}) \tag{3.21}$$

$$X^0_{DME,1} = \frac{Y^0_{DME,1} W_{N_2}}{W_{DME}} \qquad X^0_{O_2,2} = \frac{Y^0_{O_2,2} W_{N_2}}{W_{O_2}} \tag{3.22}$$

By solving this Formulation in Mathcad following results can be obtained:

$Y^0_{DME,1}$ =   0,301
$Y^0_{O2,2}$ =   0,214

These values agree well with the Points of pure DME in Figure 3.4.

2) Case 1: Addition of DME to the Oxidizer Stream ($\Phi_1^{-1} = 0$; $\Phi_2 > 0$)

As there is no addition of air to the fuel stream ($\Phi_1^{-1} = 0$) the oxygen mass fraction of the fuel stream can be set to $Y_{O2,1} = 0$.

The mass fraction of oxygen in the oxidizer stream is set to the value of the non premixed case and will stay constant during all experiments where DME is added to the oxidizer stream. ($Y_{O2,2} = 0,214$)

To calculate the mass fractions of the other reactants certain values between zero and one are chosen for the equivalence ratio Φ_2 of the oxidizer stream.

Now the DME mass fraction of the oxidizer stream $Y_{DME,2}$ can be calculated.

$$\Phi_2 = 2,087\left(\frac{Y_{DME,2}}{Y_{O_2,2}}\right) \tag{3.23}$$

After calculating variable n with following equations

$$n = \frac{1}{\sqrt{Le_{DME}}}\frac{X_{DME,2}}{Z_{DME,ST}}\left\{\exp\left[\frac{x_{ST}^2\left(1-Le_{DME}\right)}{2}\right]\right\} \tag{3.24}$$

$$X_{DME,1} = \frac{Y_{DME,1}W_{N_2}}{W_{DME}};X_{O_2,1} = \frac{Y_{O_2,1}W_{N_2}}{W_{O_2}};$$

$$X_{DME,2} = \frac{Y_{DME,2}W_{N_2}}{W_{DME}};X_{O_2,2} = \frac{Y_{O_2,2}W_{N_2}}{W_{O_2}}; \tag{3.25}$$

Variable m can be calculated.

$$m = \frac{c}{3} - n \tag{3.26}$$

$$c = 3\frac{c_p W_{N_2}(T_{AD}-T_U)}{Q_{DME}Z_{ST}(1-Z_{ST})} \tag{3.27}$$

Now the mass fraction of DME in the fuel stream $Y_{DME,1}$ can be calculated by solving equations 3.25 and 3.28.

$$m = \frac{1}{\sqrt{Le_{DME}}}\frac{X_{DME,1}}{1-Z_{DME,ST}}\left\{\exp\left[\frac{x_{ST}^2\left(1-Le_{DME}\right)}{2}\right]\right\} \tag{3.28}$$

Following Table 3.2 shows the mass fractions of the selected measuring points for equivalence ratios Φ_2 from 0 to 0,3 for the oxidizer stream to stay outside of the flammability limits.

Table 3.2: Mass fractions of the reactants in fuel and oxidizer stream chosen for the experiment for $\Phi_1 = 0$ and $\Phi_2 = [0;0,3]$

Φ_2 [ ]	$Y_{O2,2}$ [ ]	$Y_{N2,2}$ [ ]	$Y_{DME,2}$ [ ]	$Y_{N2,1}$ [ ]	$Y_{DME,2}$ [ ]	$Y_{O2,2}$ [ ]
0,000	0,214	0,786	0,000	0,699	0,301	0,000
0,050	0,214	0,781	0,005	0,712	0,288	0,000
0,100	0,214	0,776	0,010	0,7253	0,275	0,000
0,150	0,214	0,770	0,015	0,738	0,262	0,000
0,200	0,214	0,765	0,021	0,752	0,248	0,000
0,250	0,214	0,760	0,026	0,765	0,235	0,000
0,300	0,214	0,755	0,031	0,778	0,222	0,000

3) Case 2: Addition of Air to the Fuel Stream ($\Phi_1^{-1} > 0$; $\Phi_2 = 0$)

As there is no addition of fuel to the oxidizer stream ($\Phi_2 = 0$) the fuel mass fraction of the oxidizer stream can be set to $Y_{DME,2} = 0$.

The mass fraction of DME in the fuel stream is set to the value of the non premixed case and will stay constant during all experiments where air is added to the fuel stream. ($Y_{DME,1} = 0,301$)

To calculate the mass fractions of the other reactants certain values between zero and one are chosen for the equivalence ratio Φ_1^{-1} of the fuel stream.

Now the oxygen mass fraction of the fuel stream $Y_{O2,1}$ can be calculated.

$$\Phi_1^{-1} = \frac{Y_{O_2,1}}{2,087 Y_{DME,1}} \tag{3.29}$$

After calculating variable a

$$a = \frac{X_{O_2,1}}{1 - Z_{ST}} \tag{3.30}$$

Variable c can be calculated.

$$m = \frac{a + c}{3} \tag{3.31}$$

$$c = \frac{c_p W_{N_2} (T_{AD} - T_U)}{Q_{DME} Z_{ST} (1 - Z_{ST})} - a \tag{3.32}$$

Now the mass fraction of oxygen in the oxidizer stream $Y_{O2,2}$ can be calculated.

$$c = \frac{X_{O_2,2}}{Z_{ST}} \tag{3.33}$$

Following Table 3.3 shows the mass fractions of the selected measuring points for equivalence ratios Φ_1^{-1} from 0 to 0,25 for the oxidizer stream as with Φ_1^{-1} = 0,25 the maximum level of premixing oxygen in fuel is reached when air is used as oxidizer gas. Higher levels of premixing would just be possible if pure oxygen would be used as oxidizer gas.

Table 3.3: Mass fractions of the reactants in fuel and oxidizer stream chosen for the experiment for Φ_2 =0 and Φ_1^{-1} = [0;0,25]

Φ_1^{-1} [ ]	$Y_{O2,2}$ [ ]	$Y_{N2,2}$ [ ]	$Y_{DME,2}$ [ ]	$Y_{N2,1}$ [ ]	$Y_{DME,2}$ [ ]	$Y_{O2,2}$ [ ]
0,000	0,214	0,786	0,000	0,699	0,301	0,000
0,050	0,199	0,801	0,000	0,668	0,301	0,0314
0,100	0,185	0,815	0,000	0,636	0,301	0,0628
0,150	0,170	0,830	0,000	0,605	0,301	0,0942
0,200	0,156	0,844	0,000	0,573	0,301	0,126
0,250	0,141	0,859	0,000	0,542	0,301	0,157

3.2.6.   Verification of the New Short DME Mechansim of UCSD Combustion Research Group for Diffusion Flames

After comparing the experimental and the numerical results for the partial premixed DME flames investigation it was decided to verify the new developed short DME mechanism of the UCSD combustion research group for pure diffusion flames.

Starting from the non premixed case of the previous partial premixed experiment and a fixed stochiomtric mixture fraction Z_{ST} = 0,318 all the mass fractions of the fuel and oxidizer stream were calculated by reducing the O_2 mass fraction of the oxidizer stream in 0,05 steps.

Following calculations based on the previous carried out asymptotic analysis for partial premixed DME flames were carried out to calculate the measuring points.

As in this investigation no premixing is taking place $Y_{DME,2}$ and $Y_{O2,1}$ can be set to zero. The values of x_{ST}, $Z_{DME,ST}$ are the same as in 3.2.5. The mass fraction of oxygen in the oxidizer stream is $Y_{O2,2}$ = 0,214 for the starting point and is set to fixed values of 0,21, 0,205, 0,2, 0,195,....

Now the mass fraction of DME in the fuel stream $Y_{DME,1}$ can be calculated for fixed values of $Y_{O2,2}$ by using the equations of the non premixed case of 3.2.5 in following order:

1. Calculate $X_{O2,2}$ with 3.22
2. Calculate c^0 with 3.20
3. Calculate m^0 with 3.18
4. Calculate $X_{DME,1}$ with 3.19
5. Calcualate $Y_{DME,1}$ with 3.22

The adiabatic flame temperature T_{AD} can be calculated with 3.21.

Following Table 3.4 shows the calculated mass fractions of the fuel and oxidizer stream of the selected measuring points for selected values of $Y_{O2,2}$ from 0,185 up to 0,214

Table 3.4: Chosen mass fractions of the reactants in fuel and oxidizer stream and calculated adiabatic temperature T_{AD} for a fixed Z_{ST} = 0,318 for the verification of the new DME mechanism

Point	$Y_{O2,2}$ [ ]	$Y_{N2,2}$ [ ]	$Y_{DME,1}$ [ ]	$Y_{N2,1}$ [ ]	T_{AD} [K]
1	0,214	0,786	0,301	0,699	1850,0
2	0,210	0,790	0,295	0,705	1820,0
3	0,205	0,795	0,288	0,712	1783,7
4	0,200	0,800	0,281	0,719	1747,4
5	0,195	0,805	0,274	0,726	1711,1
6	0,190	0,810	0,267	0,733	1674,9
7	0,185	0,815	0,260	0,740	1638,6

4. Computional Simulations

Computional simulations become more and more important in all fields of engineering. In the area of combustion research the ever growing power of computers enabled the simulation of detailed chemical kinetics in recent years. Computational modelling and simulations have become very useful tools in combustion as with kinetic modelling it´s possible to solve a great variety of problems and in contrast to experimental investiagtions simulations are not restricted by physical limitations. The computational simulation is often much faster, cheaper and easier to apply than detailed experimental investigations. However, computing detailed chemical kinetic mechanisms still requires a lot of time and extremely powerful processors. In order to reduce the computational time and respectively costs complexity and dimensions of the chemical kinetic mechanisms are reduced by adopting analogy rules and symplifying assumptions. [18]

In this thesis computational simulations are carried out for pure DME fuels. The Lawrence Livermore National Laboratory Dimethly Ether 2000 mechansim and a new reduced DME mechanism devloped by [17] of the University of California, San Diego are used. Unfortunately chemical kinetic mechanisms which include iso-octane are too detailed to be solved with the available computer in the combustion Lab and would require CHEMKIN PRO for processing.

4.1. CHEMKIN

Chemkin is a very useful software tool which enables the simulation of complex chemical reactions. It was orignially developed by Sandia National Labaratories. For computional simulations of chemical kinetic mechanisms CHEMKIN requires three input files and the input settings for the boundary conditions.

- Gas-phase kinetics file also called input file
- Thermodynamic file also called thermo data file
- Gas transport file also called transport data file
- Input settings

The input file normally contains four blocks of informations in following order, the thermo block may be skipped if all species are registered in the thermo data file.

- Elements block
- Species block
- Thermo block
- Reactants block

Elements and species block are a list of all relevant elements and species, if there is a thermo block, it contains thermodynamic data for the relevant species.

The most interesting block is the reactants block which contains all chemical reactions that take place, the Arrhenius rate coefficents A, β and E_A for each reaction as well as information about the reversibility and pressure dependence of the reactions and if a third body is involved in the reaction.

The thermo data file contains names and elemental composition of all species together with the polynomial coefficient for entropy, enthalpy and isobanic heat with the associated temperature range.

The transport data file contains several molecular properties like the dipole moment and the Lennard-Jones-Potential for all species to evaluate thermal conductivities, diffusion coefficients and thermal diffusion components.

All species listed in the input file also have to be listed in the thermodynamic file and the transport data file. Out of these three files the complier is creating a gase-phase kinetics-linking file (chem.asc) that contains all relevant information of the mechanisms that is accessed permanently during the reactor-model simulation.

As mentioned before the boundary conditions are included in the input settings which contain reactor physical properties, grid properties, stream properties and species-specific properties.

Several idealized reactor models can be selected in CHEMKIN. For all carried out simulations in this thesis the „Diffusion or Premixed Opposed-flow-Flame" reactor model was used.

For the simulations the solver is using the CHEMKIN application code, the input settings, the gas-phase kinetics linking file and the reactor model to calculate each data point. [2–4, 9]

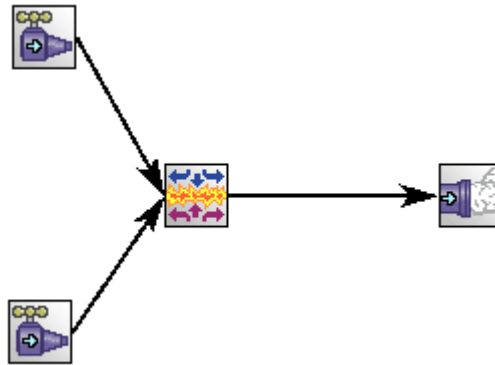## 4.2. Computional Simulations

Figure 4.1 CHEMKIN Reactor model „Diffusion or Premixed Opposed-flow-Flame"

As mentioned in 4.1 the „Diffusion or Premixed Opposed-flow-Flame" reactor model (figure 4.1) is chosen for the invesigations. The pressure is set to 1 atm and the ambient pressure is set to 296 K. The maximum temperature for the initial temperature profile is set to 400 K for autoignition and 2100 K for extinction. A manual approach is chosen to find the autoignition temperature and the extinction strain rate. Figure 4.2 shows the mathematicall boundary conditions to solve the gas energy equation for all computations carried out in this thesis.

Pseudo Time Steps (Fixed Temperature)	
Number of Time Steps	100.0
Initial Size of Time Step	1.0E-6 sec ▼
Pseudo Time Steps (Energy Equation)	
Number of Time Steps	100.0
Initial Size of Time Step	1.0E-6 sec ▼
Minimum Pseudo Time Step	1.0E-10 sec ▼
Maximum Pseudo Time Step	0.01 sec ▼
Number Time Steps Before Increasing	25
Time Step Decrement Factor	2.0
Time Step Increment Factor	2.0
Number of Transient Iterations before Updating Jacobian	20
Maximum Number of Iterations per Pseudo Time Step	25
Maximum Number of Pseudo Time Stepping Operations Allowed	100
Number of Initial Pseudo Time Steps	0
Number of Iterations before Updating Jacobian	20
Maximum Number of Iterations per Steady State Search	100
Pseudo Time Stepping Only	
Number of Time Steps	
Initial Size of Time Step	sec ▼
Output Frequency during Integration	100
Minimum Bounds on Species Fractions	-0.0001
Positive Value to Reset Species Fractions	0.0
◉ Windward Differencing	
○ Central Differencing	

Figure 4.2: Mathematical boundary conditions for computations

4.2.1.   Autoignition

For autoignition experiments only the pure DME flames are investigated. The species-specific properties are selected according to the fuel mass fractions of the carried out experiments ($Y_{DME,1}$ = 0,4) The reactor physical properties are set like described in 4.2. The number of uniform grid points is set to 100, with the further specifications (grid properties)

- adaptive grid control based on solution gradient: 0,1
- adaptive grid control based on solution Curvature: 0,5
- maximum number of grid points allowed: 500
- number of adaptive grid points

The distance between the ducts is set to 1,45 cm with an estimated flame center position of 0,5 cm.

To determine the autoignition temperature a manual approach with the help of a parameter study is chosen. The concept is very similar to the experimental procedure as the temperature is increased until autoignition occurs. To satisfy the momentum balance the fuel velocity has to be decreased when the gas temperature is increased. With the oxidizer strain rate and the gas temperature as input parameters all the densities, strain rates and inlet velocities for fuel and oxidizer stream can be calculated in an excel file. The gas temperature and the inlet fuel velocity are used as input parameters for the parameter study and the simulations are carried out as long as the autoignition temperature is found. The criteria for autoignition is the temperature profile over the distance between fuel and oxidizer duct. As soon as a steep temperature increase can be identified, a flame is established and this run is where autoignition first occurs. By comparing the input parameters of this run and the results of the excel file the gas temperature can be determined. For the simulations of DME the Lawrence Livermore National Laboratory Dimethly Ether 2000 mechansim was used and the during the experiment measured inlet temperature of the fuel duct was averaged and set to T_1 = 383 K for all computations.

4.2.2. Extinction

The number of uniform Grid Points is set to 30, with the further specifications

- adaptive grid control based on solution gradient: 0,1
- adaptive grid control based on solution curvature: 0,5
- maximum number of grid points allowed: 500
- number of adaptive grid points

The distance between the ducts is set to 1,25 cm with an estimated flame center position of 0,5 cm.

To determine the oxidizer strain rate for extinction a different manual approach is applied. In contrast to the parameter study used to find the autoignition temperature continuations are used. The difference between continuations to a parameter study is that continuations use the results of the previous run as input parameters for the following run. Similar to the autoignition simulations before the inlet velocities of the fuel and oxidizer stream can be calculated with the oxidizer strain rate, the inlet fuel and oxidizer temperature as input parameters by using the momentum balance in an excel file. The inlet velocities are the input parameters for the continuations and can be imported in CHEMKIN by saving as .csv file before. The criteria for extinction is again the temperature profile over the distance between the ducts and as soon as a negative temperature step can be identified the flame extinguishes. By comparing the input parameters of this run with the calculated parameters in the excel file the oxidizer strain rate for extinction can be determined.

Different simulations for extinction are carried out in this thesis. For the pure DME point in the extinction experiments for DME/iso-octane fuel blends the inlet fuel temperature is set to $T_1 = 395 \text{ K}$ like in the experiment and the Lawrence Livermore National Laboratory Dimethly Ether 2000 mechansim is used.

For simulation of partial premixed DME flames the inlet fuel temperature is set to $T_1 = 310 \text{ K}$ and the Lawrence Livermore National Laboratory Dimethly Ether 2000

and a new develped short DME mechanism of [17] is used. The inlet temperature of the oxidizer stream is set to T_2 **= 296 K** for all extinction computations carried out in this thesis and the mass fractions of the species are chosen according to the previous carried out experiments.

For the verification of the new short DME mechanism of the UCSD combustion research group for diffusion flames the same settings are used as in the numerical analysis of partial premixed DME flames.

5. Experimental and Numerical results

In this chapter the results of the experiments and the numerical simulations are summarized. The detailed experimental data is attached in Appendix A.

5.1. Autoignition of DME/Iso-Octane Fuel Mixtures in Non-Premixed Flows

The temperatures of autoignition shown in the following figures are corrected for losses according to 3.1.2. The symbols represent arithmetically averaged temperature measurements and the lines are polynomial second order best-fit-curves.

The autoignition temperature separates the figures in two regions. For a given fuel autoignition will never occur at temperatures below the autoignition temperature, but it will always occur at temperatures above the autoigntion temperature.

Generally there is a link between the oxidizer strain rate a_2 and the autoignition temperature T_2. An increase of the oxidizer strain rate a_2 leads to a raise of the autoignition temperature T_2. This rise in temperature occurs because the increasing of the oxidizer strain rate a_2 involves an increase of the inlet velocities V_1 and V_2 of fuel and oxidizer stream that on the other hand decreases the time for chemical reactions. Therefore the mixture is harder to ignite and requires higher temperatures for autoignition.

Figure 5.1 shows the autoignition temperature T_2 of different fuel blends of DME and iso-octane as a function of the oxidizer strain rate a_2. The data showed in the figure shows fuel compositions from 100 %DME/ 0% iso-octane up to 50% DME/ 50% iso-octane with a fuel mass fraction of $Y_{F,1} = 0.4$
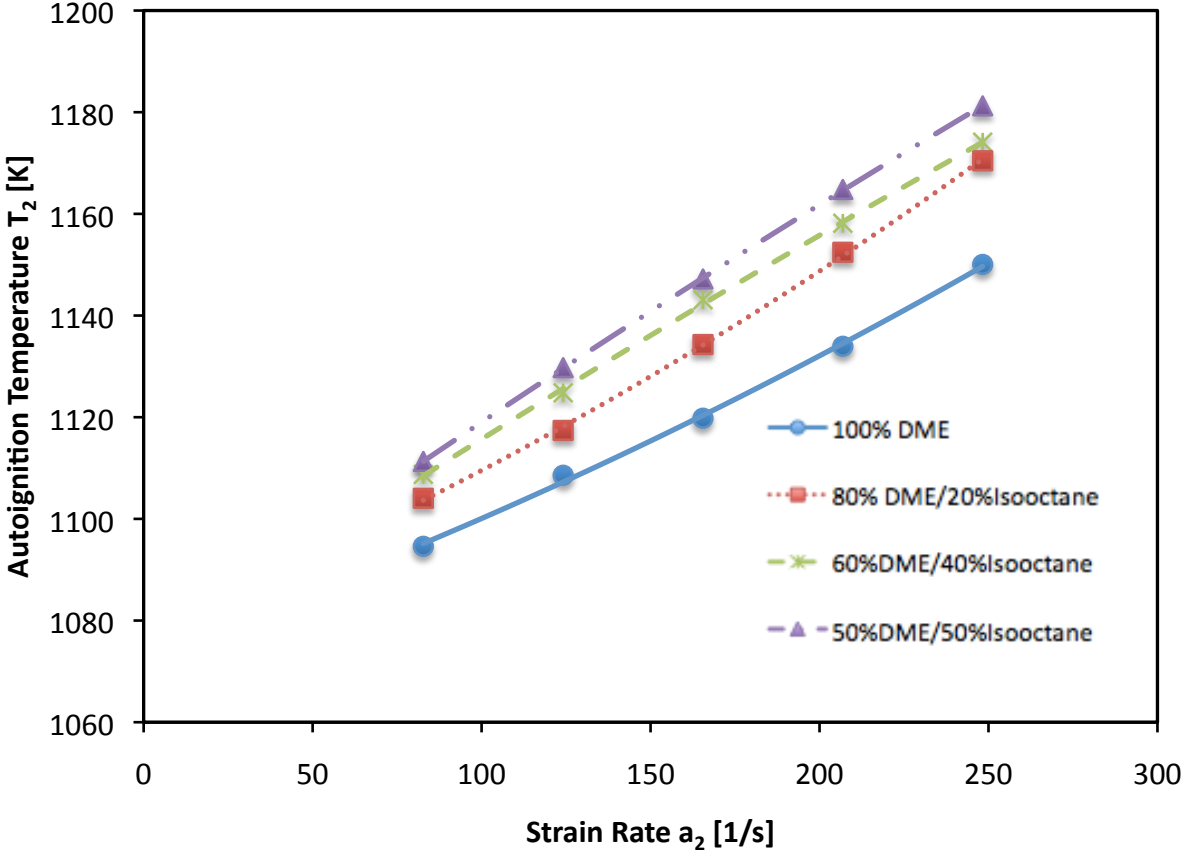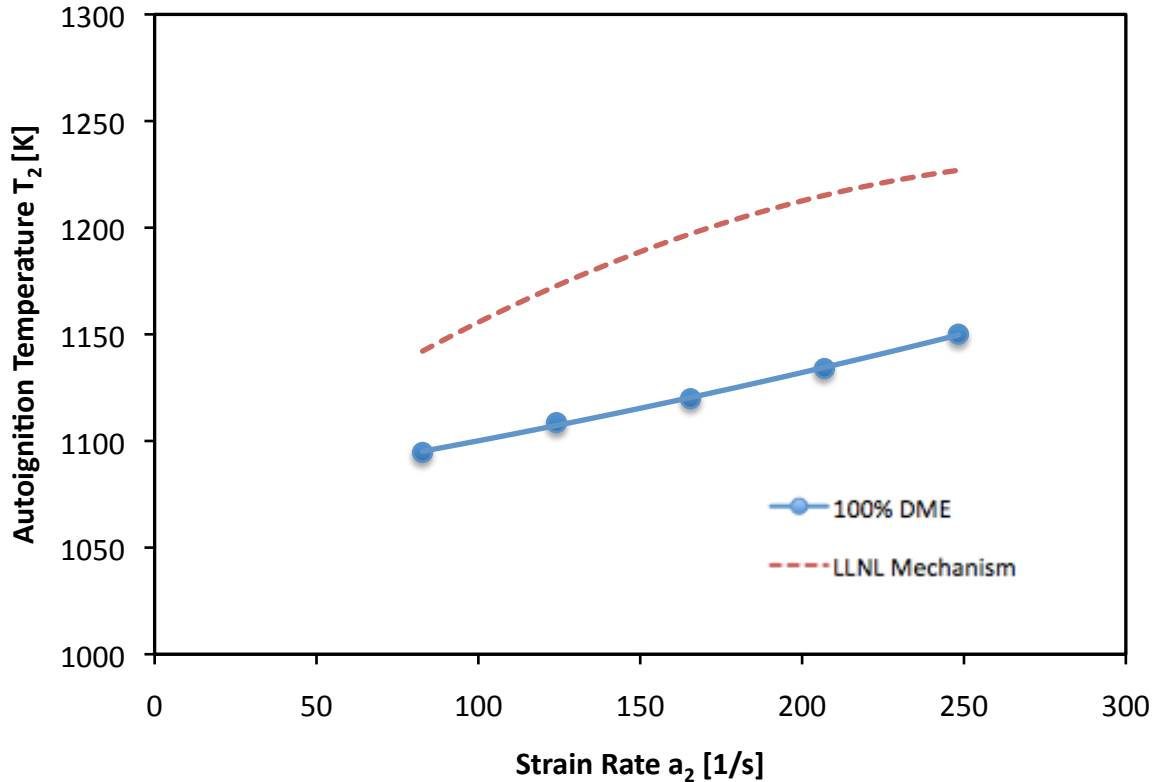

Figure 5.1: The temperature of autoignition of the oxidizer stream T_2 as function of the oxidizer strain rate a_2 at a constant fuel mass fraction $Y_{F,1} = 0,4$ for different fuel mixtures of DME and iso-octane. The figure shows data from 100%DME/0%iso-octane up to 50%DME/50%iso-octane. The symbols represent the experimental data, the lines are polynomial second order best-fit curves.

Dimethyl ether shows the lowest autoigntion temperatures at all strain rates of all displayed fuel compositions. By increasing the content of iso-octane in the mixture the autoigntition temperature T_2 rises. Increasing the iso-octane concentration of the fuel mixture seems to have an uniform increasing effect over the strain rate but at the same time the increasing effect seems to decrease with higher iso-octane concentrations. The gradient dT_2/da_2 seems to be be a bit higher for fuel mixtures containing iso-octane than for pure DME, especially for higher strain rates.

Figure 5.2: The temperature of autoignition of the oxidizer stream T_2 as function of the oxidizer strain rate a_2 at a constant fuel mass fraction $Y_{F,1}$ = 0,4 for pure DME. The figure shows the experimental data in comparison with the computational data of the LLNL DME 2000 mechanism. The figures represent the experimental data, the lines are polynomial second order best-fit curves.

Figure 5.2 shows a comparison of the autoigntion temperatures of 100% DME between the experimental data and the results of the numerical simulation using the LLNL DME 2000 mechansim as described in 4.2.1. The results of the experiments and the computations seem to agree very well as the temperature difference ΔT_2 is always in a range between 50 K at low strain rates up to 75 K at medium and higher strain rates. The numerical results in overall are slightly higher then the experimental results and show a steeper gradient dT_2/da_2 at lower strain rates. The fact that the experimental data of DME is very close to the numerical data of DME lets suppose that also the experimental data of DME/iso-octane is in the right range, even if it was not possible to run computations for iso-octane fuel mixtures.

By plotting the autoigntion temperature over the fuel composition of DME and iso-octane the experimental results can be considered from a different angle. Figure 5.3 shows the autoigntion temperature for oxidizer strain rates from a_2 = 80 s^{-1} up to a_2 = 250 s^{-1}. Fuel mixtures from 100% DME/ 0% iso-octane up to 30% DME/ 70% iso-octane were tested. Unfortunately it wasn´t possible to ignite pure iso-ocante and fuel mixtures with more then 70% iso-octane without risking to destroy the heating element of the used autoigntion top. Another interesting fact is that igniting pure DME was easier at lower strain rates and with increasing content of iso-octane igniting of the fuel mixture became easier at higher strain rates.
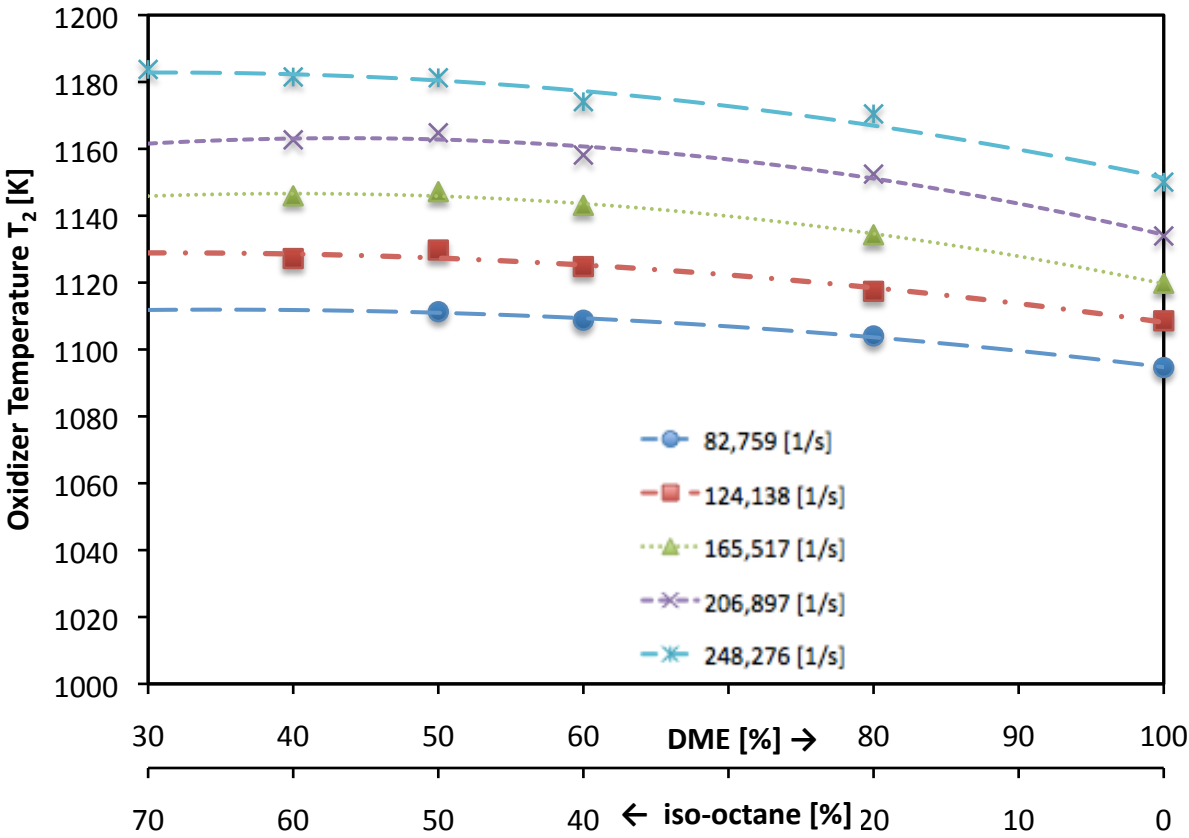
Figure 5.3: The temperature of autoignition of the oxidizer stream T_2 as a function of the fuel composition of DME and iso-octane. The figure shows data for five different oxidizer strain rates a_2. The symbols represent experimental data, the lines are polynomial second order best-fit curves.

As mentioned in the beginning the autoignition temperature is increasing by strain rate and by increasing amount of iso-octane in the fuel mixture. The increase by rising the amount of iso-octane in the fuel mixture is decreasing at higher concentrations of iso-octane. At a fuel composition of 60% iso-octane/ 40% DME even slightly lower autoignition temperatures up to ΔT_2 = 2,55K at a strain rate of a_2 = 124,138 s^{-1} were measured compared to measurements of 50% iso-octane/50%DME mixtures. At high strain rates of a_2 = 248,276 s^{-1} however a continious increasing

effect by increasing the concentration of iso-octane in the fuel mixture could be determined up to 70% iso-octane/ 30% DME fuel mixtures.

To evaluate the autoignition behaviour at higher concentrations of iso-octane in the full range a more powerful heating element is required. Such a heating element is built right now at the UCSD combustion laboratory for upcoming experiments of autoignition at elevated pressures and will soon be available.

Anyway the results show an visible effect of an rising autoigntion temperature by increasing the concentration of iso-octane for all strain rates up to 50% iso-octane/ 50% DME.

5.2. Extinction of DME/Iso-Octane Fuel Mixtures in Non-Premixed Flows

In this experiment the extinction behaviour of DME/iso-octane fuel mixtures was investigated for various blends of DME and iso-octane. The experiments were carried out at a fixed adiabatic flame temperature and a fixed stochiometric mixture fraction according to 3.2.4 Since both DME and iso-octane show a a visible blue flame, their blends also show a visible blue flame.

Figure 5.4 shows the the oxidizer strain rate a_2 at extinction as a function of the fuel composition of DME and iso-octane. The blue symbols represent the experimental results, the blue line represents a polynomial second order best-fit-curve for the experimental data. The red symbol represents the results of the numerical CHEMKIN simulation for pure DME using the using the LLNL Dimethyl Ether 2000 mechanism.

The plotted data can also be seen as a boundary between the flammable and the non-flammable region of the fuel mixture. In the condition above the boundary it is not possible to ignite the mixture. By decreasing the oxidizer strain rate (vertical shift) or by increasing the DME concentration of the fuel mixture (horizontal shift to the right) it´s possible to reenter the flammable region and to ignite the fuel mixture by an external energy source.

The obtained data shows that extinction of dimethyl ether occurs at much higher strain rates than extinction of iso-octane. The measured oxidizer strain rates a_2 of

pure DME are more than three times higher than the values of extinction for pure DME. Results for pure DME fit very well together with the results of the computations. The difference between experimental and numerical results Δa_2 is only 6 s^{-1} for pure DME. The very small deviations of experimental and numerical results let suppose that the experimental results are in the right range.
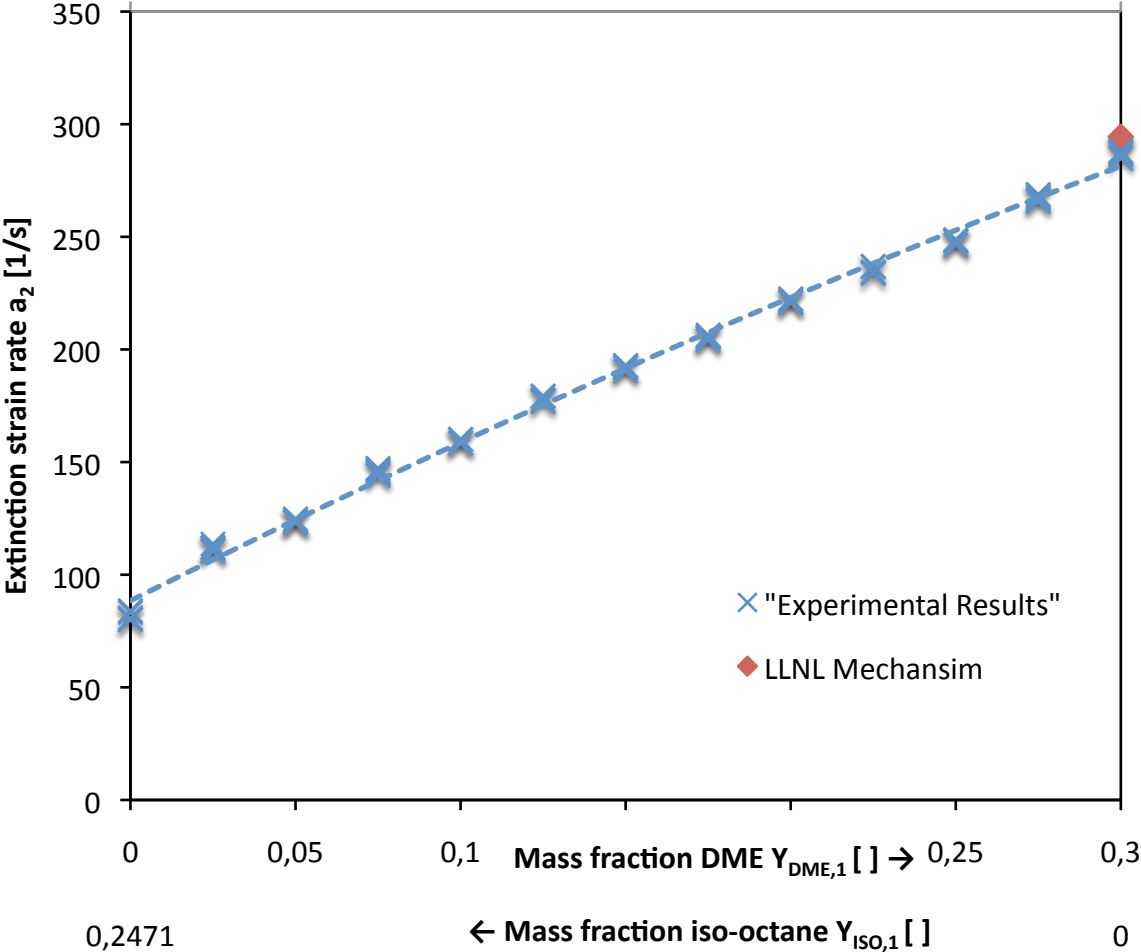

Figure 5.4: Oxidizer strain a_2 rate at extinction as a function of the fuel composition of DME and iso-octane for fixed values of the stochiometric mixture fraction Z_{ST} = 0,318 and adiabatic flame temperature T_{AD} = 1850 K. The symbols represent the experimental and the numerical data, line is a polynomial second order best-fit curve.

The data obtained in figure 5.4 shows that the extinction strain rate is increasing with higher concentrations of DME in the fuel mixture. This effect seems to be uniform through the whole range of the fuel composition. No influence in the extinction behaviour can be seen by blending DME and iso-octane. The measured values of the blends show just averaged values of the extinction strain rates of the pure fuels according to the fuel composition.

5.3. Extinction of Partial Premixed DME Flames

In this set of experiments the extinction behaviour of partial premixed DME flames was investigated. The experiments were carried out at a fixed adiabatic flame temperature and a fixed stochiometric mixture fraction according to 3.2.5.

The investigation is divided into two parts as partial premixing is possible in two ways:

- Case 1: Addition of DME to the oxidizer stream
- Case 2: Addition of air to the fuel stream

The following two figures show the extinction behaviour as a function of the level of premixing for both cases. The symbols represent the experimental data, the lines represent polynomial second order best-fit curves for the experiments as well as the computational results. For the computations the LLNL Dimethyl Ether 2000 mechanism and the newly developed short DME mechanism of [17] by the combustion research group of UCSD were used.

5.3.1. Case 1: Addition of DME to the Oxidizer Stream

Figure 5.5 shows the oxidizer strain rate a_2 at extinction as a function of the equivalence ratio Φ_2 of DME and oxygen in the oxidizer stream. The non premixed case ($\Phi_2 = 0$) shows the lowest strain rates, with an increasing level of premixing ($\Phi_2 > 0$) extinction occurs delayed and a significant rise in the oxidizer strain rate a_2 can be determined for the experimental results as well as for the computations.

The computational data underpredicts the increase of the extinction strain rate with increasing level of premixing but shows the same trend. Both mechanisms show similar values for the gradient $da_2/d\Phi_2$ but compared to San Diego mechanism the LLNL mechanism shows higher values of a_2 over the full range from $\Delta a_2 = 47,2 \text{ s}^{-1}$ at $\Phi_2 = 0$ up to $\Delta a_2 = 79,2 \text{ s}^{-1}$ at $\Phi_2 = 0,35$.

The San Diego mechanism shows especially for pure diffusion flames ($\Phi_2 = 0$) and small levels of premixing a very well agreement with the experimental results, the LLNL mechanism on the other hand overpredicts the extinction strain rate for the non

premixed case but fits very well with the experimental data at medium levels of premixing. The difference between measurement and prediction is just Δa_2 = 3,8 s^{-1} at Φ_2 = 0,2.

As in the previous extinction investigation the plotted data can also be seen as a boundary between the flammable and the non-flammable region of the fuel mixture. In the condition above the boundary it´s not possible to ignite the mixture. By decreasing the oxidizer strain rate (vertical shift) or by increasing the level of premixing (horizontal shift to the right) it´s possible to reenter the flammable region and to ignite the fuel mixture by an external energy source.
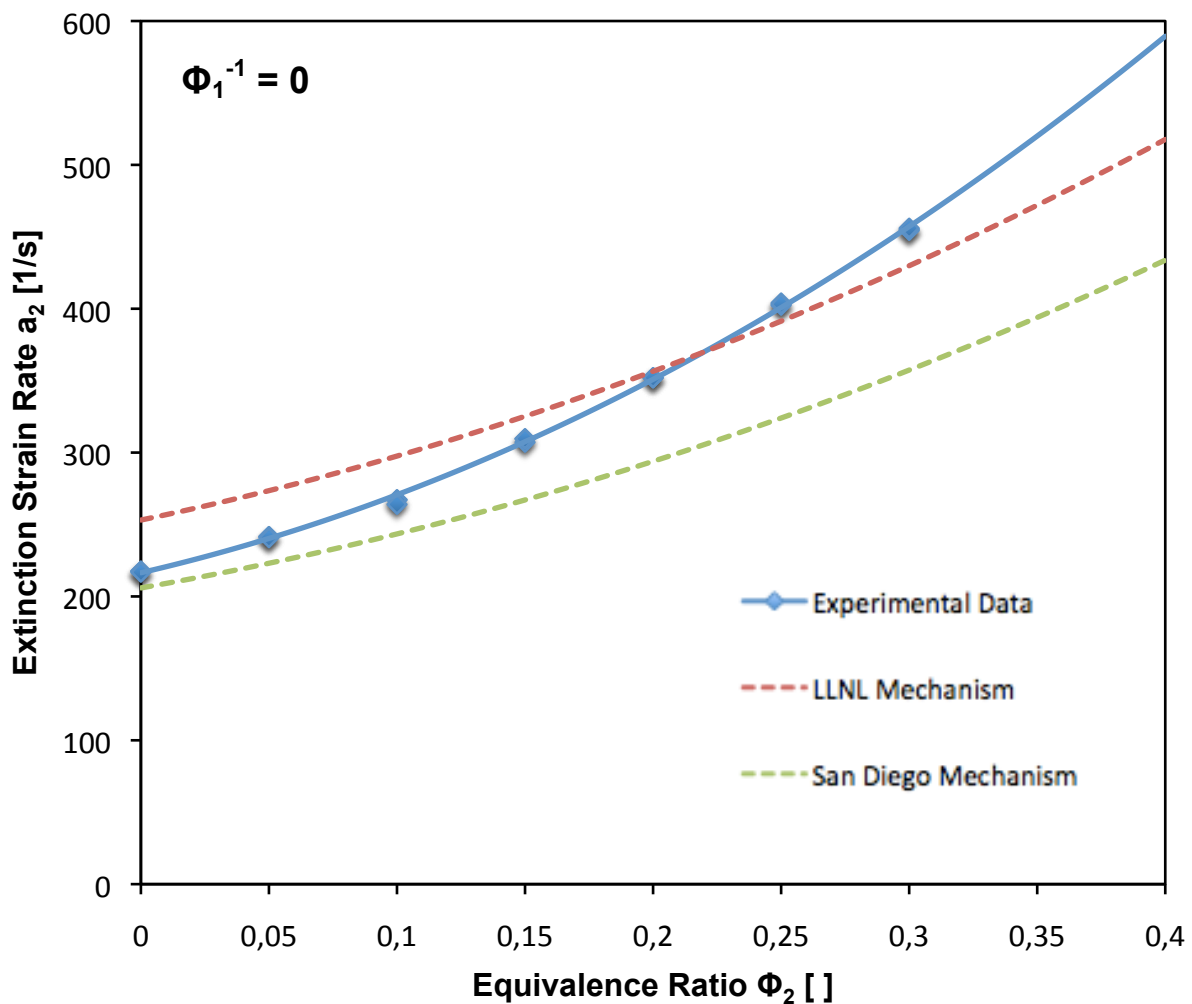
Figure 5.5: Oxidizer strain rate a$_2$ at extinction as a function of the equivalence ratio Φ_2 of the oxidizer stream. The values of the stochiometric mixture fraction Z_{ST} = 0,318 and adiabatic flame temperature T_{AD} = 1850 K are fixed. The figure shows experimental data in comparison with the computational results of the LLNL DME 2000 mechansim and the San Diego Mechanism. The symbols represent the experimental and the numerical data, lines are polynomial second order best-fit curves.

5.3.2. Case 2: Addition of Air to the Fuel Stream

Figure 5.6 shows the oxidizer strain rate a_2 at extinction as a function of the equivalence ratio Φ_1^{-1} of oxygen and DME at the fuel stream. For the experimental data no influence is visible for partial premixing. The extinction strain rate stays almost constant until $\Phi_1^{-1} = 0{,}15$ and increases by $\Delta a_2 \approx 3s^{-1}$ at $\Phi_1^{-1} = 0{,}2$ and by $\Delta a_2 \approx 9s^{-1}$ at $\Phi_1^{-1} = 0{,}25$.

Again both mechanisms show similar values for the gradient $da_2/d\Phi_1^{-1}$ but compared to San Diego mechanism the LLNL mechanism shows slightly higher values of a_2 over the full range from $\Delta a_2 = 47{,}2 \text{ s}^{-1}$ at $\Phi_2 = 0$ up to $\Delta a_2 = 58{,}4 \text{ s}^{-1}$ at $\Phi_2 = 0{,}25$.
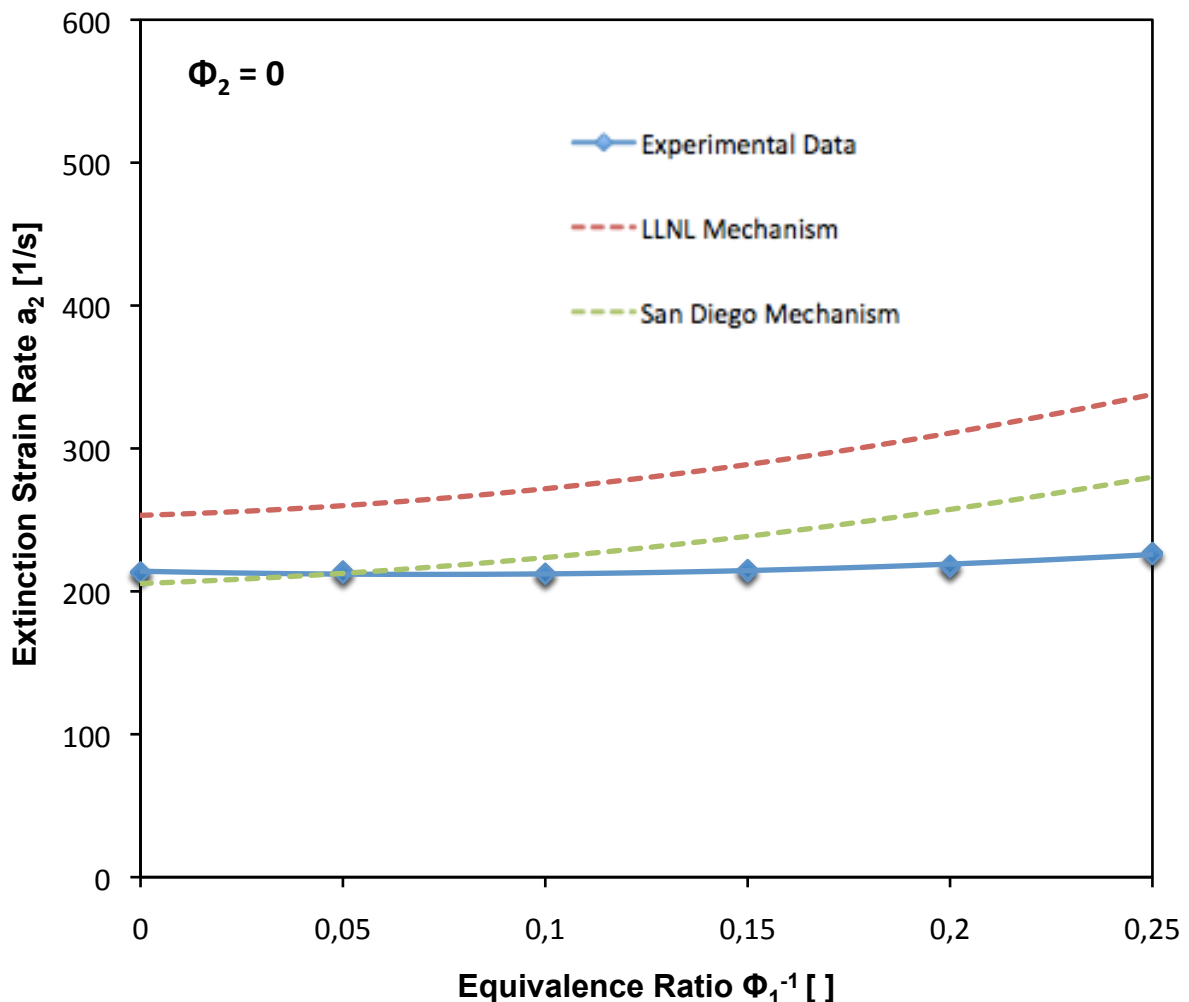
Figure 5.6: Oxidizer strain rate a_2 at extinction as a function of the equivalence ratio Φ_1^{-1} of the fuel stream. The values of the stochiometric mixture fraction $Z_{ST} = 0{,}318$ and adiabatic flame temperature $T_{AD} = 1850$ K are fixed. The figure shows experimental Data in comparison with the computational results of the LLNL DME 2000 mechansim and the San Diego Mechanism. The symbols represent the experimental and the numerical data, lines are polynomial second order best-fit curves.

Both mechanisms overpredict the increase by the level of premixing. The San Diego mechanism agrees better with the experimental results as it again shows very accurate results for diffusion flames and as well has a slightly slower gradient $da_2/d\Phi_1^{-1}$ as the LLNL mechansim.

5.3.3. Interpretation of Results

To elucidate the influence of partial premixing on flame structure and critical conditions of extinction the flame structure was calculated using the San Diego mechanism for various values of Φ_2 (with $\Phi_1^{-1} = 0$) and Φ_1^{-1} (with $\Phi_2 = 0$). Several plots of the mass fractions of O_2, DME, H_2 x 30, CO, CO_2, H_2O and the temperature T as a function of the mixture fraction Z are obtained for a chosen oxidizer strain rate $a_2 = 200$ s^{-1}.

Figure 5.6 shows the mass fractions of O_2, DME, 30 times H_2, CO, CO_2, H_2O and the flame temperature T as function of the mixture fraction Z at a strain rate $a_2 = 200$ s^{-1} for the non premixed case. ($\Phi_1^{-1} = 0$; $\Phi_2 = 0$)
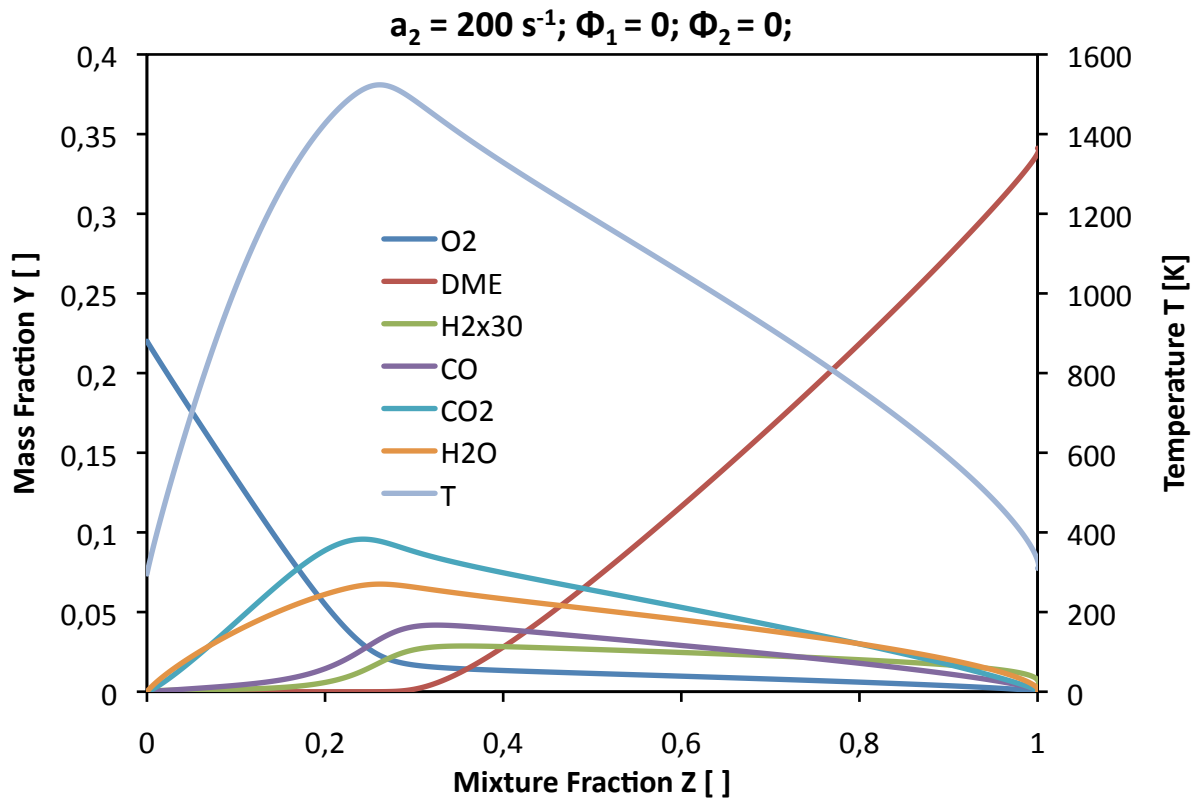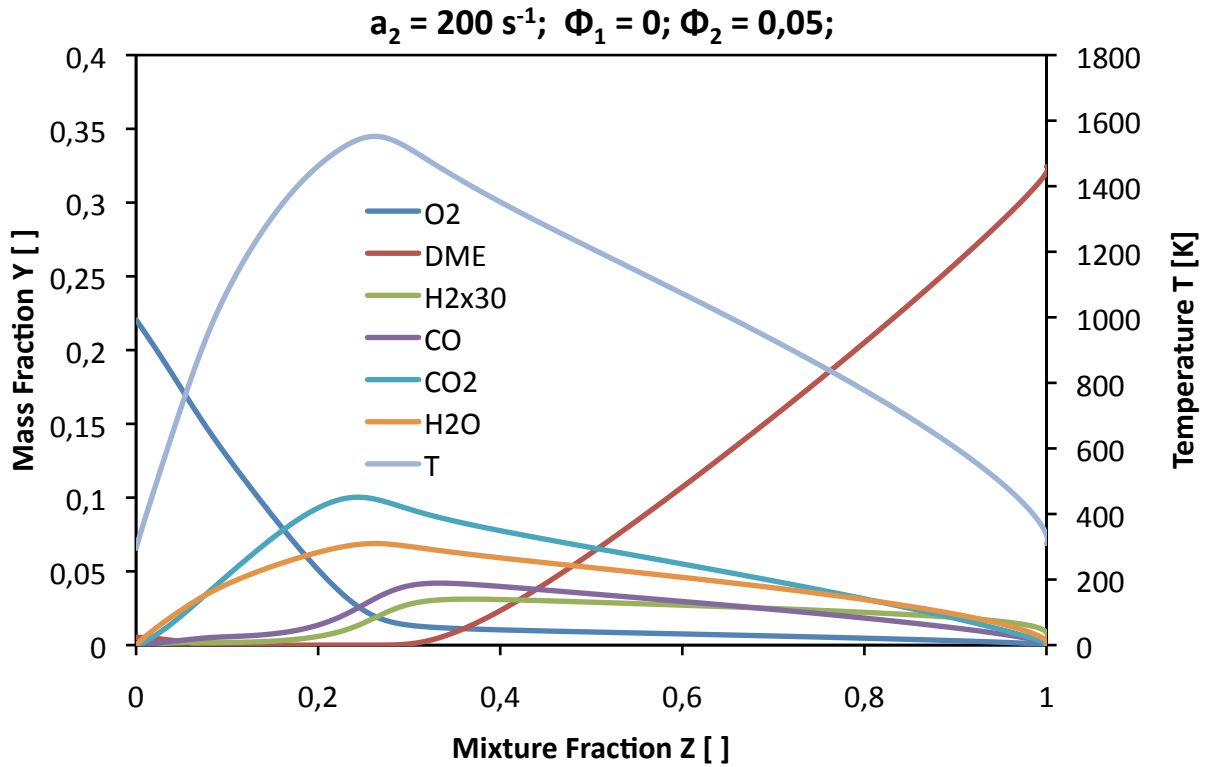

Figure 5.7: Plot of mass fractions Y_{O2}, Y_{DME}, Y_{H2} x 30, Y_{CO}, Y_{CO2}, Y_{H2O} and the flame Temperature T as function of the mixture fraction Z of non premixed ($\Phi_1^{-1} = 0$; $\Phi_2 = 0$) DME flames at an oxidizer strain rate $a_2 = 200$ s^{-1}. Plots are results of the numerical analysis using the San Diego mechanism.

Analyzing the non premixed case in figure 5.6 you can see that the DME is completely consumed ($Y_{DME} = 0$) from $Z = 0$ until the stochiometric mixture fraction $Z_{ST} = 0{,}318$. By further increasing the mixture fraction Z the value Y_{DME} is constantly rising as well. On the other hand you can see that oxygen is not completely consumed, Y_{O2} has a maximum at $Z = 0$ and decreases with increasing mixture fraction Z but is still not fully consumed at Z_{ST}. This "leaking" of oxygen is a result of incomplete chemistry.

Two very important layers can be found in this plot. At values of Z slightly below the stochiometric mixture fraction Z_{ST} H_2 (green) and CO (purple) are formed by consuming DME. This effect is visible as Y_{H2} and Y_{CO} are increasing to their maximum in this layer. Left of this layer H_2O (orange) and CO_2 (turqoise) are formed by consuming H_2 and CO. Again this layer is characterized by increasing values of Y_{H2O} and Y_{CO2} to their maximum in this layer.

Looking at the flame temperature you can see that the highest temperatures occur at values of Z slightly below Z_{ST} in the area where H_2 and CO are formed.

Case 1: Addition of DME at Oxidizer Stream

The figures 5.7 – 5.10 on the following two pages show the same plots for increased levels of premixing DME at the fuel stream from from $\Phi_2 = 0,05$ up to $\Phi_2 = 0,35$.
By increasing the level of DME in the oxidizer stream two phenomenons are visible. Firstly you can see that with increasing equivalence ratio Φ_2 the "leaking" of oxygen is decreasing which implicates that more oxygen is consumed. This effect of enhanced consumption of oxygen promotes combustion and leads to a delayed extinction at higher strain rates and will be showed more detailed in figure 5.11.

Secondly you can see that DME is not fully consumed up to values of Z around 0,1. The amount of not consumed DME (Y_{DME}) is increasing with higher levels of premixing. This effect leads to a second layer where H_2 (green) and CO (purple) are formed by consuming DME and higher values of Y_{O2} in this layer compared to the non premixed case. The layer is again visible as Y_{H2} and Y_{CO} are increasing to a local maximum in this area. In the case of addition of DME to the fuel stream there are three layers, in two layers H_2 and CO are formed by consuming DME, in the third layer between H_2O (orange) and CO_2 (turquoise) are formed by consuming H_2 and CO.

The plot of the flame temperature shows the same trend as in the non premixed case, the gradient dT/DZ at small values of Z is increasing with higher levels of premixing but the maximum temperature still occurs in the same region as before and the maximum flame temperature is increasing by more than 100 K from $\Phi_2 = 0$ to $\Phi_2 = 0,35$.

Figure 5.8: Plot of mass fractions Y_{O2}, Y_{DME}, Y_{H2} x 30, Y_{CO}, Y_{CO2}, Y_{H2O} and the flame Temperature T as function of the mixture fraction Z of partial premixed ($\Phi_1^{-1} = 0$; $\Phi_2 = 0.05$) DME flames at an oxidizer strain rate $a_2 = 200 \text{ s}^{-1}$. Plots are result of the numerical analysis using the San Diego mechanism.
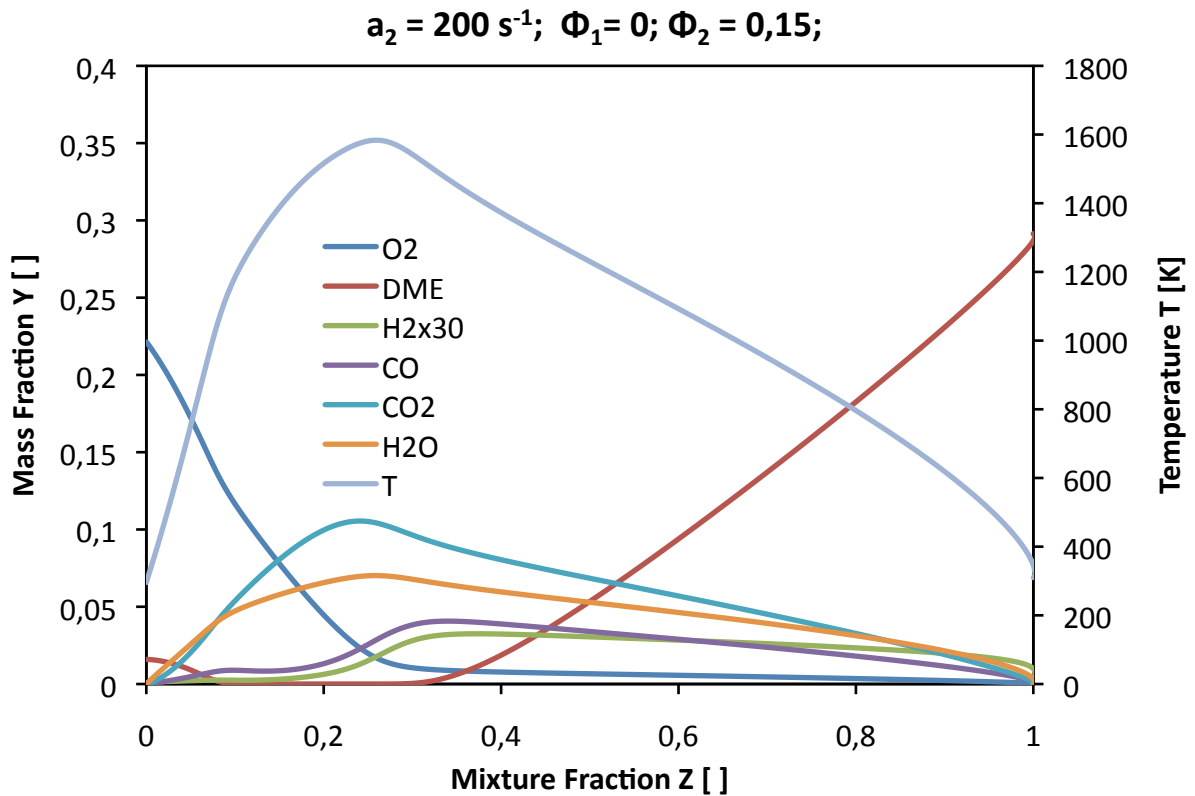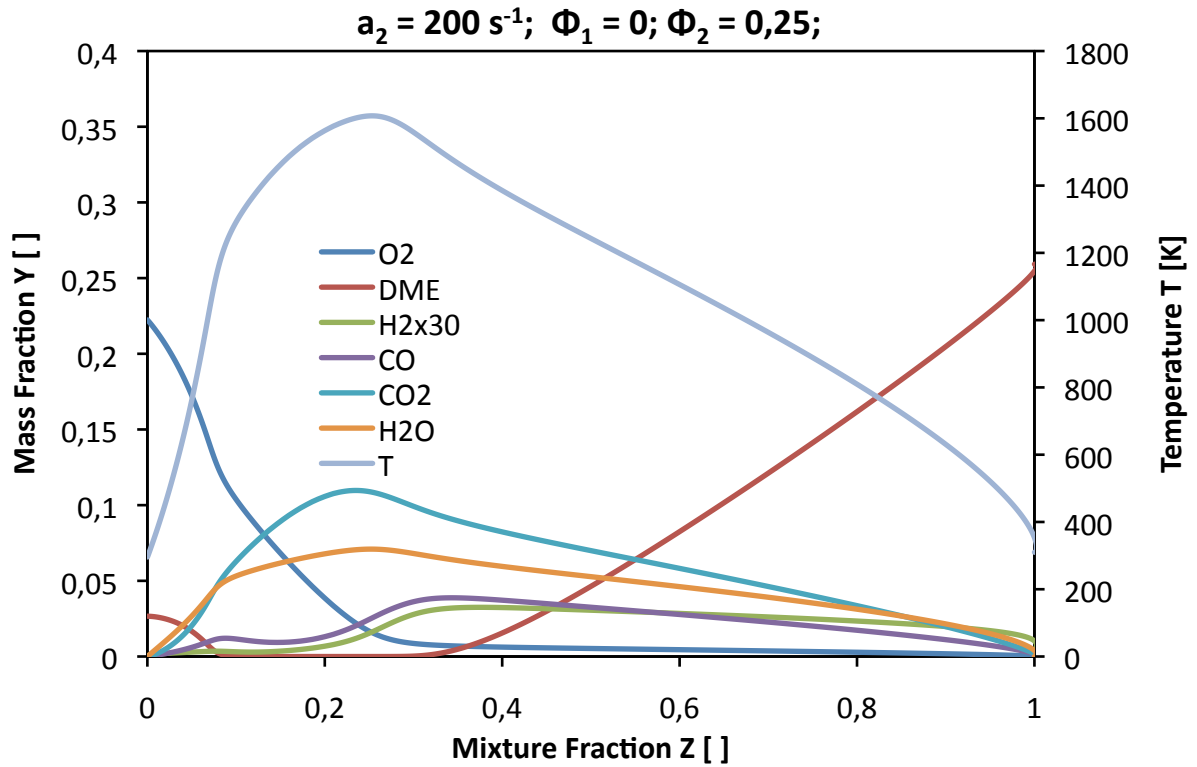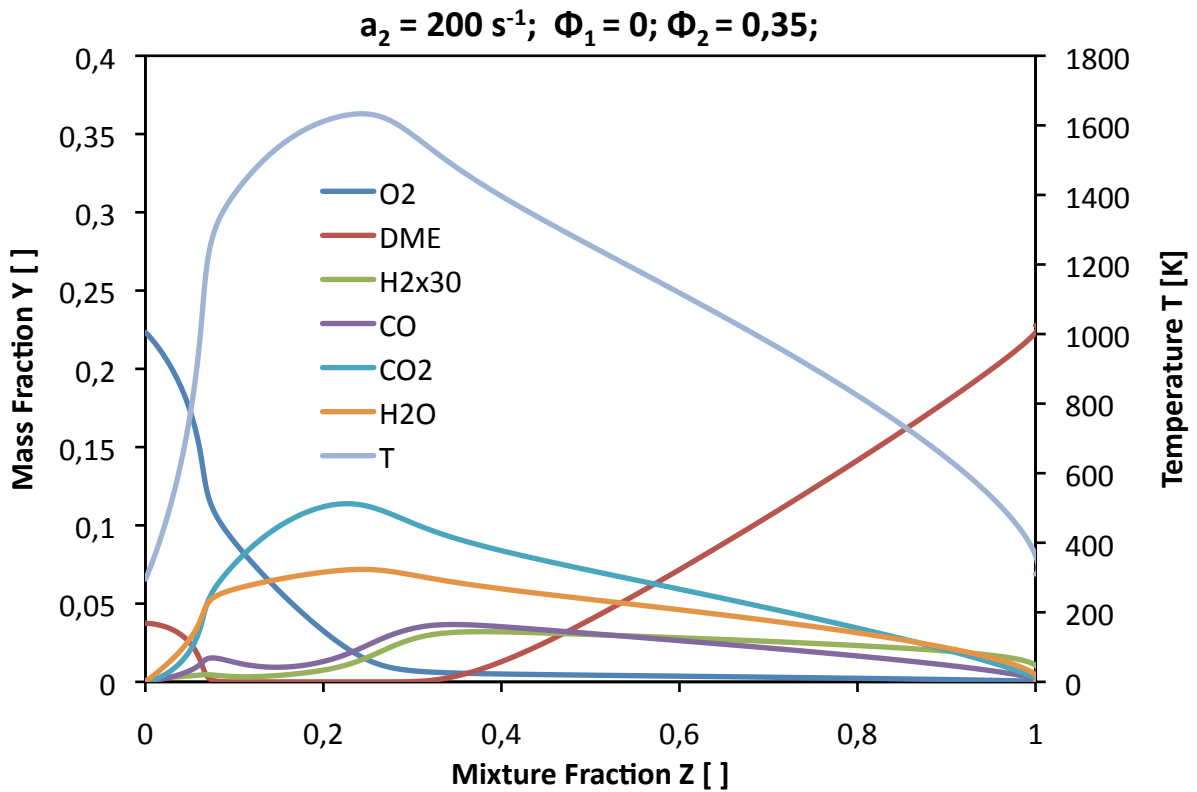

Figure 5.9: Plot of mass fractions Y_{O2}, Y_{DME}, Y_{H2} x 30, Y_{CO}, Y_{CO2}, Y_{H2O} and the flame Temperature T as function of the mixture fraction Z of partial premixed ($\Phi_1^{-1} = 0$; $\Phi_2 = 0.15$) DME flames at an oxidizer strain rate $a_2 = 200 \text{ s}^{-1}$. Plots are result of the numerical analysis using the San Diego mechanism.

Figure 5.10: Plot of mass fractions Y_{O2}, Y_{DME}, Y_{H2} x 30, Y_{CO}, Y_{CO2}, Y_{H2O} and the flame Temperature T as function of the mixture fraction Z of partial premixed ($\Phi_1^{-1} = 0$; $\Phi_2 = 0{,}25$) DME flames at an oxidizer strain rate $a_2 = 200$ s^{-1}. Plots are result of the numerical analysis using the San Diego mechanism.

Figure 5.11: Plot of mass fractions Y_{O2}, Y_{DME}, Y_{H2} x 30, Y_{CO}, Y_{CO2}, Y_{H2O} and the flame Temperature T as function of the mixture fraction Z of partial premixed ($\Phi_1^{-1} = 0$; $\Phi_2 = 0{,}35$) DME flames at an oxidizer strain rate $a_2 = 200$ s^{-1}. Plots are result of the numerical analysis using the San Diego mechanism.

Figure 5.11 shows the O_2 mass fraction Y_{O2} at Z_{ST} = 0,318 together with the extinction strain rate as a function of the equivalence ratio of DME and oxygen in the oxidizer stream. The data is obtained by the numerical analysis using the San Diego mechansim. The symbols represent the results of the numerical analysis and the lines represent polynomial second order best - fit curves.

In this figure it is visible that the oxygen „leaking" at Z_{ST} is decreasing with higher levels of premixing in the oxidizer stream. This phenomenon implies that at higher levels of premixing more oxygen is consumed and as mentioned before the effect of enhanced consumption of oxygen promotes combustion and leads to a delayed extinction at higher oxidizer strain rates a_2. It can be seen in Figure 5.11 as the extinction strain rate a_2 is increasing at the same time the O_2 mass fraction Y_{O2} is decreasing.
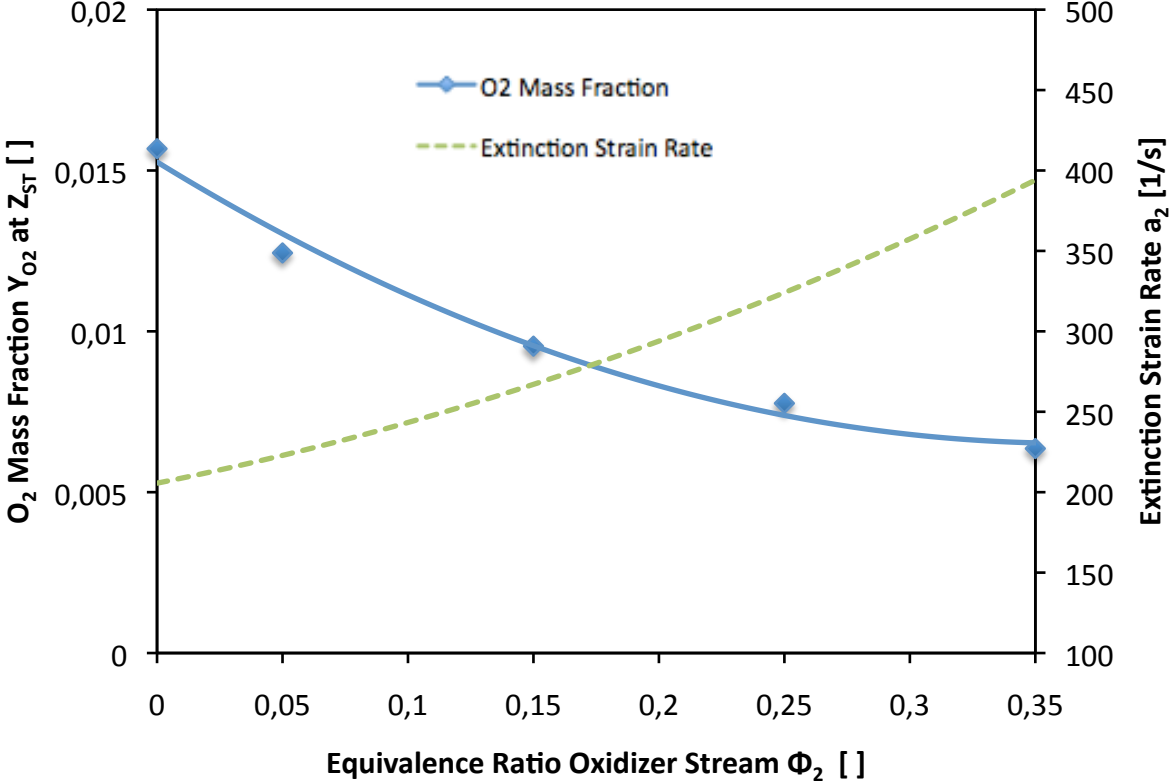
Figure 5.12: O_2 mass fraction Y_{O2} at Z_{ST} = 0,318 and extinction strain rate a_2 as a function of the equivalence ratio of the oxidizer stream (level of premixing). The symbols represent the numerical data of the San Diego mechanism, the lines are polynomial second order best-fit curves.

Case 2: Addition of Air to Fuel Stream

The following figures 5.13 – 5.15 on the following two pages show again plots of the mass fractions and the flame temperature for increased levels of premixing oxygen to the fuel stream from $\Phi_1^{-1} = 0,05$ up to $\Phi_1^{-1} = 0,25$.

By increasing the level of oxygen in the fuel stream changes are mainly visible at the plot of the oxygen mass fraction Y_{O2}. Higher levels of premixing lead to lower values of Y_{O2} at $Z = 0$ (oxidizer side) and to an increase of Y_{O2} for values of $Z > Z_{ST}$. The oxygen "leaking" at Z_{ST} stays almost constant and is not significantly decreasing until higher levels of premixing ($\Phi_1^{-1} = 0,25$). This phenomon can be seen more detailed in figure 5.16 later.

In comparison to the addition of DME to the oxidizer stream you can see that DME is completely consumed from $Z = 0$ to $Z = Z_{ST}$. Similar to that in the non-premixed case there is one layer where H_2 (green) and CO (purple) are formed by consuming DME and on the left hand side of this layer there is another one where H_2O (orange) and and CO_2 (turquoise) are formed by consuming H_2 and CO. Both of this layers are located in the same areas as in the non premixed case where their mass fractions are increasing to their maximum amounts.

The plot of the flame temperature shows the same trend as in the non-premixed case. The maximum temperature occurs still in the same region but increases by more than 100 K from $\Phi_1^{-1} = 0$ to $\Phi_1^{-1} = 0,25$ and shows even higher values then than in the case of addition of DME to the oxidizer stream.
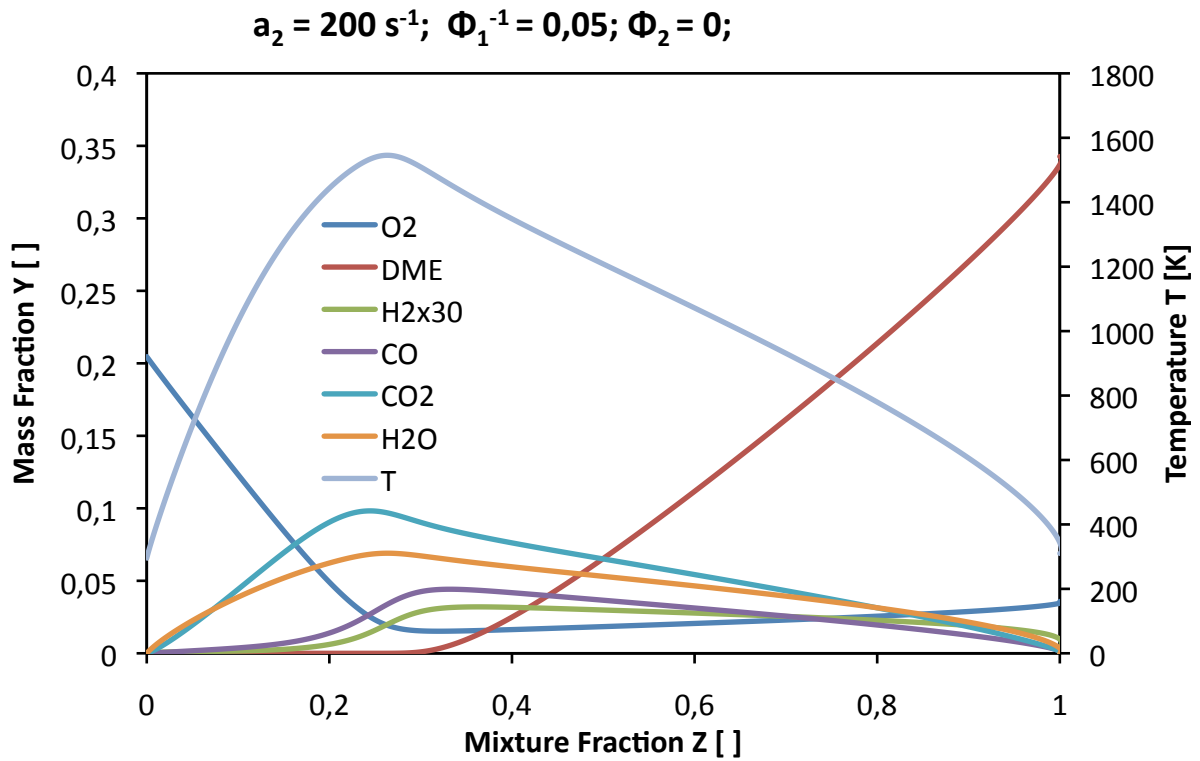
Figure 5.13: Plot of mass fractions Y_{O2}, Y_{DME}, Y_{H2} x 30, Y_{CO}, Y_{CO2}, Y_{H2O} and the flame Temperature T as function of the mixture fraction Z of partial premixed (Φ_1^{-1} = 0,05; Φ_2 = 0) DME flames at an oxidizer strain rate a_2 = 200 s^{-1}. Plots are result of the numerical analysis with the San Diego mechanism.
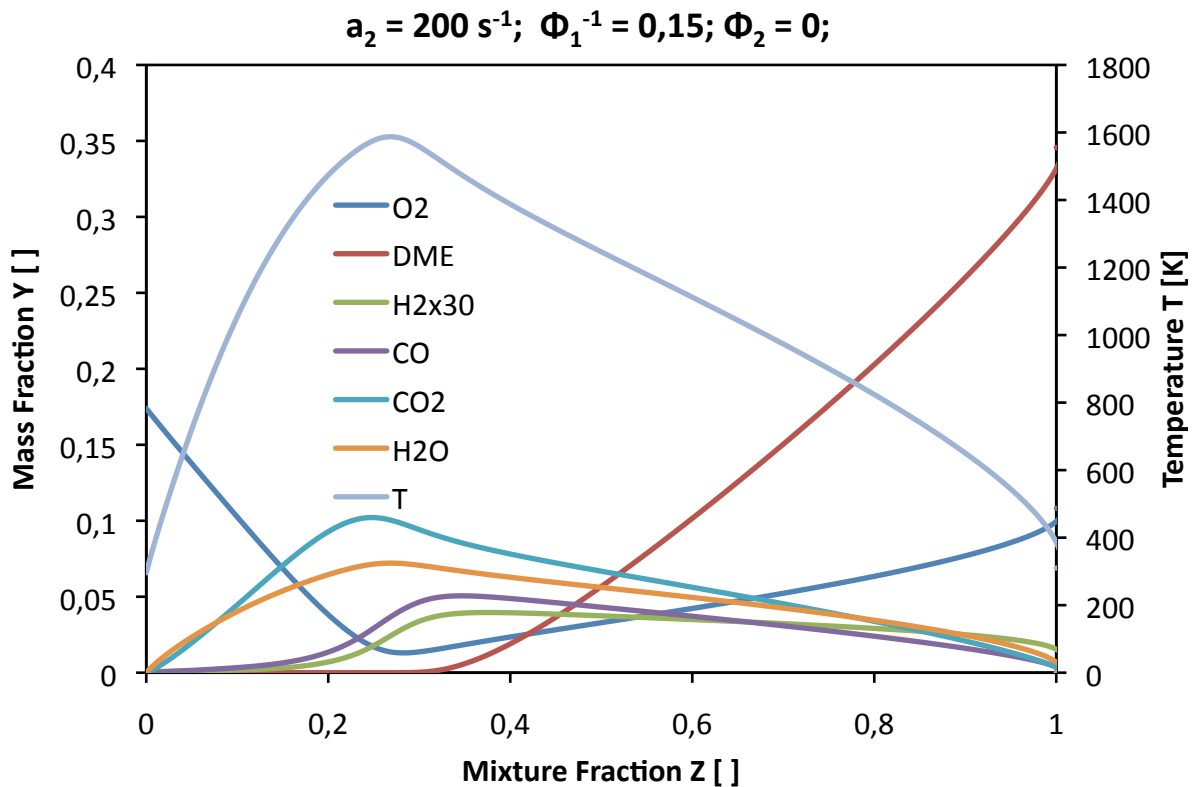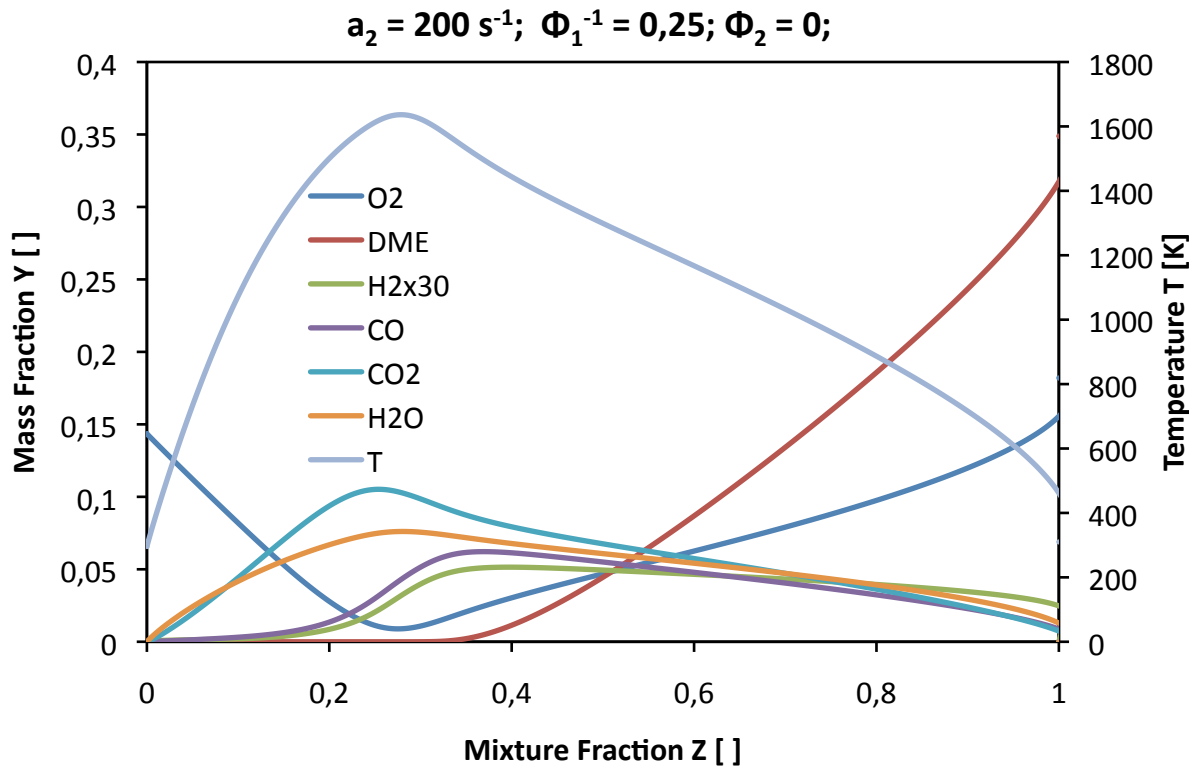

Figure 5.14: Plot of mass fractions Y_{O2}, Y_{DME}, Y_{H2} x 30, Y_{CO}, Y_{CO2}, Y_{H2O} and the flame Temperature T as function of the mixture fraction Z of partial premixed (Φ_1^{-1} = 0,15; Φ_2 = 0) DME flames at an oxidizer strain rate a_2 = 200 s^{-1}. Plots are result of the numerical analysis with the San Diego mechanism.

Figure 5.15: Plot of mass fractions Y_{O2}, Y_{DME}, Y_{H2} x 30, Y_{CO}, Y_{CO2}, Y_{H2O} and the flame Temperature T as function of the mixture fraction Z of partial premixed ($\Phi_1^{-1} = 0,25$; $\Phi_2 = 0$) DME flames at an oxidizer strain rate $a_2 = 200$ s^{-1}. Plots are result of the numerical analysis with the San Diego mechanism.

The following figure shows that the oxygen „leaking" at Z_{ST} is almost constant up to values of $\Phi_1^{-1} = 0{,}15$ and then slightly decreases for higher levels of premixing. At the same time the extinction strain rate a_2 is increasing slightly and it can be seen that the level of increase is linked to the level of decrease in oxygen "leaking". As in case 1 the decreasing oxygen „leaking" means that more oxygen is consumed and therefore we have a delayed extinction at higher oxidizer strain rates a_2.
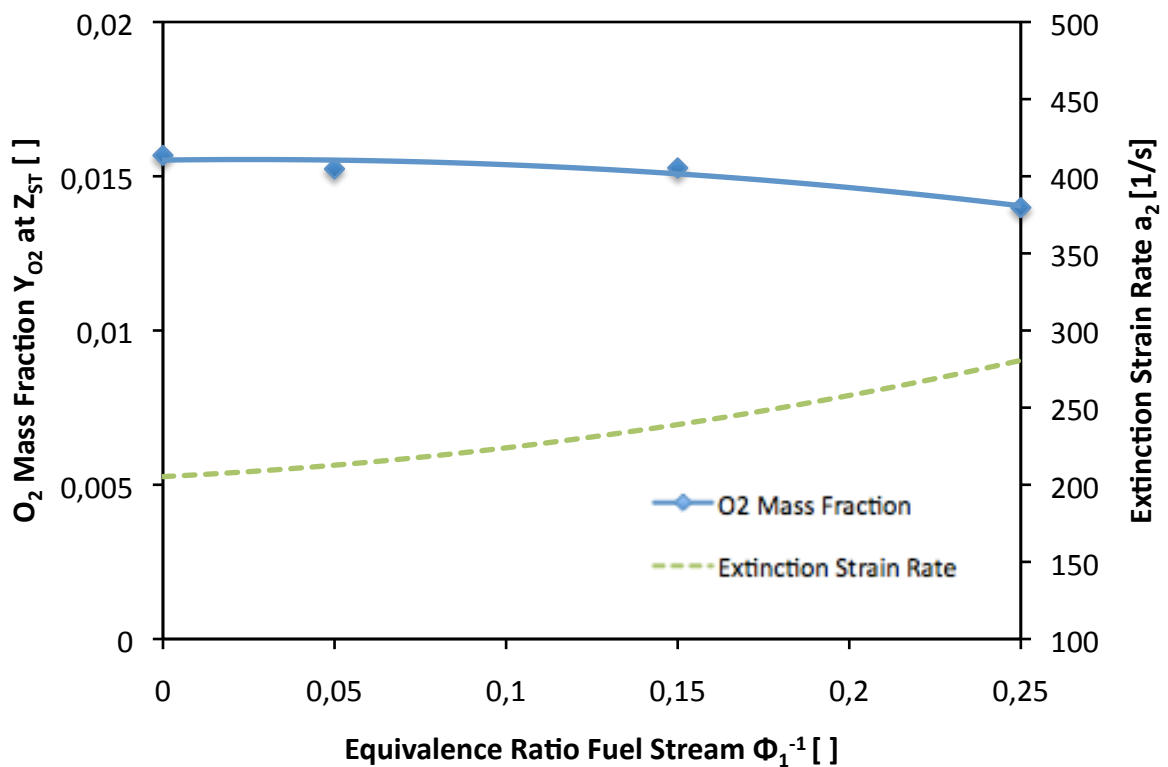
Figure 5.16: O_2 mass fraction Y_{O2} at Z_{ST} = 0,318 and extinction strain rate a_2 as a functions of the inverted equivalence ratio Φ_1^{-1} of the fuel stream (level of premixing). The symbols represent the numerical data of the San Diego mechanism, the lines are polynomial second order best-fit curves.

5.4. Verification of New DME mechanism
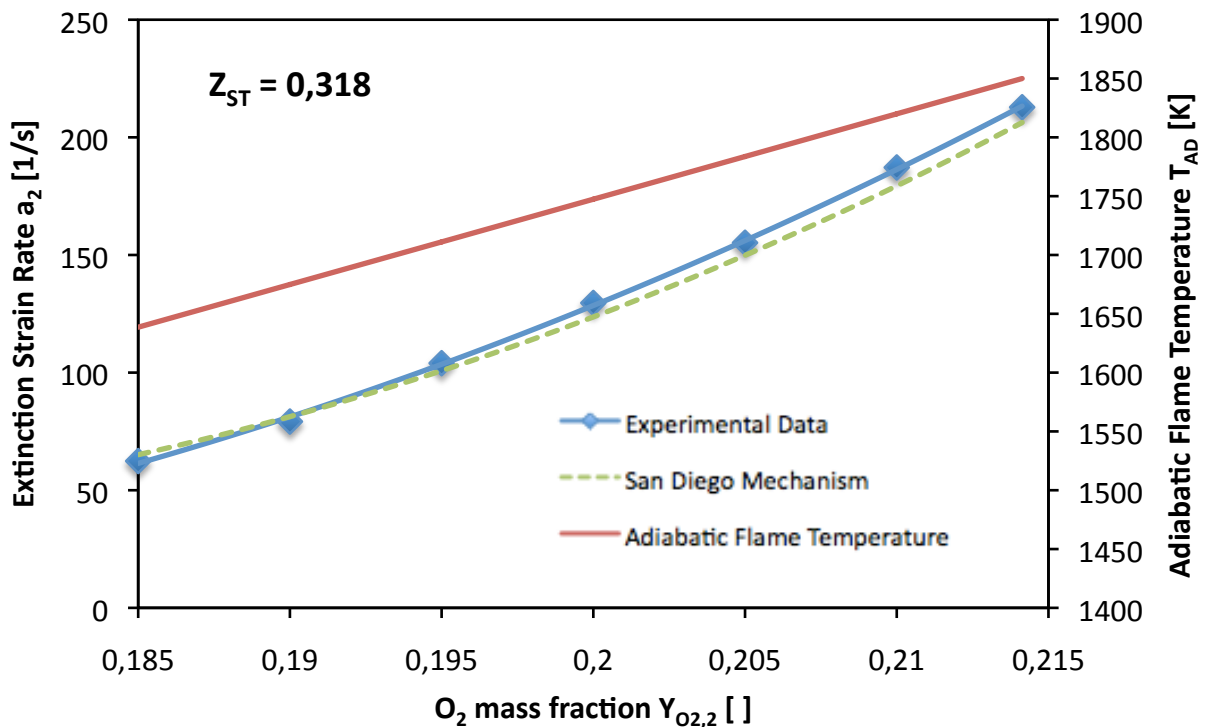
Figure 5.17: Verification of new short DME mechanism by UCSD combustion research group. The new DME mechanism is verified by comparing the numerical analysis with experiments of pure diffusion flames for a fixed stochiometric mixture fraction Z_{ST} = 0,318. The figure shows the extinction strain rate a_2 of the experiments and the numericaly analysis and the calculated adiabatic temperature T_{AD} as a function of O_2 mass fraction in the oxidizer stream $Y_{O2,2}$.

As the new developed short DME mechanism of the UCSD combustion research group showed a very well agreement with the experimental data for pure diffusion flames in the partial premixed investigations (non – premixed case; $\Phi_1^{-1} = 0$, $\Phi_2 = 0$) it was decided to verify its agreement with additional measurement points for diffusion flames. Starting from the non premixed case of the previous partial premixed experiments and a fixed stochiomtric mixture fraction Z_{ST} = 0,318 the O_2 mass fraction of the oxidizer stream $Y_{O2,2}$ is decreased in steps of 0,05 and all the related mass fractions of fuel and oxidizer stream are calculated according to 3.2.6.

The results obtained in 5.17 show the results of the experiments in comparison with the San Diego mechanism and the calculated adiabatic flame temperature T_{AD} as a function of the O_2 mass fraction $Y_{O2,2}$ in the oxidizer stream. The symbols represent the results of the experiment, the lines represent polyonomial second order best-fit-curves. Below a value of $Y_{O2,2}$ = 0,185 it was almost impossible to ignite the flame so this point was selected as starting point. The obtained data shows an almost perfect

65

agreement of the experimental results and the numerical simulation. Extinction strain rate a_2 and adiabatic temperature T_{AD} are both increasing with higher values of $Y_{O2,2}$.

6. Concluding Remarks

The main focus of this thesis was to get a better knowledge of the combustion behaviour of dimethyl ether. In the first part of this thesis the influence of mixing DME with iso-octane was investigated.

As it was not possible to ignite pure iso-octane fuel mixtures with the existing experimental site no complete conclusion can be made about autoignition of DME/iso-octane fuel mixtures. However, the experimental results show that for all strain rates the autoigntion temperature is rising by increasing the amount of iso-octane in the fuel mixture up to 50% iso-octane/ 50% DME.

For extinction of DME/iso-octane fuel mixtures the strain rate at extinction is found to be positively correleated to an increase of DME in the combustile mixture.

In the second part of this thesis the influence of partial premixing for extinction of DME flames was investigated. Partial premixing can be done both with DME in the oxidizer stream (fuel-lean boundary) or with oxygen in the fuel stream (fuel-rich boundary). The key observation is that addition of DME to the fuel-lean mixture enhance the overall recativity and an delayed extinction leads to higher values of the extinction strain rate while addition of oxygen to the fuel-rich mixture has little influence on the overall reactivity and the extinction strain rate stays nearly constant and increases only slightly for higher levels of premixing. Numerical calculations with the LLNL DME 2000 mechanism and a new short reaction mechanism for the combustion of dimethyl ether of the UCSD combustion research group show a good agreement with the experimental results. The numerical calculations of the San Diego mechanism show that for all values of Φ_2 and Φ_1^{-1}, DME is completely consumed in the reaction zone, while there is incomplete consumption of O_2. With increasing level of premixing in the oxidizer stream(increasing amounts of DME in the oxidizer stream) the consumption of O_2 increases. This is expected to be the reason for increasing reactivity.

The new developed short DME mechanism by the UCSD combustion research group showed although a very well agreement with the experimental reults for pure DME diffusion flames.

Bibiography

[1]   Bradley, D. and Entwistle, A.G. 1961. Determination of the emissivity, for total, radiation, of small diamert platinum-10% rhodium wires in the termperature range 600-1450 °C. *Br. J. Appl. Phys.* 12, 12 (1961), 708–711.

[2]   CHEMKIN 2013. *Getting Started Manual 10131, Reaction Design*, San Diego

[3]   CHEMKIN 2013. *Input Manual 10131, Reaction Design*, San Diego

[4]   CHEMKIN 2013. *Theory Manual 10131, Reaction Design*, San Diego

[5]   Dabelstein, W., Reglitzky, A., Schütze, A. and Reders, K. 2000. Automotive Fuels. *Ullmann's Encyclopedia of Industrial Chemistry*. Wiley-VCH Verlag GmbH & Co. KGaA.

[6]   Erdener, H., Arinan, A. and Orman, S. 2012. Future Fossil Fuel Alternative; DME (A review). *International Journal of Renewable Energy Research (IJRER)*. 1, 4 (2012), 252–258.

[7]   Humer, S.H. 2007. *Development of a surrogate diesel fuel,* Vienna, Austria

[8]   Incropera, F.P., DeWitt, D.P., Bergman, T.L. and Lavine, A.S. 2012. *Principles of Heat and Mass Transfer*. John Wiley & Sons, Hoboken,NJ.

[9]   Kee, R.J., Rupley, F.M., Meeks, E. and Miller, J.A. 1996. *CHEMKIN-III: A Fortran Chemical Kinetics Package for the Analysis of Gas Phase Chemical and Plasma Kinetics," Sandia National Laboratories Report*.

[10]   Mills, A.F. 1999. *Heat transfer*. Prentice Hall, Upper Saddle River, NJ.

[11]   Niemann, U., Seshadri, K. and Williams, F.A. Accuracies of laminar counterflow flame experiments. *Combustion and Flame*.

[12]   NIST Chemistry WebBook: *http://webbook.nist.gov/chemistry/*. Accessed: 2014-10-17.

[13]   Ogawa, T., Inoue, N., Shikada, T. and Ohno, Y. 2003. Direct dimethyl ether synthesis. *Journal of natural gas chemistry*. 12, 4 (2003), 219–227.

[14]   OMEGA   Engineering   Thermocouple   Reference   Tables   URL http://www.omega.com/section/thermocouples.html. Accessed: 2015-01-14.

[15]   Peters, N. 2010. *Combustion Theory. CEFRC Summer School*. Princeton.

[16]   Peters, N. *Technische Verbrennung I*. RWTH Aachen.

[17]   Prince, J.C. and Williams, F.A. A short reaction mechanism for the combustion of dimethyl-ether. *Private communication*

[18]   Ranzi, E., Dente, M., Goldaniga, A., Bozzano, G. and Faravelli, T. 2001. Lumping procedures in detailed kinetic modeling of gasification, pyrolysis, partial oxidation and combustion of hydrocarbon mixtures. *Progress in Energy and Combustion Science*. 27, 1 (Jan. 2001), 99–139.

[19]   Ritter   TG-Series   Operation   Instructions,   2010.   URL http://www.ritter.de/fileadmin/download/public/EN/Manuals/RITTER-EN-Manual-P01-TG.pdf. Accesed: 2015-02-12.

[20]   Seiser, R. *Nonpremixed Combustion of Liquid Hydrocarbon Fuels*, Graz, Austria.

[21]   Seiser, R., Seshadri, K., Piskernik, E. and Liñán, A. 2000. Ignition in the viscous layer between counterflowing streams: asymptotic theory with comparison to experiments. *Combustion and Flame*. 122, 3 (Aug. 2000), 339–349.

[22]   Seiser, R., Truett, L. and Seshadri, K. 2002. Extinction of partially premixed flames. *Proceedings of the Combustion Institute*. 29, 2 (2002), 1551–1557.

[23]   Semelsberger, T.A., Borup, R.L. and Greene, H.L. 2006. Dimethyl ether (DME) as an alternative fuel. *Journal of Power Sources*. 156, 2 (Jun. 2006), 497–511.

[24]   Seshadri, K. and Williams, F.A. 1978. Laminar flow between parallel plates with injection of a reactant at high reynolds number. *International Journal of Heat and Mass Transfer*. 21, 2 (Feb. 1978), 251–253.

[25]   Shaddix, C.R. 1999. CORRECTING THERMOCOUPLE MEASUREMENTS FOR RADIATION LOSS: A CRITICAL REVIEW. 33rd National Heat Transfer Conference (Aug. 1999).

[26]   Totten, G.E., Westbrook, S.R. and Shah, R.J. eds. 2003. *Fuels and lubricants handbook: technology, properties, performance, and testing*. ASTM International.

[27]   Tsuji, H. 1982. Counterflow diffusion flames. *Progress in Energy and Combustion Science*. 8, 2 (1982), 93–119.

[28]   Turns, S. 2011. *An Introduction to Combustion: Concepts and Applications*. McGraw-Hill Science/Engineering/Math.

[29]   Williams, F.A. 1994. *Combustion Theory: Second Edition*. Westview Press.

[30]   Williams, F.A. 2014. *Unexpected Discovery of Cool Flames in Experiments on the International Space Station*.

List of Figures

List of Tables

A. Appendix A

A.1. Experimental Data Autoignition of DME/Iso-Octane Fuel Mixtures

a₂ [1/s]	a₁ [1/s]	ρ₂ [kg/m³]	ρ₁ [kg/m³]	v₂ [m/s]	v₁ [m/s]	T₂ [K]	T₁ [K]	$Y_{O2,2}$ []	$Y_{N2,2}$ []	$Y_{DME,1}$ []	$Y_{ISO,1}$ []	$Y_{N2,1}$ []
82,759	45,522	0,322234	1,065012	0,3	0,1650	1094,6	379,81	0,233	0,767	0,4	0	0,6
124,138	67,567	0,318171	1,073998	0,45	0,2449	1108,58	376,83	0,233	0,767	0,4	0	0,6
165,517	89,615	0,314983	1,074504	0,6	0,3249	1119,8	376,47	0,233	0,767	0,4	0	0,6
206,897	111,301	0,311052	1,074834	0,75	0,4035	1133,95	376,31	0,233	0,767	0,4	0	0,6
248,276	132,691	0,306698	1,073729	0,9	0,4810	1150,05	376,52	0,233	0,767	0,4	0	0,6
82,759	44,795	0,319476	1,090447	0,3	0,1624	1104,05	384,17	0,233	0,767	0,32	0,08	0,6
124,138	66,471	0,317078	1,105885	0,45	0,2410	1117,4	378,91	0,233	0,767	0,32	0,08	0,6
165,517	87,681	0,310956	1,108091	0,6	0,3178	1134,3	377,95	0,233	0,767	0,32	0,08	0,6
206,897	108,666	0,306059	1,109487	0,75	0,3939	1152,45	377,45	0,233	0,767	0,32	0,08	0,6
248,276	129,412	0,301352	1,109165	0,9	0,4691	1170,45	377,52	0,233	0,767	0,32	0,08	0,6
82,759	43,709	0,318122	1,140465	0,3	0,1584	1108,75	380,88	0,233	0,767	0,24	0,16	0,6
124,138	64,955	0,313583	1,145332	0,45	0,2355	1124,8	379,33	0,233	0,767	0,24	0,16	0,6
165,517	85,848	0,307755	1,144011	0,6	0,3112	1143,1	379,64	0,233	0,767	0,24	0,16	0,6
206,897	106,628	0,304553	1,146638	0,75	0,3865	1158,15	378,95	0,233	0,767	0,24	0,16	0,6
248,276	127,214	0,300415	1,144260	0,9	0,4611	1174,1	379,87	0,233	0,767	0,24	0,16	0,6
82,759	44,507	0,315518	1,090924	0,3	0,1613	1111,3	405,57	0,233	0,767	0,2	0,2	0,6
124,138	65,083	0,311451	1,133090	0,45	0,2359	1129,75	390,49	0,233	0,767	0,2	0,2	0,6
165,517	85,690	0,307460	1,147139	0,6	0,3106	1147,2	385,77	0,233	0,767	0,2	0,2	0,6
206,897	106,205	0,302814	1,149195	0,75	0,3850	1164,8	385,11	0,233	0,767	0,2	0,2	0,6
248,276	126,647	0,298597	1,147538	0,9	0,4591	1181,25	385,57	0,233	0,767	0,2	0,2	0,6
124,138	63,969	0,313806	1,181753	0,45	0,2319	1127,2	381,41	0,233	0,767	0,16	0,24	0,6
165,517	84,798	0,307795	1,172661	0,6	0,3074	1145,95	384,56	0,233	0,767	0,16	0,24	0,6
206,897	105,427	0,303361	1,168318	0,75	0,3822	1162,7	386,08	0,233	0,767	0,16	0,24	0,6
248,276	125,590	0,298534	1,166682	0,9	0,4553	1181,5	386,50	0,233	0,767	0,16	0,24	0,6
248,276	124,026	0,300326	1,203477	0,9	0,4496	1183,75	382,17	0,233	0,767	0,12	0,28	0,6

a_2 [1/s]	a_1 [1/s]	ρ_2 [kg/m³]	ρ_1 [kg/m³]	V_2 [m/s]	V_1 [m/s]	T_2 [K]	T_1 [K]	$Y_{O2,2}$ []	$Y_{N2,2}$ []	$Y_{DME,1}$ []	$Y_{ISO,1}$ []	$Y_{N2,1}$ []
84	85,81	1,19151	1,14182	0,26250	0,26815	296	367,13	0,2324	0,7676	0	0,2471	0,7529
83,2	85,02	1,19151	1,14106	0,26000	0,26569	296	367,50	0,2324	0,7676	0	0,2471	0,7529
80	81,88	1,19151	1,13741	0,25000	0,25588	296	368,78	0,2324	0,7676	0	0,2471	0,7529
80,8	82,87	1,19151	1,13279	0,25250	0,25896	296	370,40	0,2324	0,7676	0	0,2471	0,7529
80	82,10	1,19151	1,13132	0,25000	0,25656	296	370,60	0,2324	0,7676	0	0,2471	0,7529
113,6	117,41	1,19125	1,11524	0,35500	0,36690	296	373,49	0,2309	0,7691	0,025	0,2266	0,7484
112	115,52	1,19125	1,11979	0,35000	0,36099	296	371,93	0,2309	0,7691	0,025	0,2266	0,7484
110,4	113,78	1,19125	1,12160	0,34500	0,35555	296	371,31	0,2309	0,7691	0,025	0,2266	0,7484
112	115,38	1,19125	1,12245	0,35000	0,36057	296	370,94	0,2309	0,7691	0,025	0,2266	0,7484
111,2	114,58	1,19125	1,12201	0,34750	0,35806	296	371,12	0,2309	0,7691	0,025	0,2266	0,7484
124,8	129,77	1,19099	1,10157	0,39000	0,40552	296	375,70	0,2294	0,7706	0,05	0,2060	0,7440
124	129,10	1,19099	1,09880	0,38750	0,40343	296	376,26	0,2294	0,7706	0,05	0,2060	0,7440
123,2	128,36	1,19099	1,09723	0,38500	0,40111	296	376,95	0,2294	0,7706	0,05	0,2060	0,7440
124	129,15	1,19099	1,09797	0,38750	0,40358	296	376,70	0,2294	0,7706	0,05	0,2060	0,7440
123,2	127,82	1,19099	1,10647	0,38500	0,39943	296	373,61	0,2294	0,7706	0,05	0,2060	0,7440
144	149,96	1,19072	1,09800	0,45000	0,46862	296	373,91	0,2279	0,7721	0,075	0,1855	0,7395
146,4	152,73	1,19072	1,09408	0,45750	0,47728	296	375,21	0,2279	0,7721	0,075	0,1855	0,7395
144,8	151,27	1,19072	1,09104	0,45250	0,47272	296	376,63	0,2279	0,7721	0,075	0,1855	0,7395
145,6	152,18	1,19072	1,08999	0,45500	0,47556	296	376,73	0,2279	0,7721	0,075	0,1855	0,7395
147,2	153,66	1,19072	1,09267	0,46000	0,48020	296	375,77	0,2279	0,7721	0,075	0,1855	0,7395
160	167,74	1,19045	1,08313	0,50000	0,52418	296	376,24	0,2263	0,7737	0,1	0,1650	0,7350
158,4	165,96	1,19045	1,08444	0,49500	0,51863	296	376,06	0,2263	0,7737	0,1	0,1650	0,7350
158,4	166,03	1,19045	1,08361	0,49500	0,51883	296	376,34	0,2263	0,7737	0,1	0,1650	0,7350
160	167,98	1,19045	1,08004	0,50000	0,52493	296	377,50	0,2263	0,7737	0,1	0,1650	0,7350
160	168,16	1,19045	1,07777	0,50000	0,52549	296	378,66	0,2263	0,7737	0,1	0,1650	0,7350
179,2	189,84	1,19018	1,06048	0,56000	0,59326	296	381,93	0,2248	0,7752	0,125	0,1444	0,7306

179,2	189,54	1,19018	1,06388	0,56000	0,59231	296	380,72	0,2248	0,7752	0,125	0,1444	0,7306
176,8	186,74	1,19018	1,06687	0,55250	0,58356	296	379,84	0,2248	0,7752	0,125	0,1444	0,7306
179,2	188,99	1,19018	1,07004	0,56000	0,59060	296	378,51	0,2248	0,7752	0,125	0,1444	0,7306
177,6	187,47	1,19018	1,06818	0,55500	0,58584	296	379,29	0,2248	0,7752	0,125	0,1444	0,7306
192,8	203,59	1,18992	1,06712	0,60250	0,63622	296	377,15	0,2233	0,7767	0,15	0,1239	0,7261
192	202,52	1,18992	1,06946	0,60000	0,63289	296	376,13	0,2233	0,7767	0,15	0,1239	0,7261
192,8	203,16	1,18992	1,07166	0,60250	0,63487	296	375,57	0,2233	0,7767	0,15	0,1239	0,7261
192	202,52	1,18992	1,06946	0,60000	0,63289	296	376,13	0,2233	0,7767	0,15	0,1239	0,7261
192,8	203,16	1,18992	1,07166	0,60250	0,63487	296	375,57	0,2233	0,7767	0,15	0,1239	0,7261
190,4	199,78	1,18992	1,08085	0,59500	0,62430	296	372,34	0,2233	0,7767	0,15	0,1239	0,7261
192	201,87	1,18992	1,07639	0,60000	0,63085	296	373,84	0,2233	0,7767	0,15	0,1239	0,7261
192,8	203,16	1,18992	1,07166	0,60250	0,63487	296	375,57	0,2233	0,7767	0,15	0,1239	0,7261
206,4	220,85	1,18966	1,03904	0,64500	0,69017	296	384,67	0,2218	0,7782	0,175	0,1034	0,7216
205,6	219,30	1,18966	1,04564	0,64250	0,68532	296	382,61	0,2218	0,7782	0,175	0,1034	0,7216
204,8	217,70	1,18966	1,05286	0,64000	0,68031	296	379,78	0,2218	0,7782	0,175	0,1034	0,7216
205,6	219,30	1,18966	1,04564	0,64250	0,68532	296	382,61	0,2218	0,7782	0,175	0,1034	0,7216
204	216,58	1,18966	1,06375	0,64000	0,67682	296	376,12	0,2218	0,7782	0,175	0,1034	0,7216
205,6	217,95	1,18966	1,05863	0,64250	0,68110	296	378,27	0,2218	0,7782	0,175	0,1034	0,7216
204,8	217,70	1,18966	1,05286	0,64000	0,68031	296	379,78	0,2218	0,7782	0,175	0,1034	0,7216
222,4	236,93	1,18940	1,04803	0,69500	0,74039	296	378,83	0,2203	0,7797	0,2	0,0829	0,7171
222,4	237,48	1,18940	1,04311	0,69500	0,74214	296	380,60	0,2203	0,7797	0,2	0,0829	0,7171
221,6	235,88	1,18940	1,04974	0,69250	0,73713	296	378,11	0,2203	0,7797	0,2	0,0829	0,7171
220,8	233,89	1,18940	1,06003	0,69000	0,73089	296	374,41	0,2203	0,7797	0,2	0,0829	0,7171
220,8	233,74	1,18940	1,06138	0,69000	0,73043	296	374,32	0,2203	0,7797	0,2	0,0829	0,7171
236,8	255,37	1,18912	1,02245	0,74000	0,79804	296	385,47	0,2187	0,7813	0,225	0,0623	0,7127
236,8	254,91	1,18912	1,02615	0,74000	0,79660	296	384,17	0,2187	0,7813	0,225	0,0623	0,7127
236,8	254,91	1,18912	1,02615	0,74000	0,79660	296	384,17	0,2187	0,7813	0,225	0,0623	0,7127
236,8	255,37	1,18912	1,02245	0,74000	0,79804	296	385,47	0,2187	0,7813	0,225	0,0623	0,7127
233,6	250,39	1,18912	1,03498	0,73000	0,78248	296	381,06	0,2187	0,7813	0,225	0,0623	0,7127
234,4	250,91	1,18912	1,03776	0,73250	0,78410	296	379,97	0,2187	0,7813	0,225	0,0623	0,7127
236,8	254,25	1,18912	1,03147	0,74000	0,79454	296	382,20	0,2187	0,7813	0,225	0,0623	0,7127
236,8	254,91	1,18912	1,02615	0,74000	0,79660	296	384,17	0,2187	0,7813	0,225	0,0623	0,7127
246,4	262,83	1,18886	1,04489	0,77000	0,82134	296	375,30	0,2172	0,7828	0,25	0,0418	0,7082
248	264,61	1,18886	1,04432	0,77500	0,82689	296	375,18	0,2172	0,7828	0,25	0,0418	0,7082
248	264,74	1,18886	1,04326	0,77500	0,82732	296	375,58	0,2172	0,7828	0,25	0,0418	0,7082
248	264,61	1,18886	1,04489	0,77500	0,82134	296	375,30	0,2172	0,7828	0,25	0,0418	0,7082
248,8	265,80	1,18886	1,04163	0,77750	0,83063	296	376,09	0,2172	0,7828	0,25	0,0418	0,7082
248	264,96	1,18886	1,04150	0,77500	0,82801	296	376,39	0,2172	0,7828	0,25	0,0418	0,7082
268,8	288,06	1,18860	1,03500	0,84000	0,90018	296	376,14	0,2157	0,7843	0,275	0,0213	0,7037
268,8	288,06	1,18860	1,03500	0,83750	0,89718	296	375,96	0,2157	0,7843	0,275	0,0213	0,7037
248	264,96	1,18886	1,04150	0,77500	0,82801	296	376,39	0,2172	0,7828	0,25	0,0418	0,7082
268	287,10	1,18860	1,03574	0,83500	0,89718	296	375,96	0,2157	0,7843	0,275	0,0213	0,7037
267,2	286,04	1,18860	1,03715	0,83500	0,89389	296	375,35	0,2157	0,7843	0,275	0,0213	0,7037
266,4	285,13	1,18860	1,03759	0,83250	0,89102	296	375,03	0,2157	0,7843	0,275	0,0213	0,7037

265,6	284,15	1,18860	1,03845	0,83000	0,88798	296	374,82	0,2157	0,7843	0,275	0,0213	0,7037
287,2	309,19	1,18834	1,02533	0,89750	0,96621	296	377,11	0,2142	0,7858	0,3	0,0008	0,6992
288	309,83	1,18834	1,02677	0,90000	0,96823	296	376,73	0,2142	0,7858	0,3	0,0008	0,6992
288	309,73	1,18834	1,02743	0,90000	0,96791	296	376,49	0,2142	0,7858	0,3	0,0008	0,6992
284,8	306,02	1,18834	1,02928	0,89000	0,95630	296	375,54	0,2142	0,7858	0,3	0,0008	0,6992
286,4	307,50	1,18834	1,03087	0,89500	0,96093	296	375,28	0,2142	0,7858	0,3	0,0008	0,6992

A.3. Experimental Data Partial Premixed DME Flames

Case 1: Addition of DME at oxidizer stream

a_2 [1/s]	a_1 [1/s]	ρ_2 [kg/m³]	ρ_1 [kg/m³]	v_2 [m/s]	v_1 [m/s]	T_2 [K]	T_1 [K]	$Y_{O2,2}$ []	$Y_{N2,2}$ []	$Y_{DME,2}$ []	$Y_{N2,1}$ []	$Y_{DME,1}$ []	$Y_{O2,1}$ []
217,60	204,76	1,1725	1,3241	0,6800	0,6399	300	292,02	0,214133	0,785867	0,000000	0,699075	0,300925	0
217,60	204,83	1,1725	1,3233	0,6800	0,6401	300	292,20	0,214133	0,785867	0,000000	0,699075	0,300925	0
216,80	204,12	1,1725	1,3227	0,6775	0,6379	300	292,37	0,214133	0,785867	0,000000	0,699075	0,300925	0
216,80	204,12	1,1725	1,3227	0,6775	0,6379	300	292,39	0,214133	0,785867	0,000000	0,699075	0,300925	0
241,60	228,58	1,1749	1,3126	0,7550	0,7144	300	292,97	0,214133	0,780737	0,005130	0,712197	0,287803	0
241,60	228,62	1,1749	1,3121	0,7550	0,7143	300	292,89	0,214133	0,780737	0,005130	0,712197	0,287803	0
240,80	227,90	1,1749	1,3117	0,7525	0,7122	300	292,67	0,214133	0,780737	0,005130	0,712197	0,287803	0
264,00	250,66	1,1774	1,3060	0,8250	0,7833	300	292,67	0,214133	0,775607	0,010260	0,725320	0,274680	0
267,20	253,57	1,1774	1,3074	0,8350	0,7924	300	292,39	0,214133	0,775607	0,010260	0,725320	0,274680	0
267,20	253,57	1,1774	1,3074	0,8350	0,7924	300	292,39	0,214133	0,775607	0,010260	0,725320	0,274680	0
307,20	292,81	1,1798	1,2986	0,9600	0,9150	300	292,67	0,214133	0,770477	0,015390	0,738442	0,261558	0
309,60	295,18	1,1798	1,2979	0,9675	0,9224	300	292,78	0,214133	0,770477	0,015390	0,738442	0,261558	0
309,60	295,21	1,1798	1,2976	0,9675	0,9225	300	292,85	0,214133	0,770477	0,015390	0,738442	0,261558	0
352,00	336,90	1,1823	1,2907	1,1125	1,0528	300	292,75	0,214133	0,765346	0,020521	0,751564	0,248436	0
352,00	336,97	1,1823	1,2901	1,1000	1,0530	300	292,88	0,214133	0,765346	0,020521	0,751564	0,248436	0
352,00	337,01	1,1823	1,2898	1,1000	1,0532	300	292,97	0,214133	0,765346	0,020521	0,751564	0,248436	0
402,40	386,82	1,1848	1,2821	1,2575	1,2088	300	293,03	0,214133	0,760216	0,025651	0,764686	0,235314	0
404,00	388,38	1,1848	1,2820	1,2625	1,2137	300	293,07	0,214133	0,760216	0,025651	0,764686	0,235314	0
403,20	387,66	1,1848	1,2817	1,2600	1,2114	300	293,12	0,214133	0,760216	0,025651	0,764686	0,235314	0
455,20	439,14	1,1873	1,2757	1,4225	1,3723	300	292,87	0,214133	0,755086	0,030781	0,777808	0,222192	0
454,40	438,36	1,1873	1,2757	1,4200	1,3699	300	292,86	0,214133	0,755086	0,030781	0,777808	0,222192	0
456,00	439,91	1,1873	1,2757	1,4250	1,3747	300	292,86	0,214133	0,755086	0,030781	0,777808	0,222192	0

Case 2: Addition of Oxygen to fuel stream

a_2 [1/s]	a_1 [1/s]	ρ_2 [kg/m³]	ρ_1 [kg/m³]	v_2 [m/s]	v_1 [m/s]	T_2 [K]	T_1 [K]	$Y_{O2,2}$ []	$Y_{N2,2}$ []	$Y_{DME,2}$ []	$Y_{N2,1}$ []	$Y_{DME,1}$ []	$Y_{O2,1}$ []
222,50	201,54	1,1725	1,3169	0,6675	0,6298	300	293,58	0,214133	0,785867	0	0,699075	0,300925	0,000000
222,50	201,53	1,1725	1,3171	0,6675	0,6298	300	293,57	0,214133	0,785867	0	0,699075	0,300925	0,000000
221,67	200,80	1,1725	1,3168	0,6650	0,6275	300	293,63	0,214133	0,785867	0	0,699075	0,300925	0,000000
221,67	199,68	1,1700	1,3288	0,6650	0,6240	300	292,45	0,199491	0,800509	0	0,667674	0,300925	0,031401
223,33	201,29	1,1700	1,3273	0,6700	0,6290	300	292,80	0,199491	0,800509	0	0,667674	0,300925	0,031401
221,67	199,89	1,1700	1,3261	0,6650	0,6246	300	293,10	0,199491	0,800509	0	0,667674	0,300925	0,031401
221,67	199,26	1,1675	1,3316	0,6650	0,6227	300	293,35	0,184849	0,815151	0	0,636272	0,300925	0,062803
220,83	198,54	1,1675	1,3312	0,6625	0,6204	300	293,39	0,184849	0,815151	0	0,636272	0,300925	0,062803
220,83	198,57	1,1675	1,3308	0,6625	0,6205	300	293,50	0,184849	0,815151	0	0,636272	0,300925	0,062803
222,50	198,84	1,1650	1,3443	0,6675	0,6214	300	292,07	0,170207	0,829793	0	0,604871	0,300925	0,094204
224,17	200,39	1,1650	1,3435	0,6725	0,6262	300	292,23	0,170207	0,829793	0	0,604871	0,300925	0,094204
224,17	200,46	1,1650	1,3427	0,6725	0,6264	300	292,38	0,170207	0,829793	0	0,604871	0,300925	0,094204
226,67	201,95	1,1625	1,3497	0,6800	0,6311	300	292,41	0,155566	0,844434	0	0,573469	0,300925	0,125606
225,83	201,39	1,1625	1,3473	0,6775	0,6293	300	292,90	0,155566	0,844434	0	0,573469	0,300925	0,125606
227,50	202,95	1,1625	1,3463	0,6825	0,6342	300	293,09	0,155566	0,844434	0	0,573469	0,300925	0,125606
236,67	210,17	1,1601	1,3557	0,7100	0,6568	300	292,61	0,140925	0,859075	0	0,542067	0,300925	0,157008
236,67	210,23	1,1601	1,3549	0,7100	0,6570	300	292,79	0,140925	0,859075	0	0,542067	0,300925	0,157008
235,00	208,80	1,1601	1,3542	0,7050	0,6525	300	292,91	0,140925	0,859075	0	0,542067	0,300925	0,157008

A.4. Experimental Data Verification of New DME Mechanism for Diffusion Flames

| a_2 [1/s]	a_1 [1/s]	ρ_2 [kg/m³]	ρ_1 [kg/m³]	V_2 [m/s]	V_1 [m/s]	T_2 [K]	T_1 [K]	$Y_{O2,2}$ [-]	$Y_{N2,2}$ [-]	$Y_{DME,1}$ [-]	$Y_{N2,1}$ [-]
212,00	199,50	1,1725	1,3240	0,6625	0,6234	300	292,05	0,2141	0,7859	0,300925	0,699075
212,80	200,33	1,1725	1,3231	0,6650	0,6260	300	292,30	0,2141	0,7859	0,300925	0,699075
212,80	200,40	1,1725	1,3220	0,6650	0,6263	300	292,47	0,2141	0,7859	0,300925	0,699075
187,20	176,83	1,1718	1,3133	0,5850	0,5526	300	293,66	0,2100	0,7900	0,29512	0,70488
188,00	177,57	1,1718	1,3134	0,5875	0,5549	300	293,62	0,2100	0,7900	0,29512	0,70488
186,40	176,04	1,1718	1,3138	0,5825	0,5501	300	293,56	0,2100	0,7900	0,29512	0,70488
156,00	147,11	1,1709	1,3167	0,4875	0,4597	300	291,99	0,2050	0,7950	0,28809	0,71191
155,20	146,40	1,1709	1,3159	0,4850	0,4575	300	292,21	0,2050	0,7950	0,28809	0,71191
154,40	145,79	1,1709	1,3133	0,4825	0,4556	300	292,76	0,2050	0,7950	0,28809	0,71191
129,60	122,36	1,1701	1,3126	0,4050	0,3824	300	291,98	0,2000	0,8000	0,28106	0,71894
130,40	123,16	1,1701	1,3116	0,4075	0,3849	300	292,23	0,2000	0,8000	0,28106	0,71894
128,80	121,75	1,1701	1,3094	0,4025	0,3805	300	292,71	0,2000	0,8000	0,28106	0,71894
103,20	97,84	1,1692	1,3008	0,3225	0,3058	300	293,72	0,1950	0,8050	0,27404	0,72596
104,00	98,64	1,1692	1,2997	0,3250	0,3083	300	293,99	0,1950	0,8050	0,27404	0,72596
104,00	98,69	1,1692	1,2984	0,3250	0,3084	300	294,29	0,1950	0,8050	0,27404	0,72596
79,20	75,58	1,1684	1,2830	0,2475	0,2362	300	296,90	0,1900	0,8100	0,26701	0,73299
78,40	74,84	1,1684	1,2820	0,2450	0,2339	300	297,14	0,1900	0,8100	0,26701	0,73299
78,40	74,84	1,1684	1,2820	0,2450	0,2339	300		0,1900	0,8100	0,26701	0,73299
62,40	59,67	1,1675	1,2769	0,1950	0,1865	300	297,36	0,1850	0,8150	0,25998	0,74002
60,80	58,17	1,1675	1,2754	0,1900	0,1818	300	297,72	0,1850	0,8150	0,25998	0,74002

B. Appendix B

Following formulations of extinction and autoignition of iso-octane/Dimethylether in Nonuniformn flows under Nonpremixed Conditions and Extinction and Autoignition of Partially Premixed dimethyl ether Flames in Nonuniform flows were developed by Professor K. Seshadri. (2014 -2015)
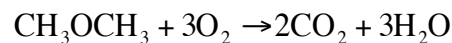
B.1. Extinction and Autoignition of Iso-Octane/Dimethyl-ether in Nonuniform Flows under Nonpremixed Conditions

Chemcial Reaction

The overall chemical reaction between iso-octane (C_8H_{18}) and O_2 is

$$C_8H_{18} + 12,5O_2 \rightarrow 8CO_2 + 9H_2O$$
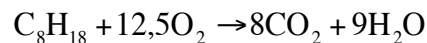
The reaction rate, ω_{ISO} with units of $1/(m^3/s)$. The overall chemcial reaction between dimethylether (CH_3OCH_3) and O_2 is

$$CH_3OCH_3 + 3O_2 \rightarrow 2CO_2 + 3H_2O$$

The reaction rate, ω_{DME} with units of $1/(m^3/s)$

Formulation

Consider two counterflowing streams flowing toward a stagnation plane. One stream called fuel stream is made up of C_8H_{18}, CH_3OCH_3 and N_2 and the other stream, called the oxidizer stream, is made up of O_2 and N_2. The mass fractions of iso-octane, dimethylether and oxygen are represented by Y_{ISO}, Y_{DME} and Y_{O_2} respectively. The mass fraction of C_8H_{18} and CH_3OCH_3 in the fuel stream respectevely are $Y_{ISO,1}$ and $Y_{DME,1}$ and that of O_2 in the oxidizer stream is $Y_{O_2,2}$.

The species balance equations are

$$\rho a \hat{x} \frac{dY_{ISO}}{d\hat{x}} + \rho D_{ISO} \frac{d^2 Y_{ISO}}{d\hat{x}^2} = W_{ISO} \omega_{ISO}$$

$$\rho a \hat{x} \frac{dY_{DME}}{d\hat{x}} + \rho D_{DME} \frac{d^2 Y_{DME}}{d\hat{x}^2} = W_{DME} \omega_{DME} \qquad (1)$$

$$\rho a \hat{x} \frac{dY_{O_2}}{d\hat{x}} + \rho D_{O_2} \frac{d^2 Y_{O_2}}{d\hat{x}^2} = 12{,}5 W_{DME} \omega_{DME} + 3 W_{O_2} \omega_{DME}$$

Here D_{DME} and D_{O_2} are respectevely the coeffecent of diffusion of CH_3OCH_3 and O_2. The energy conservation equation is

$$\rho c_p a \hat{x} \frac{dT}{d\hat{x}} + \lambda \frac{d^2 T}{d\hat{x}^2} + \sum_{i=1}^{n} \rho D_i c_{p,i} \frac{dY_i}{d\hat{x}} \frac{dT}{d\hat{x}} = -Q_{ISO} \omega_{ISO} - Q_{DME} \omega_{DME} \quad (2)$$

Here λ is the coefficient of thermal conductivity, c_p is the heat capacity of the mixture, $c_{p,i}$ is the heat capacity of species i, D_i is the coefficient of diffuion of species i, Q_{DME} is the heat released per mole of CH_3OCH_3 consumed.

Define the independent variable

$$x = \hat{x}(\rho c_p a / \lambda)^{1/2} \qquad (3)$$

For convenience, the definitions

$$X_i \equiv Y_i W_{N_2} / W_i$$
$$\tau \equiv \left(T - T_{REF}\right) \Delta T_{REF}$$
$$M_{ISO} \equiv W_{N_2} \omega_{ISO} / (\rho a)$$
$$M_{DME} \equiv W_{N_2} \omega_{DME} / (\rho a) \qquad (4)$$
$$G_{ISO} \equiv Q_{ISO} / \left(W_{N_2} c_p \Delta T_{REF}\right)$$
$$G_{DME} \equiv Q_{DME} / \left(W_{N_2} c_p \Delta T_{REF}\right)$$

are introduced. Here W_i is the molecular weight of species i, W_{N_2} is the molecular weight of nitrogen, T_{REF} is a refeerence temperature and ΔT_{REF} is a reference temperature difference. Introducing Eqs. (3) and (4) into Eq. (1) the folowing equations are obtained

$$x\frac{dX_{ISO}}{dx} + \frac{1}{Le_{ISO}}\frac{d^2X_{ISO}}{dx^2} = M_{ISO}$$

$$x\frac{dX_{DME}}{dx} + \frac{1}{Le_{DME}}\frac{d^2X_{DME}}{dx^2} = M_{DME} \tag{5}$$

$$x\frac{dX_{O_2}}{dx} + \frac{1}{Le_{O_2}}\frac{d^2X_{O_2}}{dx^2} = 12,5M_{ISO} + 3M_{DME}$$

Introducing Eqs. (3) and (4) into Eq. (2) the following equation is obtained

$$x\frac{d\tau}{dx} + \frac{d^2\tau}{dx^2} + \sum_{i=1}^{n}\frac{1}{Le_i}\frac{W_i}{W_{N_2}}\frac{c_{p,i}}{c_p}\frac{dX_i}{dx}\frac{d\tau}{dx} = -G_{ISO}M_{ISO} - G_{DME}M_{DME} \tag{6}$$

The conserved scalar quantities Z, Z_{ISO}, Z_{DME} are defined by following equations

$$x\frac{dZ}{dx^2} + \frac{d^2\tau}{dx^2} = 0$$

$$x\frac{dZ_{ISO}}{dx^2} + \frac{1}{Le_{ISO}}\frac{d^2\tau_{ISO}}{dx^2} = 0 \tag{7}$$

$$x\frac{dZ_{DME}}{dx^2} + \frac{1}{Le_{DME}}\frac{d^2\tau_{DME}}{dx^2} = 0$$

Eq. (7) is constrained to satisfy the conditions

$$Z = Z_{ISO} = Z_{DME} = 0; \; x = \infty$$
$$Z = Z_{ISO} = Z_{DME} = 1; \; x = -\infty \tag{8}$$

Integration of Eq. (7) together with Eq. (8) gives

$$Z = \frac{1}{2}\text{erfc}\left(x\sqrt{\frac{1}{2}}\right)$$

$$Z_{ISO} = \frac{1}{2}\text{erfc}\left(x\sqrt{\frac{Le_{ISO}}{2}}\right) \qquad (9)$$

$$Z_{DME} = \frac{1}{2}\text{erfc}\left(x\sqrt{\frac{Le_{DME}}{2}}\right)$$

Differntiation of Eq. (9) gives

$$\frac{dZ}{dx} = -\left(\sqrt{\frac{1}{2\pi}}\right)\exp\left(\frac{-x^2}{2}\right)$$

$$\frac{dZ_{ISO}}{dx} = -\left(\sqrt{\frac{Le_{ISO}}{2\pi}}\right)\exp\left(\frac{-x^2 Le_{ISO}}{2}\right) \qquad (10)$$

$$\frac{dZ_{DME}}{dx} = -\left(\sqrt{\frac{Le_{DME}}{2\pi}}\right)\exp\left(\frac{-x^2 Le_{DME}}{2}\right)$$

It follows from Eq. (10)

$$\frac{dZ_{ISO}}{dx} = \left(\sqrt{Le_{ISO}}\right)\frac{dZ}{dx}\left\{\exp\left[\frac{x^2(1-Le_{ISO})}{2}\right]\right\}$$

$$\frac{dZ_{DME}}{dx} = \left(\sqrt{Le_{DME}}\right)\frac{dZ}{dx}\left\{\exp\left[\frac{x^2(1-Le_{DME})}{2}\right]\right\} \qquad (11)$$

Coupling Relations at x_{ST}

Let the flame sheet be locatet at $x = x_{ST}$. At the flame sheet $Z = Z_{ST}$, $Z_{ISO} = Z_{ISO,ST}$, $Z_{DME} = Z_{DME,ST}$. At x_{ST} there is complete consumption of C_8H_{18}, CH_3OCH_3 and O_2. At x_{ST_-} the gradients are

$$\frac{1}{Le_{ISO}}\frac{dX_{ISO}}{dx} = \frac{1}{Le_{ISO}}\frac{dX_{ISO}}{dZ_{ISO}}\frac{dZ_{ISO}}{dx} = \frac{1}{Le_{ISO}}\frac{X_{ISO,l}}{1-Z_{ISO,ST}}\frac{dZ_{ISO}}{dx}$$

$$\frac{1}{Le_{DME}}\frac{dX_{DME}}{dx} = \frac{1}{Le_{DME}}\frac{dX_{DME}}{dZ_{DME}}\frac{dZ_{DME}}{dx} = \frac{1}{Le_{DME}}\frac{X_{DME,l}}{1-Z_{DME,ST}}\frac{dZ_{DME}}{dx}$$

$$\frac{dX_{O_2}}{dx} = 0$$

$$\frac{dX_{CO_2}}{dx} = \frac{dX_{CO_2}}{dZ}\frac{dZ}{dx} = -\frac{X_{CO_2,ST}}{1-Z_{ST}}\frac{dZ}{dx} \qquad (12)$$

$$\frac{dX_{H_2O}}{dx} = \frac{dX_{H_2O}}{dZ}\frac{dZ}{dx} = -\frac{X_{H_2O,ST}}{1-Z_{ST}}\frac{dZ}{dx}$$

$$\frac{d\tau}{dx} = \frac{d\tau}{dZ}\frac{dZ}{dx} = -\frac{\tau_{ST}}{1-Z_{ST}}\frac{dZ}{dx}$$

At x_{ST+} the gradient are

$$\frac{dX_{ISO}}{dx} = \frac{dX_{DME}}{dx} = 0$$

$$\frac{dX_{O_2}}{dx} = \frac{dX_{O_2}}{dZ}\frac{dZ}{dx} = -\frac{X_{O_2,2}}{Z_{ST}}\frac{dZ}{dx}$$

$$\frac{dX_{CO_2}}{dx} = \frac{dX_{CO_2}}{dZ}\frac{dZ}{dx} = -\frac{X_{CO_2,2}}{Z_{ST}}\frac{dZ}{dx} \qquad (13)$$

$$\frac{dX_{H_2O}}{dx} = \frac{dX_{H_2O}}{dZ}\frac{dZ}{dx} = -\frac{X_{H_2O,2}}{Z_{ST}}\frac{dZ}{dx}$$

$$\frac{d\tau}{dx} = \frac{d\tau}{dZ}\frac{dZ}{dx} = \frac{\tau_{ST}}{Z_{ST}}\frac{dZ}{dx}$$

The gradients at Z_{ST+} are

$$\frac{1}{Le_{ISO}}\frac{dX_{ISO}}{dZ} = \frac{1}{\sqrt{Le_{ISO}}}\frac{X_{ISO,1}}{1-Z_{ISO,ST}}\left\{\exp\left[\frac{x_{ST}^2\left(1-Le_{ISO}\right)}{2}\right]\right\} = g$$

$$\frac{1}{Le_{DME}}\frac{dX_{DME}}{dZ} = \frac{1}{\sqrt{Le_{DME}}}\frac{X_{DME,1}}{1-Z_{DME,ST}}\left\{\exp\left[\frac{x_{ST}^2\left(1-Le_{DME}\right)}{2}\right]\right\} = m$$

$$\frac{dX_{O_2}}{dZ} = 0$$

$$\frac{dX_{CO_2}}{dZ} = -\frac{X_{CO_2,ST}}{1-Z_{ST}}$$ (14)

$$\frac{dX_{H_2O}}{dZ} = -\frac{X_{H_2O,ST}}{1-Z_{ST}}$$

$$\frac{d\tau}{dZ} = \frac{\tau_{ST}}{1-Z_{ST}} = -p$$

At Z_{ST-} are

$$\frac{dX_{ISO}}{dZ} = \frac{dX_{DME}}{dZ} = 0$$

$$\frac{dX_{O_2}}{dZ} = \frac{dX_{O_2,2}}{dZ} = -c$$

$$\frac{dX_{CO_2}}{dZ} = \frac{X_{CO_2,ST}}{Z_{ST}}$$ (15)

$$\frac{dX_{H_2O}}{dZ} = \frac{X_{H_2O,ST}}{Z_{ST}}$$

$$\frac{d\tau}{dZ} = \frac{\tau_{ST}}{Z_{ST}} = s$$

Balance eqution for carbon across the reaction zone at $x = x_{ST}$ is

$$\left(\frac{8}{Le_{ISO}}\frac{dX_{ISO}}{dx} + \frac{2}{Le_{DME}}\frac{dX_{DME}}{dx} + \frac{dX_{CO_2}}{dx}\right)_{\pm} = 0$$ (16)

Balance equation for oxygen across the reation zone at $x = x_{ST}$ is

$$\left(\frac{1}{Le_{DME}}\frac{dX_{DME}}{dx} + 2\frac{dX_{O_2}}{dx} + 2\frac{dX_{CO_2}}{dx} + 2\frac{dX_{H_2O}}{dx}\right)_{\pm} = 0$$ (17)

Balance equation for hydrogen across the reaction zone at $x = x_{ST}$ is

$$\left(\frac{9}{Le_{ISO}} \frac{dX_{ISO}}{dx} + \frac{3}{Le_{DME}} \frac{dX_{DME}}{dx} + \frac{dX_{H_2O}}{dx} \right)_{\pm} = 0 \qquad (18)$$

It follows from Eqs. (16), (17) and (18)

$$\left(\frac{25}{Le_{ISO}} \frac{dX_{ISO}}{dx} + \frac{6}{Le_{DME}} \frac{dX_{DME}}{dx} - \frac{2}{Le_{DME}} \frac{dX_{O_2}}{dx} \right)_{\pm} = 0 \qquad (19)$$

Use Eqs. (14) and (15), into Eq. (19) gives

$$25g + 6m = 2c \qquad (20)$$

Coupling relations for temperature gives

$$\left(\frac{d\tau}{dx} + \frac{G_{ISO}}{Le_{ISO}} \frac{dX_{ISO}}{dx} - \frac{G_{DME}}{Le_{DME}} \frac{dX_{DME}}{dx} \right)_{\pm} = 0 \qquad (21)$$

This gives

$$\tau_{ST} = \left(G_{ISO}g + G_{DME}m \right) Z_{ST} \left(1 - Z_{ST} \right) \qquad (22)$$
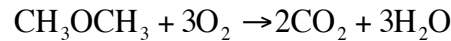
The adiabatic flame temperature T_{AD} is

$$T_{AD} = T_U + \frac{1}{c_p W_{N_2}} \left(Q_{ISO}g + Q_{DME}m \right) Z_{ST} \left(1 - Z_{ST} \right) \qquad (23)$$

B.2. Extinction and Autoignition of Partially Premixed Dimethylether Flames in Nonuniform Flows

Chemcial Reaction

The overall chemcial reaction between dimethylether (CH_3OCH_3) and O_2 is

$$CH_3OCH_3 + 3O_2 \rightarrow 2CO_2 + 3H_2O$$

The reaction rate, ω_{DME} with units of $1/(m^3/s)$

Formulation

Consdier two counterflowing streams flowing toward a stagnation plane. One stream called fuel-rich stream is injected toward the stagnation plane from the fuel-rich boundary. It is primarily made up of CH_3OCH_3 and N_2 with small amounts of O_2. The other stream, called the fuel-lean stream, is injected from the fuel-lean boundary. It is primarily made up of O_2 and N_2 with small amounts of CH_3OCH_3. The mass fractions of dimethylether and oxygen at the fuel-rich boundary are represented by $Y_{DME,1}$ and $Y_{O_2,1}$ respectively, and those at the fuel lean boundary are represented by $Y_{DME,2}$ and $Y_{O_2,2}$ respectively.

The species balance equations are

$$\rho a\hat{x} \frac{dY_{DME}}{d\hat{x}} + \rho D_{DME} \frac{d^2 Y_{DME}}{d\hat{x}^2} = W_{DME}\omega_{DME}$$

$$\rho a\hat{x} \frac{dY_{O_2}}{d\hat{x}} + \rho D_{O_2} \frac{d^2 Y_{O_2}}{d\hat{x}^2} = 3W_{O_2}\omega_{DME}$$

(1)

Here D_{ISO}, D_{DME} and D_{O_2} are respectevely the coeffcent of diffusion of C_8H_{18}, CH_3OCH_3 and O_2. The energy conservations equation is

$$\rho c_p a\hat{x} \frac{dT}{d\hat{x}} + \lambda \frac{d^2 T}{d\hat{x}^2} + \sum_{i=1}^{n} \rho D_i c_{p,i} \frac{dY_i}{d\hat{x}} \frac{dT}{d\hat{x}} = -Q_{DME}\omega_{DME}$$

(2)

Here λ is the coefficient of thermal conductivity, c_p is the heat capacity of the mixture, $c_{p,i}$ is the heat capacity of species i, D_i is the coefficient of diffuion on species i, Q_{ISO} is the heat released per mole of C_8H_{18} consumed and Q_{DME} is the heat released per mole of CH_3OCH_3 consumed.

Define the independent variable

$$x = \hat{x}(\rho c_p a / \lambda)^{1/2} \tag{3}$$

For convenience, the definitions

$$
\begin{aligned}
X_i &\equiv Y_i W_{N_2} / W_i \\
\tau &\equiv (T - T_{REF}) \Delta T_{REF} \\
M_{DME} &\equiv W_{N_2} \omega_{DME} / (\rho a) \\
G_{DME} &\equiv Q_{DME} / (W_{N_2} c_p \Delta T_{REF})
\end{aligned}
\tag{4}
$$

are introduced. Here W_i is the molecular weight of species i, W_{N_2} is the molecular weight of nitrogen, T_{REF} is a refeference temperature and ΔT_{REF} is a reference temperature difference. Introducing Eqs. (3) and (4) into Eq. (1) the folowing equations are obtained

$$
\begin{aligned}
x \frac{dX_{DME}}{dx} + \frac{1}{Le_{DME}} \frac{d^2 X_{DME}}{dx^2} &= M_{DME} \\
x \frac{dX_{O_2}}{dx} + \frac{1}{Le_{O_2}} \frac{d^2 X_{O_2}}{dx^2} &= 3M_{DME}
\end{aligned}
\tag{5}
$$

Introducing Eqs. (3) and (4) into Eq. (2) the following equation is obtained

$$x \frac{d\tau}{dx} + \frac{d^2\tau}{dx^2} + \sum_{i=1}^{n} \frac{1}{Le_i} \frac{W_i}{W_{N_2}} \frac{c_{p,i}}{c_p} \frac{dX_i}{dx} \frac{d\tau}{dx} = -G_{DME} M_{DME} \tag{6}$$

The conserved scalar quantities Z, Z_{DME} are defined by following equations

$$x\frac{dZ}{dx^2} + \frac{d^2\tau}{dx^2} = 0$$

$$x\frac{dZ_{DME}}{dx^2} + \frac{1}{Le_{DME}}\frac{d^2\tau_{DME}}{dx^2} = 0 \tag{7}$$

Eq. (7) is constrained to satisfy the conditions

$$Z = Z_{DME} = 0; x = \infty$$

$$Z = Z_{DME} = 1; x = -\infty \tag{8}$$

Integration of Eq. (7) together with Eq. (8) gives

$$Z = \frac{1}{2}\text{erfc}\left(x\sqrt{\frac{1}{2}}\right)$$

$$Z_{DME} = \frac{1}{2}\text{erfc}\left(x\sqrt{\frac{Le_{DME}}{2}}\right) \tag{9}$$

Differentiation of Eq. (9) gives

$$\frac{dZ}{dx} = -\left(\sqrt{\frac{1}{2\pi}}\right)\exp\left(\frac{-x^2}{2}\right)$$

$$\frac{dZ_{DME}}{dx} = -\left(\sqrt{\frac{Le_{DME}}{2\pi}}\right)\exp\left(\frac{-x^2 Le_{DME}}{2}\right) \tag{10}$$

It follows from Eq. (10)

$$\frac{dZ_{DME}}{dx} = \left(\sqrt{Le_{DME}}\right)\frac{dZ}{dx}\left\{\exp\left[\frac{x^2(1 - Le_{DME})}{2}\right]\right\} \tag{11}$$

Coupling Relations at x_{ST}

Let the flame sheet be located at $x = x_{ST}$. At the flame sheet $Z = Z_{ST}$, $Z_{DME} = Z_{DME,ST}$. At x_{ST} there is complete consumption of CH_3OCH_3 and O_2.

At x_{ST-} the gradients are

$$\frac{1}{Le_{DME}}\frac{dX_{DME}}{dx} = \frac{1}{Le_{DME}}\frac{dX_{DME}}{dZ_{DME}}\frac{dZ_{DME}}{dx} = \frac{1}{Le_{DME}}\frac{X_{DME,1}}{1-Z_{DME,ST}}\frac{dZ_{DME}}{dx}$$

$$\frac{dX_{O_2}}{dx} = \frac{dX_{O_2}}{dZ}\frac{dZ}{dx} = -\frac{X_{O_2,1}}{1-Z_{ST}}\frac{dZ}{dx}$$

$$\frac{dX_{CO_2}}{dx} = \frac{dX_{CO_2}}{dZ}\frac{dZ}{dx} = -\frac{X_{CO_2,ST}}{1-Z_{ST}}\frac{dZ}{dx} \tag{12}$$

$$\frac{dX_{H_2O}}{dx} = \frac{dX_{H_2O}}{dZ}\frac{dZ}{dx} = -\frac{X_{H_2O,ST}}{1-Z_{ST}}\frac{dZ}{dx}$$

$$\frac{d\tau}{dx} = \frac{d\tau}{dZ}\frac{dZ}{dx} = -\frac{\tau_{ST}}{1-Z_{ST}}\frac{dZ}{dx}$$

At x_{ST+} the gradients are

$$\frac{1}{Le_{DME}}\frac{dX_{DME}}{dx} = \frac{1}{Le_{DME}}\frac{dX_{DME}}{dZ_{DME}}\frac{dZ_{DME}}{dx} = -\frac{1}{Le_{DME}}\frac{X_{DME,2}}{Z_{DME,ST}}\frac{dZ_{DME}}{dx}$$

$$\frac{dX_{O_2}}{dx} = \frac{dX_{O_2}}{dZ}\frac{dZ}{dx} = -\frac{X_{O_2,2}}{Z_{ST}}\frac{dZ}{dx}$$

$$\frac{dX_{CO_2}}{dx} = \frac{dX_{CO_2}}{dZ}\frac{dZ}{dx} = -\frac{X_{CO_2,ST}}{Z_{ST}}\frac{dZ}{dx} \tag{13}$$

$$\frac{dX_{H_2O}}{dx} = \frac{dX_{H_2O}}{dZ}\frac{dZ}{dx} = -\frac{X_{H_2O,ST}}{Z_{ST}}\frac{dZ}{dx}$$

$$\frac{d\tau}{dx} = \frac{d\tau}{dZ}\frac{dZ}{dx} = -\frac{\tau_{ST}}{1-Z_{ST}}\frac{dZ}{dx}$$

The gradients at Z_{ST+} are

$$\frac{1}{Le_{DME}}\frac{dX_{DME}}{dZ} = \frac{1}{\sqrt{Le_{DME}}}\frac{X_{DME,1}}{1-Z_{DME,ST}}\left\{\exp\left[\frac{x_{ST}^2\left(1-Le_{DME}\right)}{2}\right]\right\} = m$$

$$\frac{dX_{O_2}}{dZ} = \frac{X_{O_2,1}}{1-Z_{ST}} = -a$$

$$\frac{dX_{CO_2}}{dZ} = -\frac{X_{CO_2,ST}}{1-Z_{ST}} \tag{14}$$

$$\frac{dX_{H_2O}}{dZ} = -\frac{X_{H_2O,ST}}{1-Z_{ST}}$$

$$\frac{d\tau}{dZ} = \frac{\tau_{ST}}{1-Z_{ST}} = -p$$

The gradients at Z_{ST-} are

$$\frac{1}{Le_{DME}}\frac{dX_{DME}}{dZ} = \frac{1}{\sqrt{Le_{DME}}}\frac{X_{DME,2}}{Z_{DME,ST}}\left\{\exp\left[\frac{x_{ST}^2\left(1-Le_{DME}\right)}{2}\right]\right\} = -n$$

$$\frac{dX_{O_2}}{dZ} = \frac{X_{O_2,2}}{Z_{ST}} = -c$$

$$\frac{dX_{CO_2}}{dZ} = \frac{X_{CO_2,ST}}{Z_{ST}}$$

$$\frac{dX_{H_2O}}{dZ} = \frac{X_{H_2O,ST}}{Z_{ST}}$$

$$\frac{d\tau}{dZ} = \frac{\tau_{ST}}{Z_{ST}} = s$$

$$(15)$$

Balance equation for carbon across the reaction zone at $x = x_{ST}$ is

$$\left(\frac{2}{Le_{DME}}\frac{dX_{DME}}{dx} + \frac{dX_{CO_2}}{dx}\right)_{\pm} = 0 \qquad (16)$$

Balance equation for oxygen acroos the reation zone at $x = x_{ST}$ is

$$\left(\frac{1}{Le_{DME}}\frac{dX_{DME}}{dx} + 2\frac{dX_{O_2}}{dx} + 2\frac{dX_{CO_2}}{dx} + 2\frac{dX_{H_2O}}{dx}\right)_{\pm} = 0 \qquad (17)$$

Balance equation for hydrogen across the reaction zone at $x = x_{ST}$ is

$$\left(\frac{3}{Le_{DME}}\frac{dX_{DME}}{dx} + \frac{dX_{H_2O}}{dx}\right)_{\pm} = 0 \qquad (18)$$

It follows from Eqs. (16), (17) and (18)

$$\left(\frac{3}{Le_{DME}}\frac{dX_{DME}}{dx} - \frac{dX_{O_2}}{dx}\right)_{\pm} = 0 \qquad (19)$$

Use Eqs. (14) and (15), into Eq. (19) gives

$$3(m+n) = a+c \tag{20}$$

Coupling relations for tempertature gives

$$\left(\frac{d\tau}{dx} + \frac{G_{DME}}{Le_{DME}} \frac{dX_{DME}}{dx}\right)_{\pm} = 0 \tag{21}$$

This gives

$$\tau_{ST} = G_{DME}(m+n)Z_{ST}(1-Z_{ST}) \tag{22}$$

The adiabatic flame temperature T_{AD} is

$$T_{AD} = T_U + \frac{1}{c_p W_{N_2}} Q_{DME}(m+n)Z_{ST}\left(1-Z_{ST}\right) \tag{23}$$